Narrow Urban Vehicles with an Integrated Suspension Tilting System: Design, Modeling, and Control

by

Chen Tang

A thesis
presented to the University of Waterloo
in fulfillment of the
thesis requirement for the degree of
Doctor of Philosophy
in
Mechanical and Mechatronics Engineering

Waterloo, Ontario, Canada, 2018

I hereby declare that I am the sole author of this thesis. This is a true copy of the thesis, including any required final revisions, as accepted by my examiners.

I understand that my thesis may be made electronically available to the public.

Abstract

Narrow urban vehicles are proposed to alleviate urban transportation challenges like congestion, parking, fuel consumption, and pollution. They are designed to seat one or two people in tandem, which saves space in road infrastructures as well as improves the fuel efficiency. However, to overcome the high rollover tendency which comes as a consequence of reduced track-width ratio, tilting systems for vehicle roll motion control are suggested.

Existing tilting solutions, which mechanically connect the wheel modules on both sides for motion synchronization, are not space-friendly for the narrow vehicle footprint. The mechanical linkages also add extra weight to those urban vehicles initially designed to be light-weighted. A novel integrated suspension tilting system (ISTS) is proposed in this thesis, which replaces rigid mechanical linkages with flexible hydraulic pipes and cylinders. In addition, combining the suspension and tilting into an integrated system will result in even more compact, light-weighted, and spacious urban vehicles.

The concept is examined, and the suspension mechanism for the tilting application is proposed after examining various mechanisms for their complexity and space requirements. Kinematic and dynamic properties of the tilting vehicle under large suspension strokes are analyzed to optimize the mechanism design.

Control of the active tilting systems for vehicle roll stability improvement is then discussed. Rather than tilting the vehicle to entirely eliminate the lateral load transfer during cornering, an integrated envelope approach considering both lateral and roll motion is proposed to improve the energy efficiency while maintaining the vehicle stability. A reconfigurable integrated control structure is also developed for various vehicle configurations as well as enhancing the system robustness against actuator failures.

The model predictive control (MPC) scheme is adopted considering the non-minimum phase nature of active tilting systems. The predictive feature along with the proposed roll envelope formulation provides a framework to balance the transient and steady-state performances using the tilting actuators. The suggested controller is firstly demonstrated on a vehicle roll model, and then applied to high-fidelity full vehicle models in CarSim including a four-wheeled SUV as well as a three-wheeled narrow urban vehicle. The SUV simulation results indicate the potential of using the developed envelope controller on conventional vehicles with active suspensions, while the narrow urban vehicle simulations demonstrate the feasibility of using the suggested ISTS on narrow tilting vehicles. By adopting the integrated envelope control approach, actuation effort is reduced and the vehicle handling, along with the stability in both lateral and roll, can be further improved.

Acknowledgements

Table of Contents

List of Tables

List of Figures

Chapter 1

Introduction

1.1 Motivation for Urban Vehicles

With the increasing number of vehicles, people in big cities have to face urban transportation issues like congestion, parking, and pollution. Research in the US shows the average number of occupants per vehicle is 1.58 [5]. Conventional four-wheeled vehicles, which are designed to accommodate four to six passengers comfortably as well as providing sufficient space for their cargo, are considered unnecessarily large for their average passenger load in normal city driving [6]. The surplus sizing of the vehicle takes more space when driving on the road as well as parking, and the extra weight comes along with the increase in fuel consumption.

Two-wheeled vehicles such as bicycles, mopeds, and motorcycles are considered space saving and extremely fuel-efficient [7]. However, such vehicles can seat limited occupants and provides small cargo space. Apart from this, passenger safety and weather protection designs of such two-wheelers are not as good as their four-wheeled counterparts. Drivers of two-wheelers also need to learn how to balance the vehicle as it is inherently unstable at low speeds, which also limits its public acceptance.

Therefore, a need exists for vehicles which are designed to carry one or two passengers with space and comfort offered by standard four-wheeled vehicles as well as significantly improved fuel efficiency [7]. It is natural, therefore, to consider three or four-wheeled narrow vehicles as a means to address these challenges. Such vehicles can be designed to provide just the right space to seat two people in tandem for normal urban commuter driving, and the reduced sizing requirement enables them to operate on reduced size lanes

and park in compact spaces. Such designs are also more stable in rollover compared with two-wheelers, and the enclosed cabin makes it possible to design a weatherproof interior and a crash-worthy body structure.

1.2 Tilting Mechanism and Tilting Control for Narrow Vehicles

Because such narrow vehicles will be operated with ordinary vehicles on highways, they still have to maintain the same height as conventional vehicles to provide good visibility for drivers. This makes the track width ratio of such vehicles problematic [8]. Stability in cornering is compromised as the reduced track width diminishes the vehicles resistance to roll moment [6]. The static stability factor (SSF) which was used by new car assessment program (NCAP) as the ratings for vehicle rollover resistance during 2001-2003 [9] is shown in Figure 1.1. It measures vehicle roll stability by considering only the vehicle geometry factors.
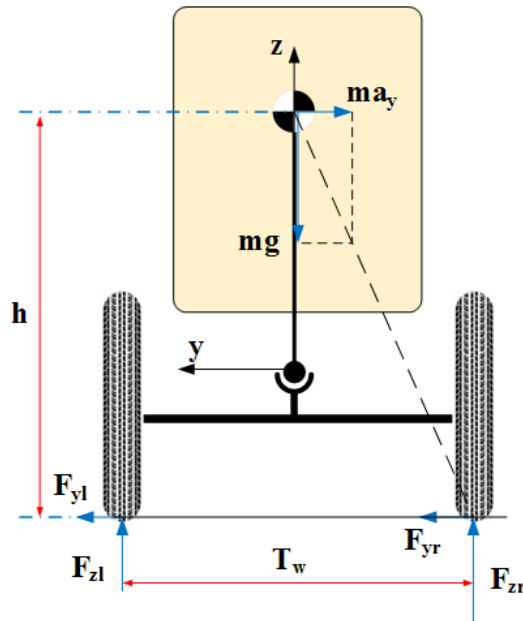
Figure 1.1: Vehicle Static Rollover and Static Stability Factor

To cause the inner wheel lifting off the ground which is regarded as the rollover, the

acceleration threshold (a_y^*) is solved as Eq.(1.1),

$$a_y^* = \frac{T_w}{2h}g \triangleq SSF \cdot g \tag{1.1}$$

Generally speaking, a narrow vehicle is defined as any vehicle with an SSF smaller than 0.6 [6]. Vehicles with high SSF cannot generate enough moment to cause rollover due to tire force saturation, which works as a fail-safe system to prevent rollover. However, this does not hold for narrow vehicles. Such vehicles can reach their tipping limit at lateral accelerations less than 0.7g while the tires skidding limit is at around 0.6 to 0.8g [6].

The solution is again inspired by two-wheelers. If such tall and narrow vehicles can lean into the curve during cornering, like bicycles and motorcycles, the rollover stability can be significantly enhanced. Such tilting systems are thus crucial in the design of narrow vehicles. Apart from this, the tilting system, in the ideal case, should be designed to require no extra control efforts from human drivers, so that any driver who can operate a conventional vehicle can quickly adapt to a narrow vehicle counterpart. This leads to the need for an active tilting system that controls the tilting mechanism to ensure the stability of the vehicle and the safety of the driver [10].

Vehicles equipped with the above-mentioned mechanical and control systems are referred to as Narrow Tilting Vehicles (NTV). Figure 1.2 summarizes the motivation for a tilting three-wheeler.
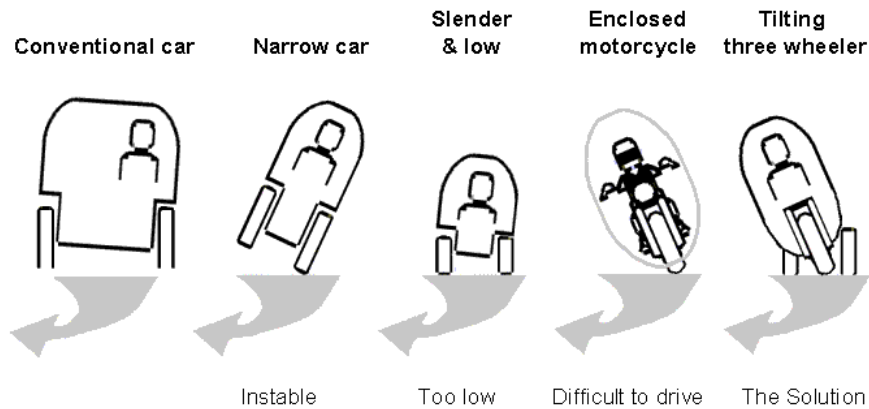
Figure 1.2: Motivation for Three-wheeled Narrow Tilting Vehicles [1]

1.3   Thesis Objectives

The objective of this thesis is to improve the design and control of narrow tilting vehicles. A compact multi-functional integrated suspension tilting system (ISTS) is proposed for narrow vehicle applications. This new design eliminates the mechanical linkages in conventional tilting mechanisms and incorporates the suspension functionality into the titling system, which results in lighter and more spacious urban vehicles. Integrated stability control is proposed for both lateral and roll motions of tilting vehicles. The controller is intended to be re-configurable to cover various wheel as well as actuators configurations for narrow urban vehicles. A strategy to properly coordinate available actuators like active steering, torque vectoring, differential braking and active tilting for integrated stability enhancement is also developed and evaluated.

1.4   Thesis Outline

The rest of the thesis is composed of the followings. Literature review in Chapter 2 starts with reviewing urban vehicles applications, their strengths, and weaknesses. Various tilting and control solutions to increase the vehicle roll stability are reviewed and discussed. Chapter 3 presents the proposed integrated suspension tilting system. The system is modeled, and its functionalities are examined. Chapter 4 deals with the design and optimization of the integrated suspension tilting system. Control of narrow tilting vehicles begins with the study of the vehicle roll model in Chapter 5. A roll envelope based on the rollover index is suggested, and a model predictive controller (MPC) is developed for the integrated control of both lateral and roll stability. Chapter 6 summarizes the conclusions and discusses the future work.

Chapter 2

Literature Review

This chapter starts with reviewing urban vehicle applications and their various configurations. Then, existing tilting mechanisms for vehicle roll stability enhancement are examined. Finally, active vehicle stability control systems are reviewed.

2.1 Urban Vehicles

To resolve the issues like congestion, parking, fuel consumption and pollution in urban transportation systems, narrow tilting vehicles (NTV) are proposed as a solution [6, 11]. They are in many ways similar to ordinary street cars but are designed to be narrow to seat one or two people in tandem. The reduced size in lateral direction saves the space and thus proves to be more efficient in utilizing the current road infrastructure like lane space and parking space. The reduced total mass as a consequence of compact size also helps to improve fuel efficiency and cut the pollution.

The narrow cabin design seems to be the cure for many of the transportation problems, but it also introduces a vital problem to such vehicles they can easily roll over without proper control. To enable narrow vehicles to be operated with conventional vehicles on street, their riding height needs to be similar to other vehicles, but the reduced track width significantly decreased such vehicles capability to resist rollover. The track width ratio, which is a rough measure of vehicle rollover stability, is almost doubled for narrow vehicles compared with the regular width automobiles. Stability in cornering is compromised since the reduced track width diminishes the vehicles resistance to roll moment [6].

Such tilting cars have an actuator to tilt the vehicle into the inner bend of the curve, like a motorcycle, to negotiate the curve at a higher speed for roll stability and also provides a fun driving experience. Conceptual and mechanism designs have been proposed [12, 13, 14, 15, 16], and several models have been built, as shown in Figure 2.1. Their configurations are summarized in Table 2.1.

Model	Wheel Config	Steerable Wheels	Driven Wheels	Tilting Parts
i-Road	2F1R[1]	Rear	Front	All
Carver	1F2R[1]	Front	Rear	Partial
Smera	2F2R[2]	Front	Rear	All
F-300 Life-jet	2F1R[3]	Front	Rear	All

Table 2.1: Comparison of Tilting Vehicle Configurations

Three wheelers, due to their simplicity and low cost [6], are ideal for narrow urban vehicle applications. Tadpole and delta are commonly adopted configurations for three-wheeled urban vehicles. The tadpole configuration refers to three-wheelers which have two wheels at the front, while the delta refers to the configuration with two wheels in the back. Dynamics analysis shows that tadpole configuration is more stable during braking while delta configuration improves the stability in acceleration [7]. Since stability in braking is more critical, and the magnitude of deceleration during emergency braking can be much higher than acceleration in normal driving, the tadpole configuration is preferred.

Several prototypes of NTVs have been built by the automotive industry since 1950. The Ford Gyron, which was a gyroscopically stabilized two-wheel vehicle with retractable wheels pods. The gyroscope, which weighted 180lbs, stabilized the vehicle and allowed it to travel at a lateral acceleration up to 1g while cornering [6], but the extra weight, at the same time, also became a limitation of the vehicle.

Another try was made by General Motors in the 1970s, when a three-wheeler called Lean Machine was fabricated. It was composed of a tilting cabin and a non-tilting engine assembly with a motorcycle front end for steering [6]. The body can rotate up to 55deg with respect to the non-tilting part. This movement was operated by the driver through foot pedal, which requires extra control effort from riders.

---

[1]Tadpole configuration: 2 wheels at the front and 1 wheel at rear;

[2]Delta configuration: 1 wheel at the front and 2 wheels at rear axle;

[3]Conventional vehicle configuration: 2 wheels at both front and rear.
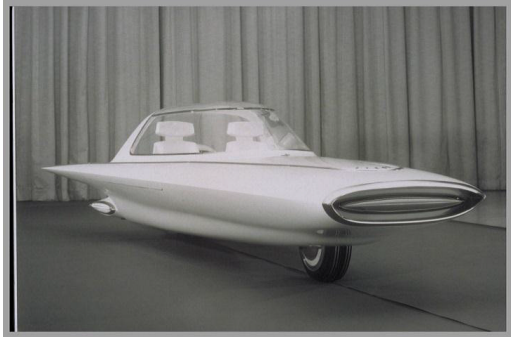
(a) Ford Gyron [6]

(b) GM Lean Machine [6]

(c) Mercedes-Benz F300 Life Jet [17]

(d) Carver [18]

(e) Lumeneo Smera [19]

(f) Toyota i-Road [20]

Figure 2.1: Examples of Narrow Tilting Vehicles

In 1997, Mercedes-Benz unveiled their NTV concept called F-300 Life-jet [17]. The vehicle was characterized by a two-wheeled front axle which can lean up to 30 degrees and a single rear wheel with the trailing arm suspension. An Active Tilt Control system was equipped, but the car was still designed to be almost as wide as a small conventional car with a front track width of 1560mm.

Carver One and the CLEVER (compact low emission vehicle for urban transport) were models developed in 2002 and 2003 respectively. Both of them had a single steerable front wheel mounted on the tilting cabin and equipped with a non-tilting axle with two wheels at the back. Their configuration was similar to that of the GM Lean Machine. They could tilt up to 45 degrees under the control of a hydraulically actuated Direct Tilt Control (DTC) system [18].

Smera [19] was a four-wheeled tilting vehicle developed by Lumeneo. This electric vehicle was regulated as a car in Europe and had a maximum speed of 128.7 km/h with a range of 145 kilometers on a single charge. The Direct Tilt Control (DTC) system installed was able to tilt the vehicle by a maximum angle of 20 degrees.

One of the recent endeavors in NTV was the Toyota i-Road [20] released in 2013. The three-wheeled electric vehicle was equipped with the active tiling system to balance the vehicle automatically. The car was designed to travel at a top speed of 45 km/h with a track width of 850mm.

2.2 Tilting Mechanisms

Even though various NTV models have been built, there are mainly three types of tilting mechanism being used in current models. Figure 2.2 shows the schematic view of single body tilting, chassis tilting and body separation tilting respectively.
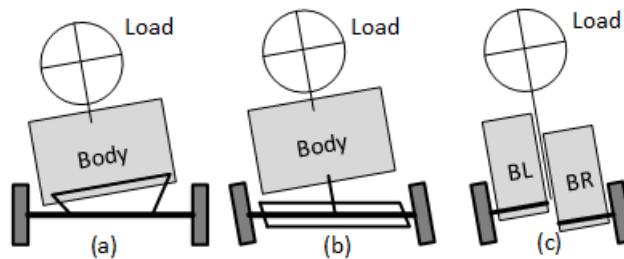
Figure 2.2: Different Types of Tilting Mechanisms [2]
(a) Single Body Tilting; (b) Chassis Tiling; and (c) Body Separation Tilting

2.2.1 Single Body Tilting

This type of tilting mechanism is shown in 2.2(a). Only the load along with the body shell tilts, while the chassis still acts as a fixed base like a regular car. Such mechanisms have been widely used in trains to tilt their heavy payload, and several tilting cars like GM Lean Machine, Carver One and the CLEVER [2, 21, 22] adopt this idea for the design[23].

The schematic view of the main tilting components used in Carver is shown in Figure 2.3. The tilting cylinders are installed between the rear (non-tilting) and front (tilting) part of the vehicle. Activation of these cylinders causes a tilting action of the passenger compartment [1]. The torque applied to the steering wheel is measured and used to drive the hydraulic pump to pressurize the hydraulic oil to one individual cylinder and withdraws the oil from the counteracting cylinder [1], thus creating the tilting motion of the body.
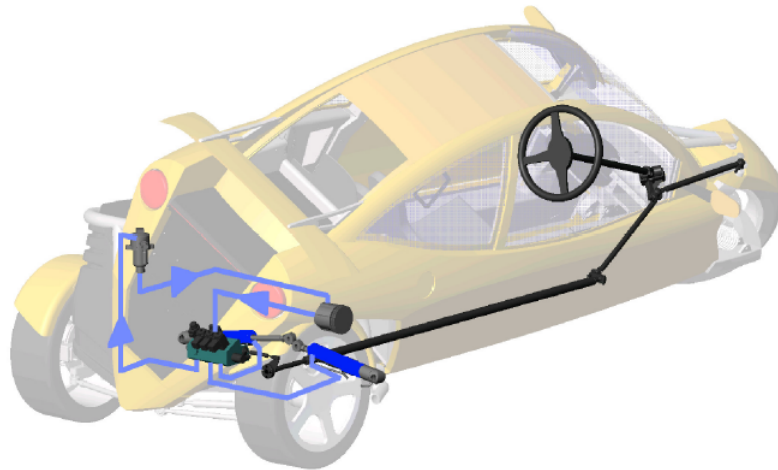
Figure 2.3: Body Tilting System in Carver [1]

2.2.2 Chassis Tilting

For chassis tilting, as shown in 2.2(b), the chassis, along with the body lean into the curve, and parallelogram mechanisms are the common designs to achieve this, as seen on Mercedes-Benz F-300, as well as recent research prototypes [13, 4, 3]. Such design is believed to be more compatible with light-weighted vehicles.

The leaning mechanism is extended from the four-bar linkage systems. The body frame, upper arm, lower arm, and wheel assemblies form the primary links. The lengths of the

arms are designed to guarantee that the wheels incline with the body. The angle between the suspension control arms and the vehicle frame can be altered by using hydraulic or electric actuators, which generates the tilting of the whole chassis as well as the camber motion of the wheels. In Figure 2.4, configuration A shows the vehicle in tilting mode, while configuration B shows the vehicle going over a bump while tilting [3].
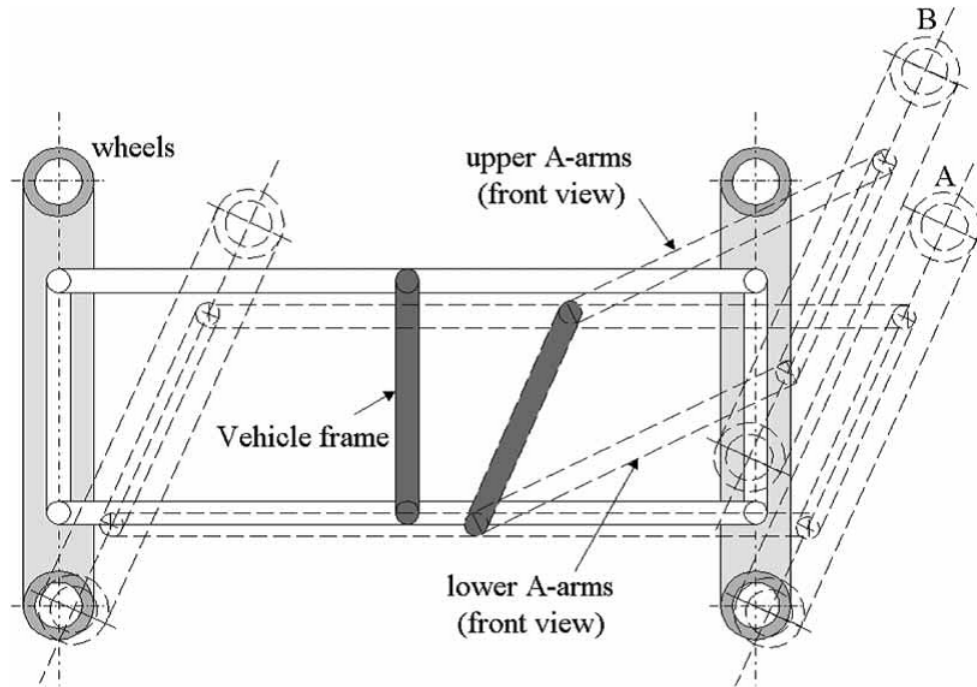
Figure 2.4: Chassis Tilting System using Parallelogram Mechanism [3]

2.2.3 Body Separation Tilting

Body separation tilting is another version of chassis tilting but achieved with a different approach. Its schematic drawing is shown in 2.2(c). The idea stems from the fact that if the wheel assembly on both sides can move independently with regard to the body, the vehicle can then lean as a whole by vertically by moving the left and right wheel assembly in opposite directions.

The swing arm mechanism used by J. Edelmann et al.[4] is shown in Figure 2.5. The suspension sub-frame and both wheel carriers are connected to the chassis by revolute joints. Actuators are attached in-between to generate the desired tilting angle. A swing

arm, along with the rods (br, bl, tr, tl) creates the coupling of motion between the wheel carriers on the left and right sides. When one of the wheel carriers goes up, the swing arm mechanism will cause the other wheel carrier to move downwards and thus generates the tilting motion. However, when both wheel carriers move uniformly, the suspension sub-frame will rotate relative to the chassis, and the suspension strut can thus absorb the road excitation.
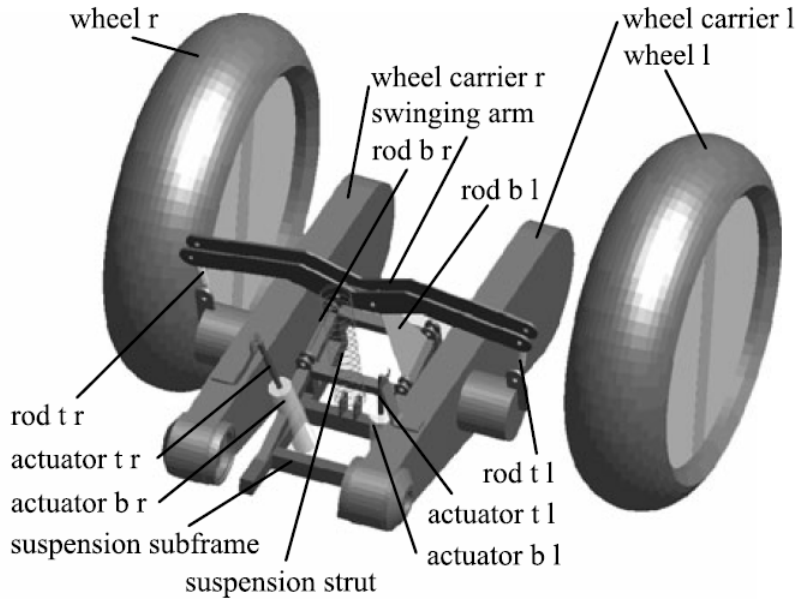
Figure 2.5: The Swing Arm Mechanism on Tilting Vehicles [4]

2.3 Vehicle Dynamics Control

In order to improve vehicle performance and enhance their stability, handling, and comfort, active control systems are widely designed and implemented [24] since the late 1970s. Generally, these systems are referred to as vehicle dynamics control (VDC) systems and can be classified as following [25]:

1. Vertical control systems such as active suspension systems (ASS), semi-active suspension systems, and active body control (ABC). They are developed for improvement in vehicle riding comfort and to some extent for vehicle handling.

2. Longitudinal control systems that are related to braking and traction including

anti-lock brake systems (ABS), traction control systems (TCS), and electronic stability program (ESP).

3. Lateral control systems that control yaw and lateral motions are developed for improvement of stability and handling of vehicles. They are used to prevent the vehicle from skidding or spinning out, and to improve vehicle response in yaw and lateral motions. Electric power steering system (EPS), active front steering (AFS), active four-wheel steering (4WS), differential braking, and differential traction are some examples of this category.

4. Roll control systems. Roll motion strongly affects handling and safety of vehicles, so active roll control is considered for performance improvements. Active suspension systems and active anti-roll bar are two examples of these control systems.

2.3.1 Lateral Stability Control

Lateral stability systems are designed to track the desired yaw rate of the vehicle. Yaw control systems are categorized into two distinct groups [26]:

Direct Yaw Control (DYC): Yaw moment can be applied to the vehicle by an unequal distribution of longitudinal forces on the left and right wheels. This method is called DYC and can be performed by differential braking and traction. The most practical method for development of DYC systems is differential braking that can be implemented by modifying ABS systems.

Indirect Yaw Control (IDYC): Steering creates side-slip angles and generates lateral force changes on tires. Such changes affect the yaw motion of the vehicle. This yaw control carried out from vehicle steering is known as indirect yaw control systems.

2.3.2 Rollover Control

The vehicle rollover is known as a major cause of severe and fatal injuries in traffic accidents. According to the research by the National Highway Traffic Safety Administration (NHTSA) [27], rollover accidents are ranked as the second most dangerous form of accident in the United States, after head-on collisions. Statistics also suggest that although a small portion of all accidents involves rollover, they constitute a disproportionately large portion of fatal ones [28].

Large vans and sport utility vehicles are prone to rollover accidents due to their high CoG positions [29, 30], and vehicles with narrow track width can also have rollover problems

before losing grip [6]. For vehicle rollover mitigation control, most of the existing researches are on un-tripped rollovers [31, 32], which are caused by extreme maneuvers like excessive speed cornering and obstacle avoidance maneuvers. The studies on tripped rollover are relatively few although the statistics [33] suggests that tripped rollover is the majority type of rollover accidents. Methods to improve vehicle rollover stability can be categorized as:

1. The methods that directly influence the roll motion and rollover behavior such as active suspensions, active anti-roll bars, and active stabilizers.

2. The methods that indirectly affect the roll motion by control of the vehicle yaw such as differential braking systems and active steering methods.

In the approach of using active suspension for rollover prevention, lateral load transfer is controlled to affect the rollover [28, 29] directly. The stability margin improved through the suggested approach is limited. Also, the drawback of this approach is that it influences the lateral stability of the vehicle and causes an over-steer characteristic [34].

The most common approach for indirect control of rollover is based on the reduction of the lateral acceleration by decreasing the yaw rate. This approach is implemented through differential braking and active front steering [35, 36]. The limitation of this approach is the loss of maneuverability, which may cause another accident [34, 37]. Some studies have been conducted to solve this problem for having both rollover prevention and good lateral stability [38, 39].

2.3.3 Active Tilting Control

Different from bicycles and motorcycles, narrow tilting cars are expected to be operated by drivers without sufficient skill and experience to lean the vehicle when cornering. The increased net weight along with the enclosed passenger cabin for comfort and safety improvement makes the balancing control much more difficult, especially in emergency situations. Consequently, active tilting control systems have been developed to keep vehicles in balance without the drivers direct intervention. These systems determine the desired tilting angle and use appropriate actuators to provide safe and comfortable driving experiences [1]. There are three different types of tilt control schemes for NTVs known as Direct Tilt Control (DTC), Steering Tilt Control (STC) and a combination of Steering and Direct Tilt Control (SDTC).

Direct Tilting Control (DTC)

For DTC systems, there is a tilting actuator to rotate the body relative to the chassis, and the steering system is used exclusively for lateral control [10]. The desired tilting angle is firstly determined by considering the vehicle speed, the curve radius and states of the vehicle. The lower-level controller then tracks the desired angle using the tilting actuator. So, the way to determine an appropriate tilting angle is crucial for DTC system design.

The common method to calculate the desired tilting angle is based on balancing the centrifugal force that occurs during steady state cornering [10]. This idea was adopted in [6, 35, 36] for DTC system design. A more complicated model suggested by [10] takes the vehicle lateral acceleration and gyroscopic moments of rotating wheels into consideration. The author claimed that the incorporation of the gyroscopic term ensured that no tilting torques were required from actuators in steady state.

Steering Tilting Control (STC)

For STC systems, there are no specific actuators for the tiling motion. Instead, the steering effort is used to track the given trajectory as well as balance the vehicle.

Based on steady-state steering conditions and linear tire model assumptions, the steering angle can be written as a function of the desired tilting angle, running speed of the vehicle and curve radius. However, calculating the desired tilting angle which can stabilize the vehicle while track the road trajectory is no easy task. Opposite steering efforts are required for curve negotiation and tilting [10].

To resolve this, the drivers turning intention interpreted from the steering wheel is no longer fed to the steering system directly. Instead, it will first be sent to a feedback controller for calculating the desired tilt angle. Then, the required steering angle to track that tilt angle can be calculated from the steady-state steering conditions. As yaw rate and tilting angle are related in steady-state conditions, by tracking a certain tilting angle derived from driver intention, the desired yaw rate which tracks the desired trajectory is also obtained.

Integrated Steering and Direct Tilting Control (SDTC)

DTC system is more stable at lower speeds compared to the STC system, while STC system is more efficient at higher speed and requires less transient torque [40, 41, 42]. Thus, a

combined system is proposed, in which DTC is more dominant at lower speeds and then STC takes over at higher speeds.

A speed dependent approach was suggested by So and Karnopp in [43] to switch between STC and DTC control. Snell [44] developed a combined SDTC control system where both elements of the control strategy were active at all times and did not rely on switching in a speed-dependent manner. Kidane et al. also developed an SDTC system with both DTC and STC working and a sinusoidal weighting function was used to ensure a smooth switch [10, 45].

Chapter 3

Integrated Suspension Tilting System: Conceptual Design

This chapter presents the proposed tilting system design for NTVs. Starting with the analysis for the packaging size of existing tilting mechanisms, it is identified that a compact and modularized tilting system is desired for narrow urban vehicles. A novel hydraulic-driven tilting system is introduced in this section, which utilizes hydraulics to replace mechanical connections for tilting motion generation. The system is integrated with an interconnected hydro-pneumatic suspension to provide the desired vertical and roll stiffness for the vehicle without introducing extra components. This further reduces the system weight and packaging size. Apart from tilting, adoption of independent hydraulic actuators enables the system to change the riding height of the vehicle. All the functionalities are illustrated and examined based on a half-car model. A full vehicle simulation is also presented to validate the feasibility of the proposed system for NTV applications, which results in more functionalities at a lower complexity and less system weight.

3.1 Challenges in Tilting System Design for NTV Applications

The followings are regarded as essential aspects in a tilting system design for NTVs:

1. Effective tilting for vehicle safety improvement

As reviewed previously, compared with the full vehicle tilting schemes, partial tilting solutions like single body tilting [1, 46, 47] are less useful for roll stability control. Since

only a small portion of the whole vehicle mass is involved in the tilting, the system has the limited potential for rollover mitigation. The tilting motion is applied mostly for improving riding comfort and driving fun.

2. System packaging and modularity

The chassis tilting systems which tilt the whole vehicle are preferred due to their effectiveness in resisting rollover for narrow urban vehicles. However, existing solutions generate the tilting motion with mechanically connected linkages to form a parallelogram mechanism [13, 16, 19, 3, 47]. The connection rods for motion synchronization add extra weight to the light-weighted vehicle, occupy cabin space, and impose body design restrictions.

The modularity of the suspension system is also sacrificed by the mechanical connections. Much effort has been devoted to developing urban vehicles in a modularized manner [48, 49, 50] to promote the subsystem re-usability. The broad adoption of X-by-wire technologies (e.g., steer-by-wire, drive-by-wire, brake-by-wire) removes the steering rod and driving shafts which used to mechanically connect the wheel modules on both sides. Similar technology is expected to simplify the tilting mechanisms.

3. Energy consumption and system operational costs

The tilting system as an auxiliary active safety system is not expected to significantly increase the manufacturing cost of urban vehicles otherwise their public acceptance might be affected. Existing solutions with added tilting mechanisms and actuators for active safety will inevitably increase the system complexity and cost. A more cost-effective solution by using suspension components in a multi-functional manner is desired.

To achieve a low operational cost, activation of the active tilting control should also be minimized, which is mostly dependent on the control algorithm to be discussed in later chapters. However, a well-designed suspension system for the NTVs should provide relatively high resistance to rollover without sacrificing the riding comfort.

To address these challenges, a novel Integrated Suspension Tilting System (ISTS) is proposed in the next section.

3.2   Integrated Suspension Tilting System

The most significant feature distinguishes the proposed system is to adopt hydraulic connections to replace the mechanical synchronizer for the tilting system. A direct benefit is the reduction in system weight and complexity. Much space can be saved for passengers and cargo, and the hydraulic pipelines can be positioned more easily in the cabin and

chassis designs compared with the rigid linkages. To make the system even more compact while achieving multi-functionalities, the traditional coil spring and shock absorber are replaced by a hydro-pneumatic suspension, which is a proven technology for the automotive industry as seen in the Citrons Hydractive systems [51, 52].

The schematic drawing of the proposed system on a half-car model is shown in Figure 3.1. The double-acting hydraulic cylinders (4) with accumulators (5) attached to their lower chambers serve as the spring component in conventional suspensions. Orifices, as well as the connecting pipelines, provide the damping sources similar to shock absorbers in conventional suspension systems. The cross inter-connection of the hydraulic cylinders provides a preferable roll stiffness without introducing auxiliary anti-roll bars. Much space and weight can be saved thanks to the simplified structure. The enhanced roll stiffness also helps to reduce the energy consumption due to the less frequent activation of active tilting controls. Finally, to actively tilt the vehicle, hydraulic pump modules (2) are connected to the upper chambers to pump fluid into the system under the coordination of the controller (3), which serves as the software implementation of mechanical constraints to achieve synchronized wheel motions in existing tilting mechanism designs.
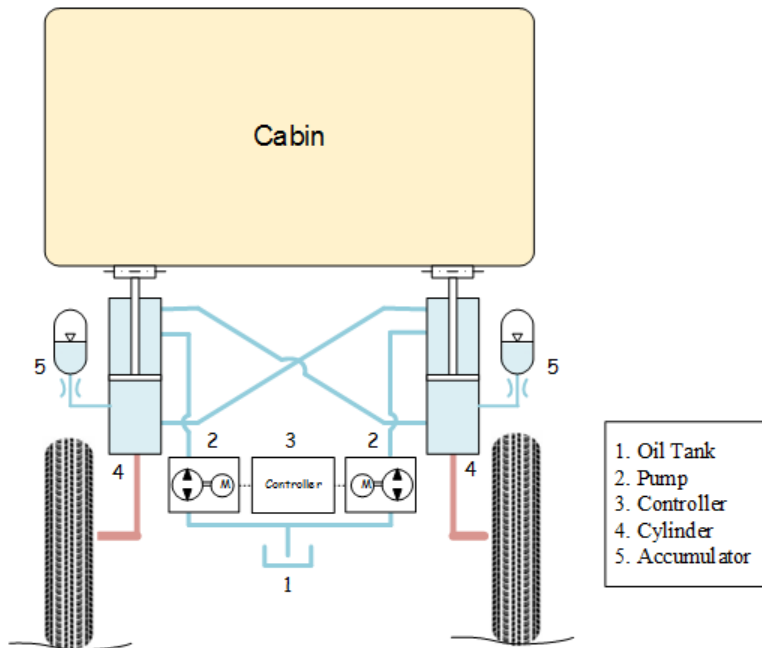
Figure 3.1: Overview of the Integrated Suspension Tilting System (ISTS)

The synchronization of wheel motions which used to be addressed by mechanical link-

ages now has a software solution: designing a controller to properly coordinate pump actuation and generate the desired motion. The adoption of separate pump modules also bring an extra degree of freedom: apart from tilting, the system can also adjust the vehicle riding height. If the piston on both sides travels in an asynchronous motion (same distance but in reverse directions), the tilting motion of the full vehicle can be achieved as shown in Figure 3.2(a). The tilting angle is determined by the piston displacement, which can be regulated by the activation of hydraulic pumps. Through the control of flow rate in the pumps, not only the tilting angle but also the tilting speed can be regulated to provide passengers a responsive feel of tilting. If the pistons move in a synchronous mode (same direction and same magnitude), vehicle height adjustment can be achieved as shown in Figure 3.2(b).
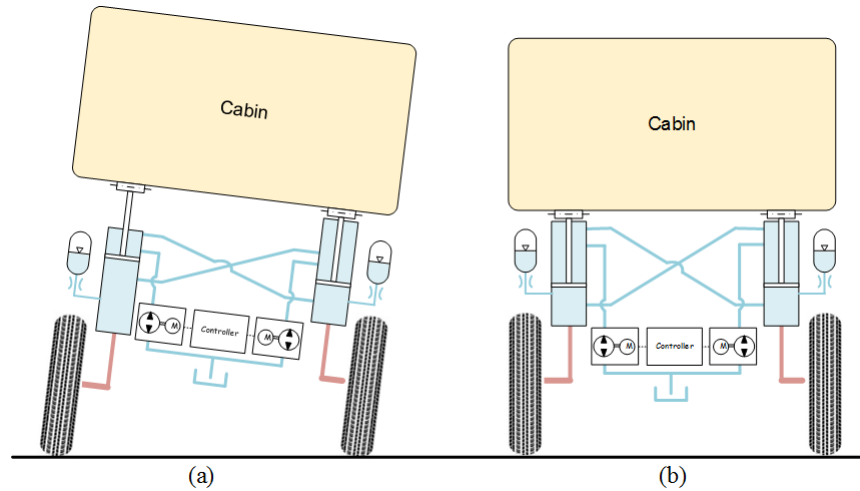
Figure 3.2: ISTS in Tilting Mode (a); and Height Adjustment Mode (b)

Such height adjustment functionality has already been applied on buses [53] to lower their floor to a kneeling position to ease entering and exiting the car, especially for the elderly population. On conventional vehicles, it has been used to improve the handling and aerodynamics, as well as to increase ground clearance for harsh environments [54].
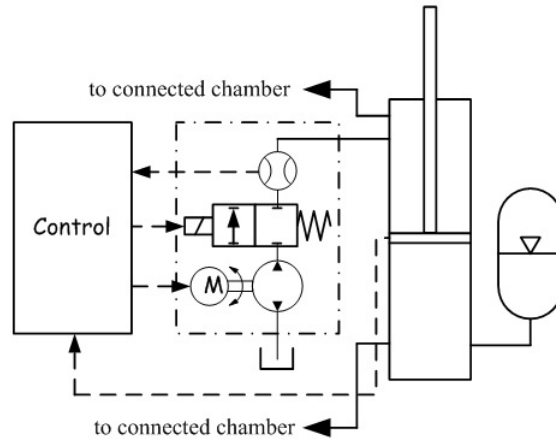
Figure 3.3: Actuator, Sensor, and Controller in ISTS

Although the idea of an integrated suspension tilting system is presented, the detailed design of the actuation and sensing module is open for implementation. An example is illustrated in Figure 3.3. The major components are: a fixed displacement pump which can rotate in either direction; a solenoid valve which can disconnect the pump from the hydraulic pipelines and eliminates the need for a motor brake; a flow meter to measure the volume of the hydraulic fluid being pumped into the cylinder; and displacement sensors to monitor the strut movements.

A typical working flow of the ISTS can be described as follows. When a tilting or height adjustment requirement is determined by the vehicle controller, the solenoid valve is firstly energized, and the fluid will be pumped into the cylinders to drive the piston to the desired position. The process is monitored by the on-board sensing system. Once the desired strut position is achieved, the solenoid valve will be closed. In that state, the cylinders and the accumulators along with the connection pipelines form the hydraulic interconnected suspension configuration [52] in a passive mode.

In summary, the proposed hydraulic-based ISTS can achieve the same tilting functionality as the existing linkage-based tilting mechanisms while it provides ride height adjustment and suspension functionalities. The reduced packaging size, as well as the system weight, can bring many benefits to the narrow urban vehicles. The system is also featured by achieving a high roll stiffness without using an anti-roll bar. All these efforts help to improve the fuel economy, safety, as well as dynamic performance in urban vehicles as a small and light-weighted carrier.

20

3.3   ISTS Modeling

To study the feasibility of the ISTS, the system is examined by the widely-adopted hydraulic and pneumatic equations [52, 55] in this section. The schematic diagram of the proposed ISTS is shown in Figure 3.4.

The pressures in the chambers are denoted as P_i ($i = 1..4$), and the flow rates in the connection pipelines are q_i ($i = 1..2$) with their positive direction shown in the figure. Flow rates contributed by the pumps are denoted as (q_{pl}, q_{pr}), while those from the accumulators are recorded as (q_{al}, q_{ar}). The air pressure and volume in the hydro-pneumatic accumulators are denoted as P_i, V_i ($i = 5..6$). The strut movements are measured as (z_{sl}, z_{sr}) respectively, while the wheel movements are (z_{ul}, z_{ur}). Finally, the suspension forces generated by the ISTS are referred to as (F_{sl}, F_{sr}).
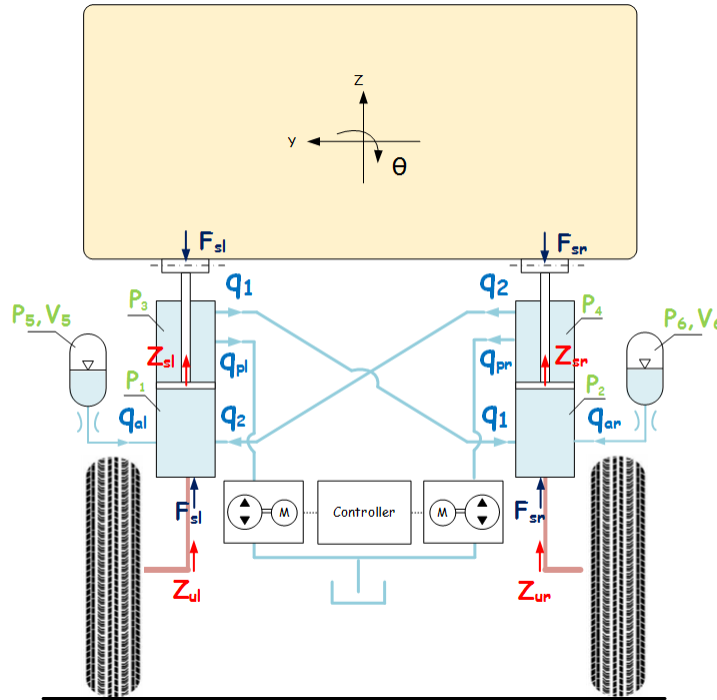
Figure 3.4: The Schematic Model of ISTS

The gas confined within the accumulator serves as the gas spring for providing the suspension stiffness for the vehicle. The ideal gas adiabatic process [56] is assumed, and the equation to relate the gas pressure (P_5, P_6) and volume (V_5, V_6) can be written as,

21

$$P_5 V_5^\gamma = P_6 V_6^\gamma = P_0 V_0^\gamma \tag{3.1}$$

where, P_0 and V_0 are the nominal charge pressure and gas volume; γ is the isentropic coefficient.

By assuming the fluid is in-compressible [57, 58], the volume change of the gas indicates the fluid flow rate leaving the accumulator as,

$$\dot{V}_5 = q_{al}, \dot{V}_6 = q_{ar} \tag{3.2}$$

By linearizing Eq.(3.1) around the nominal charge pressure and gas volume, and substituting Eq.(3.2), the fluid flow rate leaving the accumulator can be related to the gas pressure change as,

$$\dot{P}_5 = -\frac{1}{c_a} q_{al}, \dot{P}_6 = -\frac{1}{c_a} q_{ar} \tag{3.3}$$

where, $c_a = V_0/(\gamma P_0)$ is the capacitance of the accumulator.

The orifice and the cross-connected hose serve as the damping source for the suspension system. Assuming laminar fluid flow through the interconnecting pipes, and negligible entry and exit losses [56], the flow rate through the connecting pipelines are governed by the pressure difference of the connected chambers. Both of them are modeled as linear loss coefficients (r_o, r_h). According to Poiseuilles law [59], the pressure drop across the orifices and hose is proportional to the flow rate by the linear coefficient [57],

$$\begin{aligned}
P_5 &= P_1 + r_o q_{al}, P_6 = P_2 + r_o q_{ar} \\
P_3 &= P_2 + r_h q_1, P_4 = P_1 + r_h q_2
\end{aligned} \tag{3.4}$$

The cylinders serve as the boundary between the mechanical and hydraulic system. The relationship between the piston motion and the generated force represents the equivalent spring and damper of the ISTS. By assuming in-compressible fluid, the fluid volume in the four chambers can only be affected by the piston movement, fluid transported from the interconnected pipelines and the fluid from the accumulators or pumps. This leads to,

$$\begin{aligned}
q_1 &= A_U \left(\dot{z}_{sl} - \dot{z}_{ul} \right) - q_{pl}, q_2 = A_U \left(\dot{z}_{sr} - \dot{z}_{ur} \right) - q_{pr} \\
q_{al} &= A_L \left(\dot{z}_{sl} - \dot{z}_{ul} \right) - q_2, q_{ar} = A_L \left(\dot{z}_{sr} - \dot{z}_{ur} \right) - q_1
\end{aligned} \tag{3.5}$$

where, $(A_L,\ A_U)$ denotes the working area of head and rod side of the piston, respectively.

The strut force is generated by the pressure difference of upper and lower chambers. Considering the working area difference of the piston at the head and rod side, the resultant suspension force can be written as,

$$
\begin{aligned}
F_{sl} &= (P_1 - P_a)\,A_L - (P_3 - P_a)\,A_U \\
F_{sr} &= (P_2 - P_a)\,A_L - (P_4 - P_a)\,A_U
\end{aligned}
\tag{3.6}
$$

where, P_a is the atmospheric pressure.

In the rest of this chapter, the road is assumed to be flat with no disturbances. This is a commonly-adopted assumption for un-tripped rollover studies [60, 61], in which the unsprung mass displacements can be ignored. With this assumption, the equations of the proposed ISTS can be written in the state-space form with pump flow rate as inputs, pump volumetric displacements as augmented states and strut force as outputs, as,

$$
\begin{aligned}
U_{ho} &= \begin{bmatrix} q_{pl} & q_{pr} \end{bmatrix}^T \\
Y_{ho} &= \begin{bmatrix} F_{sl} & F_{sr} \end{bmatrix}^T \\
X_{ho} &= \begin{bmatrix} \dot{z}_{sl} & \dot{z}_{sr} & z_{sl} & z_{sr} & Q_{pl} & Q_{pr} \end{bmatrix}^T
\end{aligned}
\tag{3.7}
$$

The strut force produced by ISTS can be written in state space form as:

$$
Y_{ho} = A_{ho}X_{ho} + B_{ho}U_{ho} + F_{ho}
\tag{3.8}
$$

where,

$$
A_{ho} = \begin{bmatrix} A_{ds} & A_s & A_p \end{bmatrix},
$$

$$
A_{ds} = \begin{bmatrix} -\left(A_L^2 + A_U^2\right)r_o - A_U^2 r_h & 2A_L A_U r_o \\ 2A_L A_U r_o & -\left(A_L^2 + A_U^2\right)r_o - A_U^2 r_h \end{bmatrix},
$$

$$
A_s = \begin{bmatrix} -\left(A_L^2 + A_U^2\right)/C_a & 2A_L A_U / C_a \\ 2A_L A_U / C_a & -\left(A_L^2 + A_U^2\right)/C_a \end{bmatrix},
\tag{3.9}
$$

$$
A_p = \begin{bmatrix} A_U/C_a & -A_L/C_a \\ -A_L/C_a & A_U/C_a \end{bmatrix},
$$

$$
B_{ho} = \begin{bmatrix} (r_h + r_o)\,A_U & -A_L r_o \\ -A_L r_o & (r_h + r_o)\,A_U \end{bmatrix}, F_{ho} = \begin{bmatrix} (A_U - A_L)\,P_a \\ (A_U - A_L)\,P_a \end{bmatrix}
$$

23

A simple vehicle roll model with no road disturbance inputs is also adopted for the concept validation in this chapter. The half-car vehicle model which considers the vehicles vertical and roll motions can be written as,

$$
\begin{aligned}
m_s \ddot{z}_s &= F_{sl} + F_{sr} - m_s g \\
I_x \ddot{\phi} &= (F_{sl} - F_{sr})\tfrac{T_w}{2} + m_s a_y h + m_s g h \phi
\end{aligned}
\tag{3.10}
$$

where, vertical displacement and roll angle of the cabin are denoted as z_s and ϕ respectively, m_s is the cabin mass; h denotes the nominal CoG height; T_w stands for the track width; and a_y represents the measured vehicle lateral acceleration.

In the hydraulic derivations of ISTS, the strut displacements are more frequently used. The linear transform from vehicle states to suspension deflections can be written as,

$$
\begin{bmatrix} z_{sl} \\ z_{sr} \end{bmatrix} = \begin{bmatrix} 1 & +T_w/2 \\ 1 & -T_w/2 \end{bmatrix} \begin{bmatrix} z_s \\ \phi \end{bmatrix}
\tag{3.11}
$$

3.4   System Functionality Analysis

This section analyzes the feasibility of the proposed functionalities by examining the system equations developed in Section 3.3. More concretely, the decoupling of roll and bump stiffness in the passive suspension mode will be analyzed. In the active control mode, the regulation of struts movements to adjust tilting angle and riding height is also discussed.

3.4.1   Decoupled Roll and Bump Stiffness

For conventional vehicles equipped with coil springs, their bump and roll stiffness are coupled. Vehicle designers have to compromise between the handling and the riding comfort performances, or incorporate the auxiliary anti-roll bars to enhance the vehicle roll stability. However, with the proposed ISTS, the bump and roll stiffness can be separately designed to meet the comfort as well as safety requirements, with no external components. To demonstrate this, the half-car model illustrated in Figure 3.4 is adopted to analyze the vehicles nominal stiffness in vertical and roll directions.

The gas volume in both accumulators, according to Eq.(3.2) and (3.5), can be written as,

$$V_5 = V_0 + \int_0^t q_{al}dt = V_0 + A_L z_{sl} - A_U z_{sr} + Q_{pr}$$
$$V_6 = V_0 + \int_0^t q_{ar}dt = V_0 + A_L z_{sr} - A_U z_{sl} + Q_{pl}$$
(3.12)

The gas pressure can then be written as a function of vehicle states and pump inputs by combining Eq.(3.1), (3.11) and (3.12), as,

$$\begin{cases} P_5 = P_0 V_0^\gamma \left(V_0 + (A_L - A_U) z_s + (A_L + A_U) \frac{T_w}{2}\phi + Q_{pr}\right)^{-\gamma} \\ P_6 = P_0 V_0^\gamma \left(V_0 + (A_L - A_U) z_s - (A_L + A_U) \frac{T_w}{2}\phi + Q_{pl}\right)^{-\gamma} \end{cases}$$
(3.13)

In suspension mode, the pumps are not activated $(Q_{pl} = Q_{pr} = 0)$. By assuming a quasi-static pressure condition (*i.e.* $P_1 = P_4 = P_5$, $P_2 = P_3 = P_6$), the net force and moment developed by the suspension struts become:

$$\Sigma F = F_L + F_R = (P_5 + P_6 - 2P_a)(A_L - A_U)$$
$$\Sigma M = \frac{T_w}{2}(F_L - F_R) = \frac{T_w}{2}(P_5 - P_6)(A_L + A_U)$$
(3.14)

The bump and roll stiffness of the connected strut can then be determined by substituting Eq.(3.13) into (3.14), and taking derivatives around the nominal position, as:

$$K_Z|_{z_s=0,\phi=0} = -\left.\frac{\partial F}{\partial z_s}\right|_{z_s=0,\phi=0} = 2\gamma\frac{P_0}{V_0}(A_L - A_U)^2$$
$$K_\phi|_{z_s=0,\phi=0} = -\left.\frac{\partial M}{\partial \phi}\right|_{z_s=0,\phi=0} = \gamma\frac{P_0}{V_0}\frac{T_w^2}{2}(A_L + A_U)^2$$
(3.15)

The ratio between the roll and bump stiffness will become:

$$\left.\frac{K_\phi}{K_Z}\right|_{z_s=0,\phi=0} = \frac{T_w^2}{4}\frac{(A_L + A_U)^2}{(A_L - A_U)^2} = \frac{T_w^2}{4}\kappa$$
(3.16)

where, κ is amplification factor introduced by the interconnection of the hydraulic struts.

$$\kappa = \left(\frac{1 + A_U/A_L}{1 - A_U/A_L}\right)^2$$
(3.17)

Compared with the conventional coil spring suspensions where $\kappa \equiv 1$, the interconnection offers the decoupled bump and roll stiffness by providing the design flexibility through

25

this customizable amplification factor. The desired bump and roll stiffness are separately specified and substituted into Eq.(3.16) to solve for the desired amplification factor . Then, by solving Eq.(3.17), the ratio of working areas on head and rod sides are determined. Considering the vertical load balance as shown in Eq.(3.14), the head and rod side area can then be designed.

3.4.2 Strut Position Control

As illustrated in Figure 3.2, control of the strut positions can directly affect the vehicle pose and the riding height. However, due to the hydraulic interconnections, ISTS struts need to be studied in pairs for their position control. This section examines the required fluid to be pumped under steady-state assumptions to demonstrate the feasibility of ISTS for vehicle motion control.

With the flat road assumption, Eq.(3.5) can be written as,

$$
\begin{aligned}
Q_1 &= A_U z_{sl} - Q_{pl}, Q_2 = A_U z_{sr} - Q_{pr} \\
Q_2 &= A_L z_{sl} - Q_{al}, Q_1 = A_L z_{sr} - Q_{ar}
\end{aligned}
\tag{3.18}
$$

where, Q_1, Q_2, Q_{al}, Q_{ar} are the fluid volume corresponding to flow rate q_1, q_2, q_{pl}, q_{pr} respectively.

The piston movement can be represented as a function of fluid volume from the accumulators and pumps as,

$$
\begin{aligned}
z_{sl} &= \frac{A_U\left(Q_{pl}-Q_{ar}\right)+A_L(Q_{pr}-Q_{al})}{A_U^2-A_L^2} \\
z_{sr} &= \frac{A_U(Q_{pr}-Q_{al})+A_L\left(Q_{pl}-Q_{ar}\right)}{A_U^2-A_L^2}
\end{aligned}
\tag{3.19}
$$

From Eq.(3.19), to generate a synchronous strut motion $(z_{sl} = z_{sr} = s_h)$, the required volume changes in connected chambers are solved as,

$$
Q_{pl} - Q_{ar} = Q_{pr} - Q_{al} \triangleq Q_h
\tag{3.20}
$$

where, Q_h denotes the volume change for height control, and is solved by,

$$
Q_h = -\left(A_L - A_U\right) s_h
\tag{3.21}
$$

26

The negative sign in Eq.(3.21) also indicates that, to lift the cabin ($s_h > 0$), the fluid needs to be pumped into the system ($Q_h < 0$).

To tilt the cabin, the asynchronous motions of the suspension struts are desired ($z_{sl} = -z_{sr} = s_\phi$). According to Eq.(3.19), the piston movement and fluid volume change have the relationship:

$$Q_\phi = (A_U + A_L) \, s_\phi \tag{3.22}$$

For more general cases, the ISTS can produce the height adjustment (s_h) and tilting (s_ϕ) simultaneously. To achieve that, the required strut displacement are solved as,

$$z_{sl} = s_h + s_\phi, z_{sr} = s_h - s_\phi \tag{3.23}$$

The resultant fluid volume change can be determined as,

$$Q_{pl} = Q_h + Q_\phi + Q_{ar}, Q_{pr} = Q_h - Q_\phi + Q_{al} \tag{3.24}$$

where, Q_h generates the in-phase motion of the pistons for height control, while Q_ϕ generates the out-of-phase motion and sets the tilting angle of the vehicle, with their values determined in Eq.(3.21) and (3.22) respectively.

The fluid volume change contributed by accumulators (Q_{ar}, Q_{al}) can be calculated from the gas volume change due to the load transfer in the struts. From Eq.(3.10), the steady-state load transfer in the suspension struts due to tilting and lateral acceleration are,

$$\Delta F_{sl} = -\frac{1}{T_w} \left[m_s gh \sin\phi + m_s a_y h \cos\phi \right], \Delta F_{sr} = -\Delta F_{sl} \tag{3.25}$$

The load difference on struts has to be compensated by gas pressures in the corresponding accumulators. By combining Eq.(3.25) and (3.6), the gas pressure changes are solved as:

$$\Delta P_5 = \frac{\Delta F_{sl}}{A_U + A_L}, \Delta P_6 = \frac{\Delta F_{sr}}{A_U + A_L} \tag{3.26}$$

Substituting Eq.(3.26) into (3.1), the gas volume change, as well as the change in accumulator fluid volume are determined as:

$$Q_{al} = \Delta V_5 = V_0 \left[\left(\frac{P_0}{P_0 + \Delta P_5} \right)^{1/\gamma} - 1 \right]$$
$$Q_{ar} = \Delta V_6 = V_0 \left[\left(\frac{P_0}{P_0 + \Delta P_6} \right)^{1/\gamma} - 1 \right]$$
$$(3.27)$$

By properly pumping fluid into both chambers according to Eq.(3.24) and (3.27), the riding height adjustment, as well as tilting, can now be achieved.

3.5 Design Evaluation

Using the governing equations developed in Section 3.3, a mathematical model of a half car with the proposed system is developed, and the feed-forward algorithm to determine pumped fluid volume as shown in Section 3.4 based on desired riding height adjustment and tilting angle is also implemented. To demonstrate the feasibility of the proposed integrated suspension tilting system, the tilting and height adjustment functionalities are first examined using the half-car model. After that, a multi-body model for a three-wheeled tilting vehicle equipped with the proposed system is simulated in the MapleSim environment [62]. The feed-forward tilting control is adopted to examine the vehicle system behavior during a cornering maneuver. The parameters for the simulation are listed in Table 3.1.

Symbol	Parameter Description	Value	Unit
m	Vehicle mass	915	kg
I	Roll inertia	210	$\text{kg} \cdot \text{m}^2$
a	Front axle to CoG distance	0.75	m
b	Rear axle to CoG distance	1.75	m
T_w	Vehicle track width	1.2	m
H_0	Vehicle CoG height	0.55	m
P_0	Initial charge pressure	0.8	MPa
V_0	Initial gas volume	1.79	L
A_U	Area of the rod side of the piston	$3.59 \cdot 10^{-3}$	m^2
A_L	Area of the head side of the piston	$8.09 \cdot 10^{-3}$	m^2
γ	Isentropic exponent	1.4	$-$
ρ	Mass density of the fluid	900	km/m^3
C_d	Discharge coefficient	0.8	$-$
A_O	Area of the orifice	$3.0 \cdot 10^{-4}$	m^2
μ	Dynamic viscosity of the fluid	0.6	$\text{Pa} \cdot \text{s}$
L	Length of the pipe	1.5	kg
d	Diameter of the connecting pipe	$2.5 \cdot 10^{-2}$	m

Table 3.1: Parameters for the ISTS model

3.5.1   Feed-forward Height and Tilting Control

The tilting and height adjustment scenarios analyzed in the previous section are simulated using the half car model. The first scenario is to lower the vehicle CoG by 20 cm in 1 second. As shown in Figure 3.5, the system tracks the reference height and converges quickly. The fluid volume to be pumped and the resultant struts movement are shown in the figure.
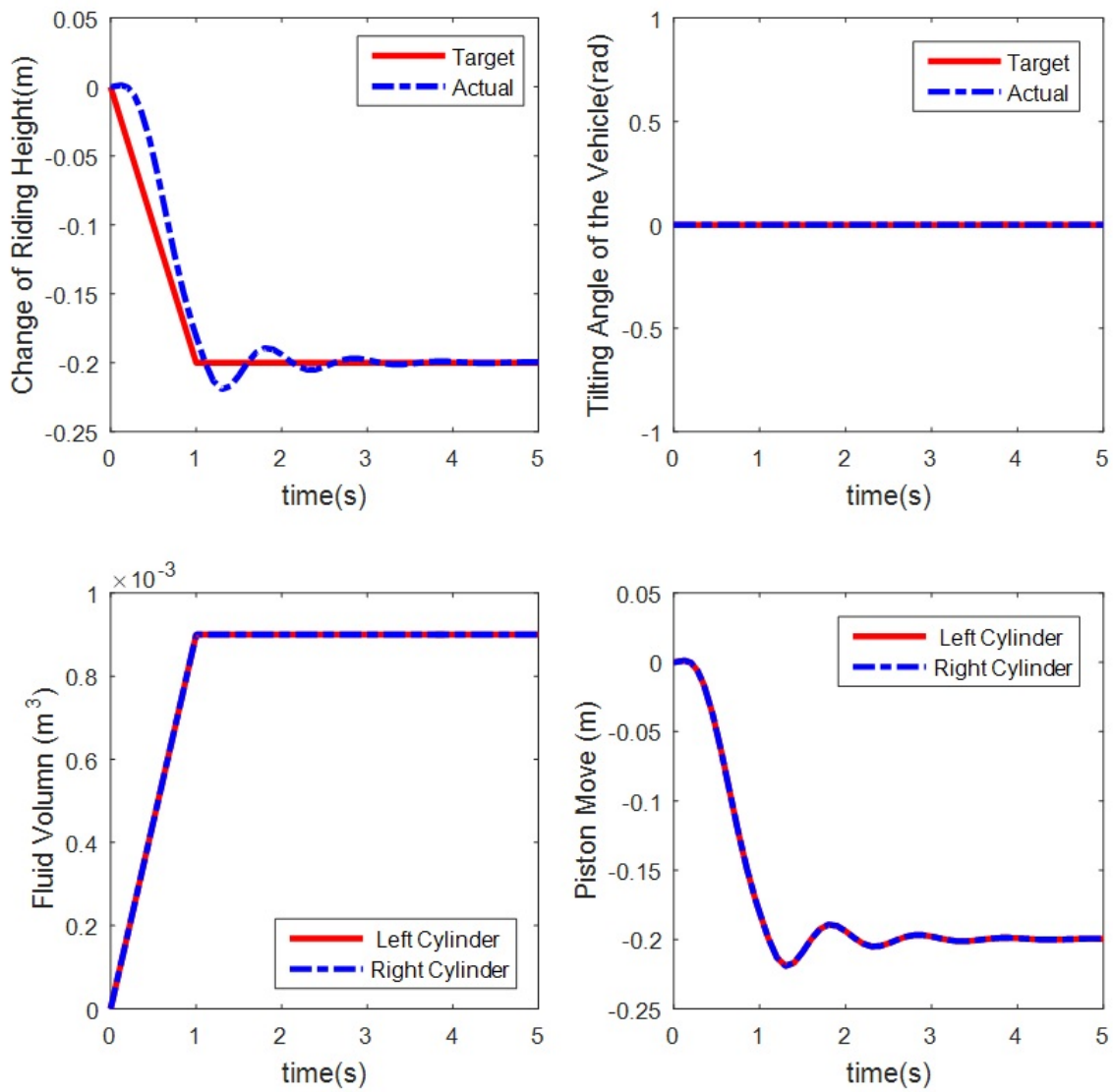
Figure 3.5: System Response for Height Adjustment

To evaluate the system capability for tilting the vehicle, the reference command is set to tilt the vehicle by 0.3 rad (18 deg) in 0.5 seconds. The quick response of the system is shown in Figure 3.6 along with the fluid being pumped and retrieved from both cylinders.
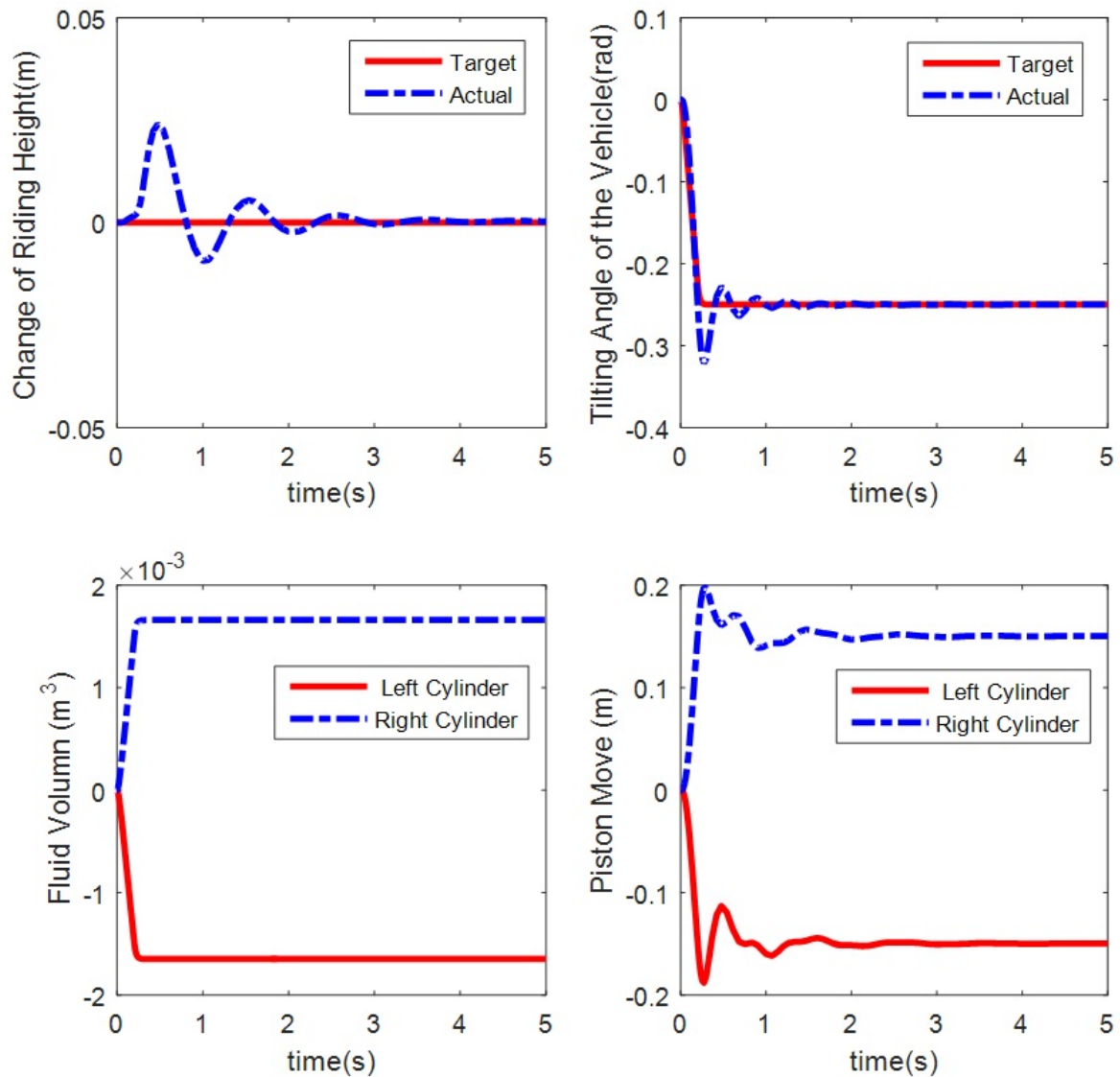
Figure 3.6: System Response for Tilting Angle Adjustment

3.5.2 Vehicle Simulation with Tilting Control

In this session, a three-wheeled tilting vehicle is modeled in the multi-body package MapleSim as shown in Figure 3.7 to demonstrate the feasibility of the proposed system on a full vehicle model under tilting control.
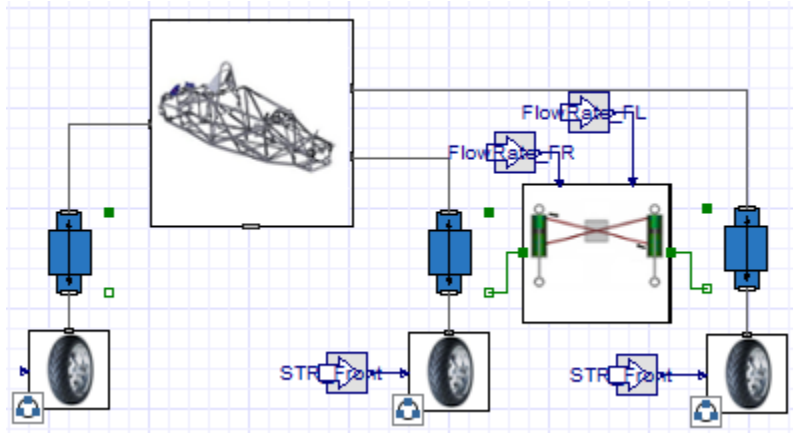
Figure 3.7: Modeling of a Three-wheeled NTV in MapleSim

The chassis is modeled as a rigid body with 6 DOFs, and the Magic Formula model [63] is adopted for the tire behavior considering camber effects. Suspensions mechanisms are simplified as a translational joint. The rear suspension is treated as a conventional strut using the linearized stiffness and damping characteristics, while the front axle with ISTS is modeled using the previously developed equations, which takes the motion states as inputs to calculate the strut forces.

The model is simulated for a cornering maneuver at the speed of 10m/s with a turning radius of 25m, which is considered a scenario for city driving at the crossroad. The trajectory of the vehicle and the steering wheel angle is shown in Figure 3.8.

(a) vehicle trajectory

(b) steering angle
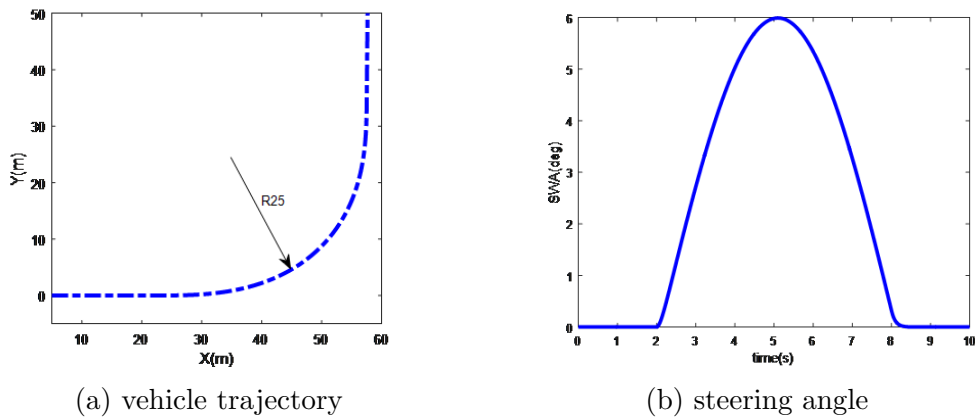
Figure 3.8: Steering Input and Vehicle Trajectory

Feed-Forward control is implemented for the feasibility study in this section. Based on the drivers steering signal, the steady-state lateral acceleration of the vehicle can be estimated [64] by,

$$a_{yss} = \frac{u^2}{a + b + K_{us}u^2}\delta \tag{3.28}$$

where, u is the longitudinal speed of the vehicle; K_{us} is the vehicle under-steer gradient; and δ is the steering angle on wheels.

As implemented in most tilting control algorithms [65][3], the desired tilting angle is calculated to balance the lateral acceleration using gravity as,

$$\phi = \arctan\left(a_{yss}/g\right) \tag{3.29}$$

Combining Eq.(3.28) and (3.29), the desired tilting angle can be determined directly from the drivers steering intention. Using the feed-forward tilting control algorithm discussed in Section 3.4.2, the required pump flow to track the desired tilting angle can then be calculated. The results for the above-mentioned cornering scenario are illustrated in Figure 3.9 and Figure 3.10.

Vehicle roll angle and rollover index [8] as performance measures are shown in Figure 3.9. It can be seen that, with the feed-forward controller, the vehicle tilts into the inner bend of the curve by about 15 degrees, while for the uncontrolled case, it rolls in the reverse direction. The uncontrolled case demonstrates a high rollover danger as indicated by the rollover index during cornering, while the proposed system shows its great potential to improve the rollover stability for the target vehicle. The maximum rollover index drops from 0.58 to 0.2 for the cornering maneuver. The required pump flow rate is shown in Figure 3.10.

(a) Roll Angle
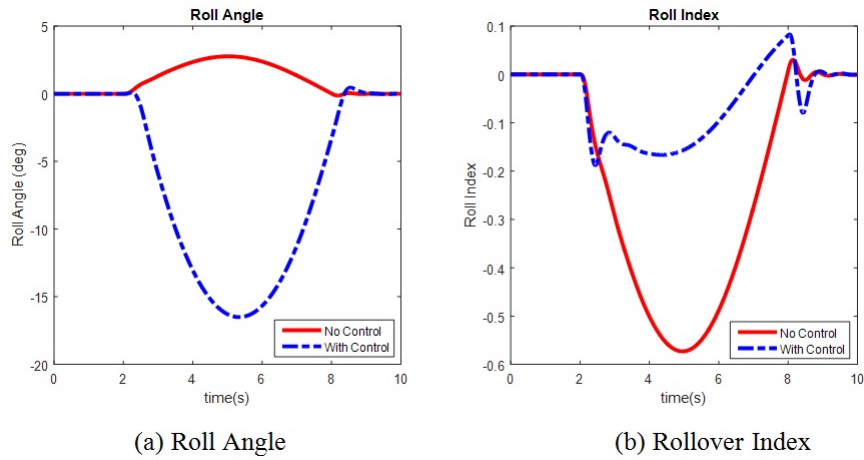
(b) Rollover Index

Figure 3.9: Vehicle Roll Angle and Rollover Index
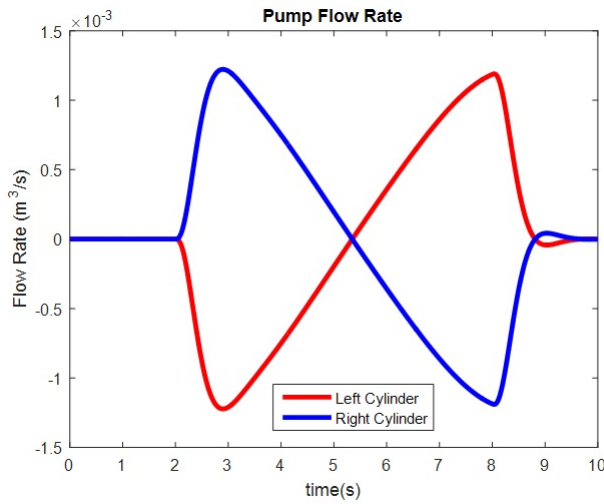
Figure 3.10: Pump Flow Rate for the Cornering Scenario

3.6 Conclusions

In this chapter, a novel Integrated Suspension Tilting System (ISTS) was proposed for narrow urban vehicles. By the adoption of interconnected hydraulic cylinders with the pump control, the system can achieve both functionalities of tilting and body height adjustments,

while satisfying the suspension requirements for comfort and stability. The system complexity, as well as the packaging size, was significantly reduced, which made it ideal for compact urban commuter vehicle applications. The proposed system in each working mode was illustrated, and its functionalities were explained with the operation of the valves and pumps. Detailed analysis demonstrated how the sizing of the components could achieve the desired bump and roll stiffness without introducing the anti-roll bar. The quasi-static fluid volume to be pumped into or out of the system to achieve the desired riding height and roll angle was also derived. Finally, a vehicle model equipped with the proposed ISTS demonstrated the feasibility of height and tilting control. Along with the more advanced controller to be developed in the following chapters, the system has the great potential to be used in narrow urban vehicles.

Chapter 4

Integrated Suspension Tilting System: Mechanism Design

The previous chapter introduced the ISTS with the widely-adopted vehicle roll plane model, in which the suspension mechanism is ignored, and struts are supposed to move vertically with respect to the cabin. This chapter proposes a proper suspension mechanism to work with the ISTS. After examining various automobile suspension mechanisms, the candidate mechanism is first identified to meet the compact packaging size requirements for urban titling cars. The kinematic and dynamic properties of the vehicle under large suspension travels during tilting are investigated. Different from the previous half-car model which neglects the longitudinal wheel movements, the full vehicle model with suspension mechanisms provides insights into the mechanism design for vehicle performances.

4.1   Challenges in Mechanism Design for NTV Applications

To understand the challenges in the suspension mechanism design, the requirements for suspension travel to fulfill the tilting task should be identified at the first place. Since the titling cars are expected to have the capability to perfectly balance the lateral acceleration [10, 66] during cornering, as shown in Figure 4.1(a).

$$\tan(\phi_x) = \frac{a_y}{g} \tag{4.1}$$

If the cabin is then virtually rotated back to the upright position as shown in Figure 4.1(b), the required wheel travel Δz from their nominal position to generate the tilting angle ϕ_x can be solved as,

$$\tan(\phi_x) = \frac{2\Delta z}{T_{w0}} \tag{4.2}$$
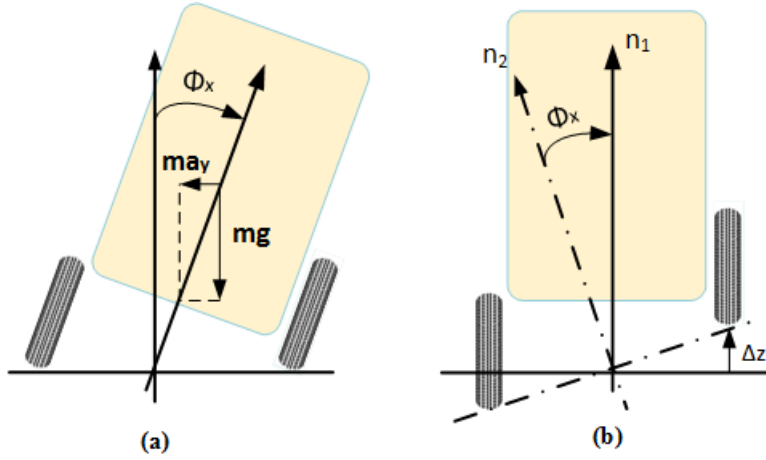
Figure 4.1: Suspension Travel and Tilting Angle

The relationship between the wheel travel and the acceleration balancing capacity of the vehicle can be derived by combining Eq.(4.1) and (4.2), as,

$$\Delta z = \frac{a_y}{g}\frac{T_{w0}}{2} \tag{4.3}$$

For an urban cornering scenario, assume the target vehicle is designed to perfectly balance itself during cornering at the speed of $u = 15km/h$ with a turning radius $R = 30m$, the steady-state lateral acceleration can be calculated as $a_y = u^2/R = 0.58g$. Substitute this value into Eq.(4.3) leads to the required tilting capability as $\phi_x = 30°$ and $\Delta z = 0.29m$. Since the road excitation can introduce extra wheel bump motions, a more practical requirement for the suspension mechanism design is to allow a vertical wheel displacement of $\Delta z = 0.35m$ from their nominal position.

Conventional suspension mechanisms are not designed to meet such specifications, and for narrow urban vehicle applications, the desired mechanism also have to remain compact

to leave enough spaces for passengers and cargo. After identifying the candidate mechanisms with the packaging size constraints, the suspension kinematics under large wheel bump motions will be analyzed in detail.

4.2   Suspension Mechanism for NTVs

This section starts examining proper suspension mechanisms for NTVs with the requirements on the system compactness in addition to the large suspension travel for tilting.

The independent suspensions that can generate pure translational motions are first examined. Sliding pillar suspension [67] was one of the solutions, which could realize the required suspension travel in a compact manner. However, the bending moment and the resulting friction forces in the guidance rail made the manufacturing and maintenance of such a mechanism very difficult. There are also linear mechanisms discussed in the literature [68, 69, 70], which generate pure bump motion, but their drawbacks are the system complexity (which requires 6 to 8 linkages), and size.

Apart from the mechanisms which generate a purely translational motion in the vertical direction, the auto industry has widely adopted the wishbone-type and trailing-arm-type mechanisms, which allows the unsprung mass to move laterally or longitudinally as it bumps. Such mechanisms are much easier to be manufactured and maintained. The multi-link [71] and double wishbone [72] mechanism, as examples of the wishbone-type mechanisms, provide a better motion control at the cost of a complex structure. More importantly, the lateral space required to generate the desired suspension stroke does not fit in the limited lateral footprint of narrow vehicles. Trailing arm mechanism [67] seems to provide a right balance between simplicity and performance. The structure is simple, cost-effective, and easy to maintain compared to the above-mentioned mechanisms which makes it quite suitable for narrow vehicle applications. Apart from that, the mechanism only sits on the side of the narrow cabin which leaves more space for passengers and cargo. The proposed ISTS can be mounted as the suspension strut connecting the trailing-arm and the chassis.

The difficulty that could hinder the successful application of the trailing-arm mechanism on NTVs is the longitudinal wheel movement during tilting. This effect has not been well studied in conventional vehicles due to the small magnitudes of wheel longitudinal movements on non-tilting vehicles. For example, the widely-adopted roll plane analysis as shown in Figure 4.1 does not consider the wheel motion in the longitudinal plane.

A schematic drawing in Figure 4.2 illustrates the longitudinal wheel travel with a

trailing-arm structure. The relationship between the longitudinal movement Δx and vertical movement of the wheel Δz can be written as,

$$\Delta x = L_{Arm} - \sqrt{L_{Arm}^2 - \Delta z^2} \tag{4.4}$$

where, L_{Arm} is the length of the trailing arm.
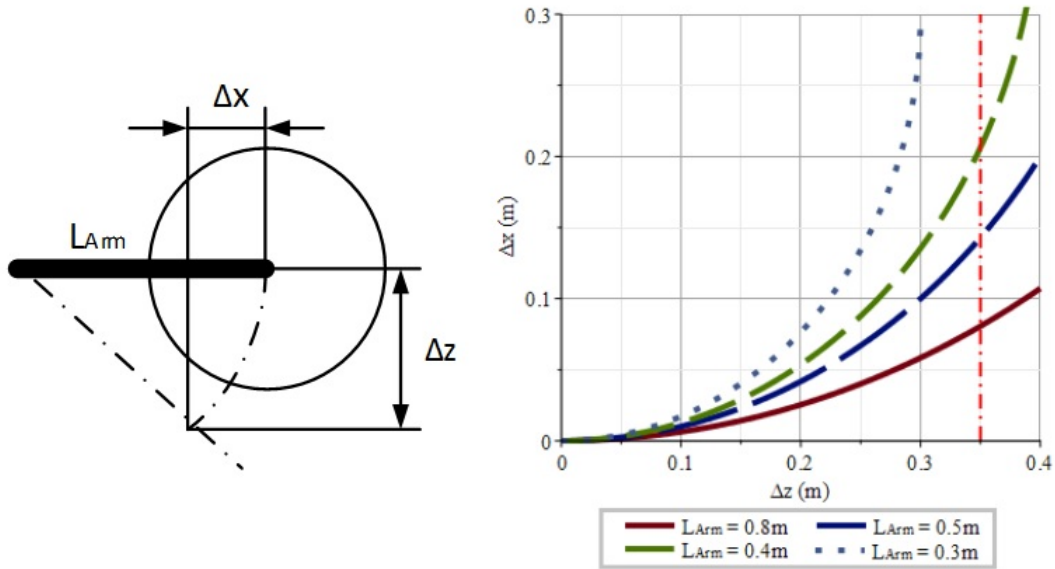
Figure 4.2: Longitudinal Movement of the Wheel

Several candidate lengths of the trailing arm are chosen to visualize Eq.(4.4) in Figure 4.2. The vertical line in red indicates the demand for vertical wheel movement as calculated in Section 4.1. A short arm (e.g., $L_{Arm} = 0.3m$) is incapable of generating the required suspension stoke, while a long arm (e.g., $L_{Arm} = 0.8m$) is restricted by the structural stiffness and the vehicle wheelbase. According to Figure 4.2, a rough estimation of longitudinal wheel movement is found to be around $0.10 - 0.25m$.

Conventional automobile suspension mechanisms will hardly see such longitudinal wheel movements. Their impact on tilting vehicle performances will be analyzed in the next section. The analytical results could be used towards the design of a trailing-arm mechanism for tilting vehicle applications.

4.3 Tilting Vehicles with Wheelbase Variation

4.3.1 Roll Angle Analysis

As illustrated in Figure 4.1, the asynchronous motion of the wheels can generate the vehicle tilting motion. However, the previous analysis does not consider the character of the suspension mechanism. More concretely, the longitudinal wheel movements shown in Figure 4.2 as a consequence of wheel bump motion is ignored. In this section, a three-dimensional vehicle model with suspension kinematics is adopted for tilting analysis.

A tadpole-configured NTV with the trailing arm mechanism is shown in Figure 4.3. The idea demonstrated in Figure 4.1 is applied in this section for the three-dimensional roll kinematics analysis. Instead of analyzing the vehicle in a tilted position as Figure 4.1(a), it would be much easier to visualize the wheel movement with an upright cabin as shown in Figure 4.1(b). The ground plane is then defined by the three contact points on wheels. By comparing the normal direction of the contact plane and that of the horizontal ground plane, the vehicle rotation as a consequence of wheel movement can then be analyzed.
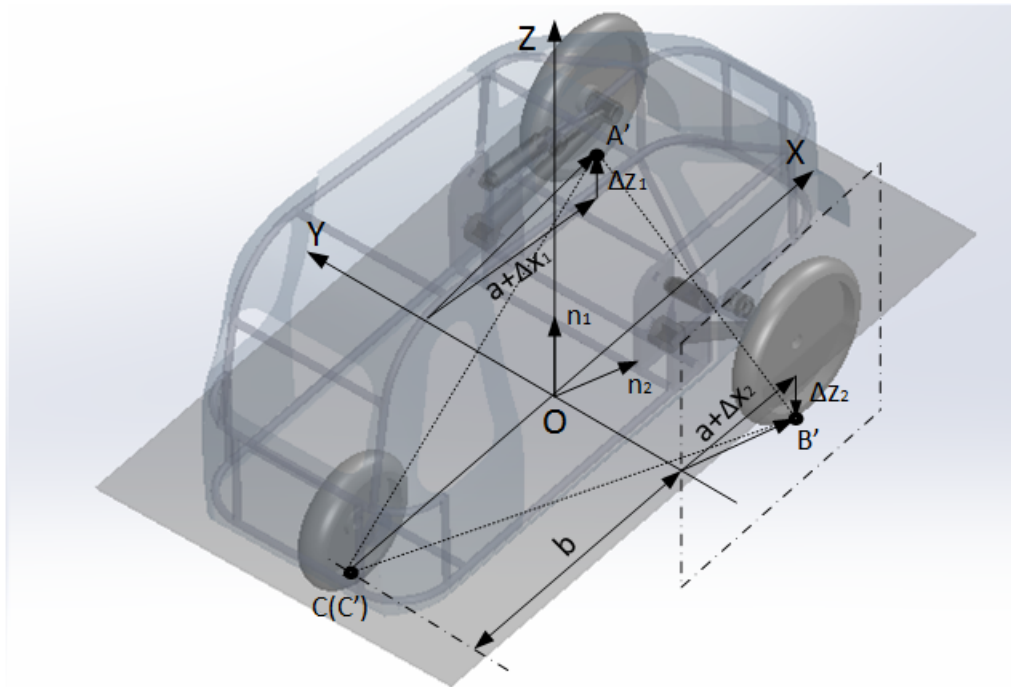
Figure 4.3: Kinematic Analysis of the Trailing Arm Mechanism

The global coordinate system $OXYZ$ is fixed to the ground with OZ axis points upward. The un-tilted pose of the vehicle can be defined with OXZ plane be the symmetrical plane of the vehicle; OX axis points at the forward direction; OZ axis goes through the vehicle center of gravity (CoG) and points upward. As described, the cabin pose remains unchanged during the kinematic analysis; however, the wheels can move from their nominal position to generate the tilting. The contact points are assumed at the bottom of the wheels. Points A, B, C denote the nominal contact points for the front-left, front-right, and rear wheel, while A', B', C' denotes their new positions after the wheel movement. The normal directions of the contact planes are denoted as $\hat{n}_1$ and $\hat{n}_2$ accordingly.

The position vectors of the nominal contact points in the global $OXYZ$ system can be written as,

$$\begin{aligned}
\overrightarrow{OA} &= \left[\begin{array}{ccc} a & +\frac{T_{w0}}{2} & 0 \end{array}\right]^T \\
\overrightarrow{OB} &= \left[\begin{array}{ccc} a & -\frac{T_{w0}}{2} & 0 \end{array}\right]^T \\
\overrightarrow{OC} &= \left[\begin{array}{ccc} -b & 0 & 0 \end{array}\right]^T
\end{aligned} \tag{4.5}$$

Since all contact points are located on the ground plane at their nominal position, the normal direction $\hat{n}_1$ is,

$$\hat{n}_1 = \left[\begin{array}{ccc} 0 & 0 & 1 \end{array}\right]^T \tag{4.6}$$

For a general tilting scenario, Δz_1 and Δz_2 are applied respectively as the vertical displacements of the two front wheels. Since the wheels are constrained by the trailing arm mechanism, no lateral displacement is produced, but both wheels move Δx_1 and Δx_2 respectively in the longitudinal direction. The global position vectors of the new contact points are written as,

$$\begin{aligned}
\overrightarrow{OA'} &= \overrightarrow{OA} + \left[\begin{array}{ccc} \Delta x_1 & 0 & \Delta z_1 \end{array}\right]^T \\
\overrightarrow{OB'} &= \overrightarrow{OB} + \left[\begin{array}{ccc} \Delta x_2 & 0 & \Delta z_2 \end{array}\right]^T \\
\overrightarrow{OC'} &= \overrightarrow{OC}
\end{aligned} \tag{4.7}$$

The normal direction of the new contact plane $A'B'C'$ as shown in Figure 4.3 can be represented as,

41

$$\hat{n}_2 = \frac{\overrightarrow{C'B'} \times \overrightarrow{C'A'}}{|\overrightarrow{C'B'}||\overrightarrow{C'A'}|} = \frac{1}{\sqrt{n_{21}^2 + n_{22}^2 + n_{23}^2}} \begin{bmatrix} n_{21} \\ n_{22} \\ n_{23} \end{bmatrix} \tag{4.8}$$

where, n_{21}, n_{22}, n_{23} are the vector components of the cross product $\overrightarrow{C'B'} \times \overrightarrow{C'A'}$:

$$\begin{aligned} n_{21} &= -\tfrac{T_{w0}}{2}\left(\Delta z_1 + \Delta z_2\right) \\ n_{22} &= -\left(a + b + \Delta x_2\right)\Delta z_1 + \left(a + b + \Delta x_1\right)\Delta z_2 \\ n_{23} &= \tfrac{T_{w0}}{2}\left(2a + 2b + \Delta x_1 + \Delta x_2\right) \end{aligned} \tag{4.9}$$

The vehicle rotation ϕ, as demonstrated in Figure 4.1, is nothing but the angle between normal vectors of the contact planes, which can be solved by referring Eq.(4.6) and (4.8):

$$\phi = \arccos\left(\hat{n}_1 \cdot \hat{n}_2\right) = \arctan\left(\sqrt{\frac{n_{21}^2 + n_{22}^2}{n_{23}^2}}\right) \tag{4.10}$$

The instantaneous rotation axis $\hat{e}_r$ is determined by the cross product of the normal vectors:

$$\hat{e}_r = \hat{n}_2 \times \hat{n}_1 = \frac{1}{\sqrt{n_{21}^2 + n_{22}^2 + n_{23}^2}} \begin{bmatrix} n_{22} \\ -n_{21} \\ 0 \end{bmatrix} \tag{4.11}$$

It is shown in Eq.(4.11) that the rotation axis has zero component in the global coordinate system, which indicates no yaw motion can be generated by arbitrary movement of trailing arms. The projected rotation on the OX and OY axis can be interpreted as the tilting motion and pitch motion respectively. To eliminate the undesired pitch, the term n_{21} in Eq.(4.11) has to be zero. From Eq.(4.9), this leads to,

$$\Delta z_1 + \Delta z_2 = 0 \tag{4.12}$$

The condition shown in Eq.(4.12) suggests that to generate a pure tilting motion without pitch, the two wheels should move in reversed directions but of the same magnitude (asynchronous mode), just as shown in the 2D roll plane model in Figure 4.1. This also agrees with the intuition that any synchronous wheel movements will change the cabin height at the front axle and finally generate pitch motion of the vehicle.

Substituting Eq.(4.9) into (4.10), the tilting angle ϕ can be written as:

$$\phi = \arctan \left(\sqrt{\frac{\left(\frac{T_{w0}}{2}\right)^2 (\Delta z_1 + \Delta z_2)^2 + \left((a+b)(\Delta z_2 - \Delta z_1) + \Delta x_1 \Delta z_2 - \Delta x_2 \Delta z_1\right)^2}{\left(\frac{T_{w0}}{2}\right)^2 (2a + 2b + \Delta x_1 + \Delta x_2)^2}} \right) \tag{4.13}$$

If the pure tilting condition derived in Eq.(4.12) is considered, the tilting angle as a particular case of Eq.(4.13) is solved by:

$$\phi_x = \phi \Big|_{\substack{\Delta z_1 = +\Delta z \\ \Delta z_2 = -\Delta z}} = \arctan\left(\frac{2\Delta z}{T_{w0}}\right) \tag{4.14}$$

Under a pure-tilting condition, as suggested by Eq.(4.2) and (4.14), the longitudinal movement of the wheels will not affect the tilting angle. Its value is the same as the one calculated by using the 2D roll plane model, which neglects the longitudinal movement of the wheels. However, once the no-pitch condition Eq.(4.12) does not hold, it has been demonstrated that both tilting and pitch angle will be produced, and the general rotation angle should be solved from Eq.(4.13). Under those circumstances, both longitudinal and vertical movement of the wheels can affect the final tilting angle.

4.3.2 Rollover Index Analysis

Apart from changing the tilting angle of the vehicle, the longitudinal movements of the wheels also affect the normal force distributions due to the contact patch movements, which might degrade vehicle roll stability. In this section, the rollover index [73] as the stability measure is adopted to analyze the impact of wheel movements on vehicle rollover stability. The model for force analyze of a tadpole NTV is illustrated in Figure 4.4. The vehicle is placed in the quasi-static position with a tilting angle ϕ_x and is assumed to be experiencing positive longitudinal and lateral accelerations, with the inertia forces applied at CoG. To balance the positive lateral acceleration, the vehicle needs to tilt to the left, so the left wheel will be lifted while the right wheel should be lowered down as discussed.
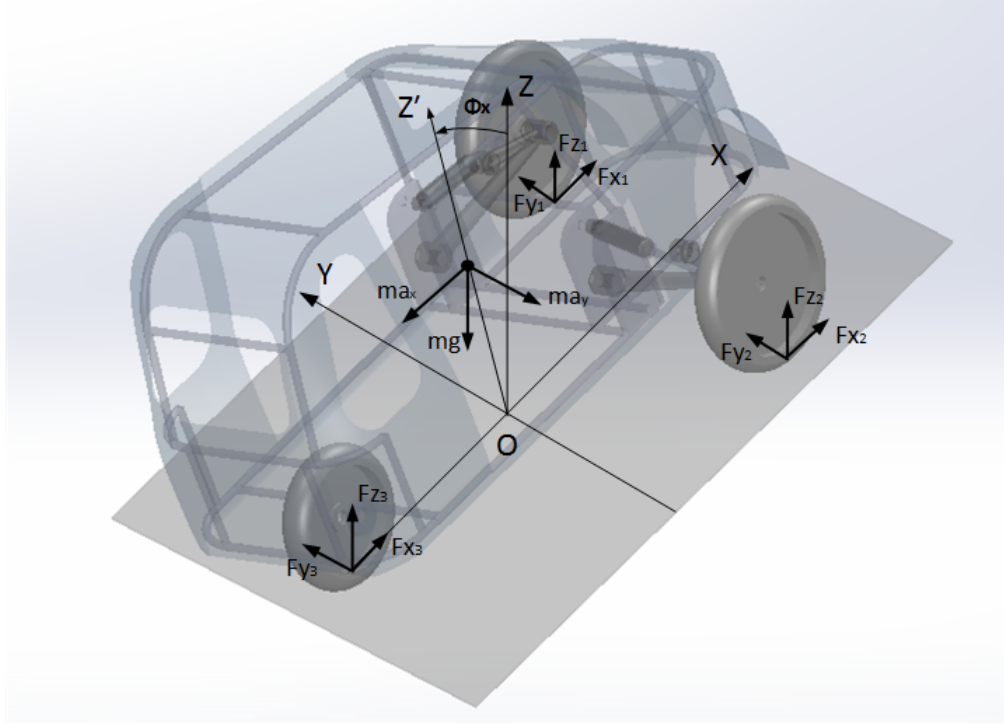
Figure 4.4: Force Analysis of the Vehicle in Tilting Motion

Using D'Alembert's principle, the force balance equation considering tilting and longitudinal wheel movements can be written as:

$$\begin{cases} F_{z1} + F_{z2} + F_{z3} = mg \\ mgh_0 \sin(\phi_x) + ma_y h_0 \cos(\phi_x) + (F_{z1} - F_{z2})\frac{T_w}{2} = 0 \\ ma_x h_0 \cos(\phi_x) + F_{z1}(a + \Delta x_1) + F_{z2}(a + \Delta x_2) - F_{z3}(b) = 0 \end{cases} \quad (4.15)$$

The normal force on each tire in steady-state can then be solved from Eq.(4.15), as:

$$\begin{cases} F_{z1} = \frac{b}{2l}mg - \frac{mh}{2l}a_x - \frac{l_0 + \Delta x_2}{l}\frac{mh}{T_{w0}}a_{ynb} \\ F_{z2} = \frac{b}{2l}mg - \frac{mh}{2l}a_x + \frac{l_0 + \Delta x_1}{l}\frac{mh}{T_{w0}}a_{ynb} \\ F_{z3} = \frac{a + (\Delta x_1 + \Delta x_2)/2}{l}mg + \frac{mh}{l}a_x - \frac{\Delta x_1 - \Delta x_2}{l}\frac{mh}{T_{w0}}a_{ynb} \end{cases} \quad (4.16)$$

where,

44

l is the wheelbase considering the longitudinal movement of the wheels, as:

$$l = l_0 + \frac{\Delta x_1 + \Delta x_2}{2} \qquad (4.17)$$

a_{ynb} is the unbalanced lateral acceleration by subtracting the gravity balanced terms:

$$a_{ynb} = a_y \cos{(\phi_x)} + g sin{(\phi_x)} \qquad (4.18)$$

It is confirmed in Eq.(4.16) that the normal force on each tire can be affected by lateral and longitudinal accelerations, as well as wheel movements. The effects of a_x and a_y on normal force changes are referred to as longitudinal and lateral load transfer, respectively [8]. When either of the normal forces at the front axle reaches zero, it indicates the rollover danger. Rollover index [8, 74] is adopted as a measure of the roll stability of the vehicle. By considering the solved normal force expressions in Eq.(4.16), the rollover index (RI) for a tadpole NTV with longitudinal wheel moves can be written as,

$$RI \triangleq \frac{F_{z1} - F_{z2}}{F_{z1} + F_{z2}} = \frac{(\Delta x_1 + \Delta x_2)/2 + l_0}{-(\Delta x_1 - \Delta x_2)/2 + p} \qquad (4.19)$$

where p is the parameter defined as:

$$p = \frac{1}{2} \frac{\frac{a_x}{g} h - b}{\frac{a_{ynb}}{g} \frac{h}{T_{w0}}} \qquad (4.20)$$

Compared with the definition of classical rollover index, the derived RI explicitly considers the effect of longitudinal wheel movements on vehicle roll stability. The classical rollover index expression can be treated as a special case of the derived form as shown in Eq.(4.19) with $\Delta x_1 = \Delta x_2 = 0$.

By observing Eq.(4.18) and (4.20), for a vehicle that does not over-lean [74]:

$$sign{(p)} = -sign(a_y) \qquad (4.21)$$

4.3.3 Preferred Longitudinal Wheel Motion

It can be seen from Eq.(4.19) that both the synchronous and asynchronous longitudinal motion of the wheels can affect the vehicle roll stability. For a vehicle about to rollover,

the absolute value of the rollover index is close to one. A practical bound of the parameter p for non-tipping vehicles is $|p| \geq l_0$. Since magnitudes of wheel longitudinal movements $(\Delta x_1, \ \Delta x_2)$ should be less than the nominal wheelbase l_0, the signs of the nominator and denominator for the rollover index in Eq.(4.19) are determined as,

$$\begin{cases} sign\left((\Delta x_1 + \Delta x_2)/2 + l_0\right) = sign\left(l_0\right) > 0 \\ sign\left(-(\Delta x_1 - \Delta x_2)/2 + p\right) = sign\left(p\right) = -sign(a_y) \end{cases} \tag{4.22}$$

By the above observation of the general rollover index expression with wheel longitudinal movements, a necessary condition for Δx_1 and Δx_2 to improve the vehicle roll stability by minimizing the magnitude of Eq.(4.19), is,

$$\begin{cases} \Delta x_1 + \Delta x_2 \leq 0 \\ sign(a_y)\left(\Delta x_1 - \Delta x_2\right) \geq 0 \end{cases} \tag{4.23}$$

Since a_y always points towards the inner bend of the curve, if the front two wheels are denoted as inner and outer wheels respectively, Eq.(4.23) can be simplified as,

$$\begin{cases} \Delta x_{in} + \Delta x_{out} \leq 0 \\ \Delta x_{in} - \Delta x_{out} \geq 0 \end{cases} \quad \Leftrightarrow \quad \begin{cases} \Delta x_{out} \leq 0 \\ |\Delta x_{in}| \leq -\Delta x_{out} \end{cases} \tag{4.24}$$

where, Δx_{in} and Δx_{out} denotes the wheel longitudinal movement on inner- and outer- side respectively.

This necessary condition is also visualized in Figure 4.5. In order to realize the preferred wheel longitudinal movement and improve the rollover stability during tilting, the outer-wheel is expected to move backward, while the inner-wheel is free to move in both forward and backward directions, with the magnitude bounded by that of the outer wheel.
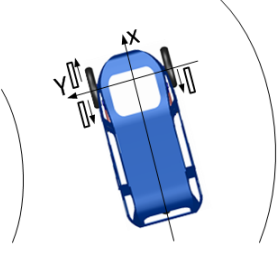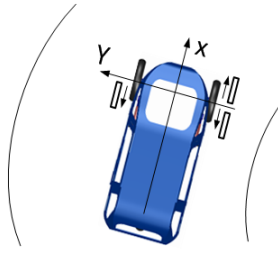
$RI = \dfrac{(\Delta x_1 + \Delta x_2)/2 + l_0}{-(\Delta x_1 - \Delta x_2)/2 + p}$	$a_y > 0$	$a_y < 0$
$\Delta x_{out} \leq 0$ $\left\| \Delta x_{in} \right\| \leq -\Delta x_{out}$		

Figure 4.5: Preferred Wheel Longitudinal Motion for Vehicle Roll Stability Improvement

4.4 Design Example

From the kinematic and dynamic analysis in the previous section, it has been shown that longitudinal displacements of the trailing arm mechanism can be beneficial to vehicle roll stability, if the suspension arm is properly designed. This section demonstrates a design example by utilizing the previous analytical results.

A schematic drawing of the mechanism at the nominal position is shown in Figure 4.6. Point D represents the hinge of the trailing arm on the chassis and is chosen as the origin of the local coordinate system for the mechanism design. The wheel is connected to the trailing arm at Point G. Point E and F are the mounting points of the actuator on chassis and arm respectively. All angles are measured in counter-clockwise directions. Since the mechanism has only one degree of freedom, the generalized coordinate is chosen as the actuator length l_{EF}, and the resultant rotation of the arm is denoted as φ.
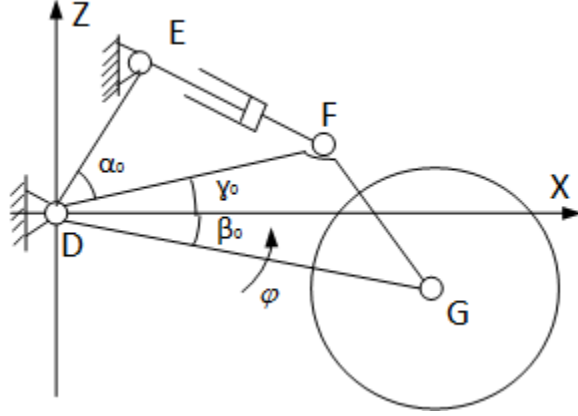
Figure 4.6: Schematic Drawing of the Trailing Arm Mechanism

The design variables of the above mechanism are identified as:
1. l_{EF0} - the initial length of the actuator at the nominal position;
2. l_{ED} - the distance between the mounting point E and D on chassis;
3. l_{FD} - the distance between the actuation point F and the hinge point D;
4. l_{GD} - the distance between wheel connection point G and the hinge point D;
5. γ_0 - the initial angle of Line FD with respect to the horizontal direction;
6. β_0 - the initial angle of Line GD with respect to the horizontal direction.

From the geometry shown in Figure 4.6, the actuator length change can be solved as:

$$\Delta l = l_{EF} - l_{EF0} = \sqrt{l_{ED}^2 + l_{FD}^2 - 2l_{ED}l_{FD}\cos\left(\alpha_0 - \varphi\right)} - l_{EF0} \qquad (4.25)$$

where, α_0 is the angle between line ED and FD as shown at the nominal position:

$$\cos\left(\alpha_0\right) = \frac{l_{ED}^2 + l_{FD}^2 - l_{EF0}^2}{2l_{ED}l_{FD}} \qquad (4.26)$$

The wheel center movement in the vertical direction can be solved as:

$$\Delta z = z_G - z_{G0} = l_{GD}\sin\left(\beta_0 + \varphi\right) - l_{GD}\sin\beta_0 \qquad (4.27)$$

where, z_{G0} is the nominal vertical position of wheel center.

Combining Eq.(4.25) and (4.27), the relationship between vertical wheel displacement and actuator length change can be written as:

$$\Delta z = l_{GD} \cos\left(\beta_0\right) \sin\left(\alpha_0 - arccos\frac{l_{ED}{}^2 + l_{FD}{}^2 - (\Delta l + l_{EF0})^2}{2l_{ED}l_{FD}}\right) +$$
$$+ l_{GD} \sin\left(\beta_0\right) \left[\cos\left(\alpha_0 - arccos\frac{l_{ED}{}^2 + l_{FD}{}^2 - (\Delta l + l_{EF0})^2}{2l_{ED}l_{FD}}\right) - 1\right] \tag{4.28}$$

According to the desired tilting capability, the required wheel travel Δz_{req} can be solved from Eq.(4.14). Denote the wheel center positions under the limiting conditions as z_{max} and z_{min}:

$$\begin{cases} z_{\max} = z_{G0} + \Delta z_{\text{req}} \\ z_{\min} = z_{G0} - \Delta z_{\text{req}} \end{cases} \tag{4.29}$$

By adopting the monotonic relationship between Δl and φ during the working range, the actuator length changes at limiting positions are solved from Eq.(4.25) as:

$$\begin{cases} \Delta l_{\max} = \Delta l|_{\varphi=\varphi_{\min}} = \sqrt{l_{ED}{}^2 + l_{FD}{}^2 - 2l_{ED}l_{FD}\cos\left(\alpha_0 - \varphi_{\min}\right)} - l_{EF0} \\ \Delta l_{\min} = \Delta l|_{\varphi=\varphi_{\max}} = \sqrt{l_{ED}{}^2 + l_{FD}{}^2 - 2l_{ED}l_{FD}\cos\left(\alpha_0 - \varphi_{\max}\right)} - l_{EF0} \end{cases} \tag{4.30}$$

where φ_{min}, φ_{max} are also solved by the monotonic relationship between Δl and φ from Eq.(4.27):

$$\begin{cases} \varphi_{max} = \varphi|_{z=z_{\max}} = \arcsin\left(+\frac{\Delta z_{\text{req}}}{l_{GD}} + sin\beta_0\right) - \beta_0 \\ \varphi_{min} = \varphi|_{z=z_{\min}} = \arcsin\left(-\frac{\Delta z_{\text{req}}}{l_{GD}} + sin\beta_0\right) - \beta_0 \end{cases} \tag{4.31}$$

Since the motion of the wheel center is constrained by the trailing arm, the coordinate x_G is solved by:

$$x_G = \sqrt{l_{GD}^2 - z_G^2} \tag{4.32}$$

The inner wheel is lifted while the outer one is lowered during cornering. The longitudinal displacements of the inner and outer wheels can be calculated by using Eq.(4.32), as:

$$\begin{cases} \Delta x_{in} = \sqrt{l_{GD}^2 - (z_{G0} + \Delta z)^2} - \sqrt{l_{GD}^2 - z_{G0}^2} \\ \Delta x_{out} = \sqrt{l_{GD}^2 - (z_{G0} - \Delta z)^2} - \sqrt{l_{GD}^2 - z_{G0}^2} \end{cases} \tag{4.33}$$

To form the optimization problem, the following constraints are considered:

1. A necessary condition for longitudinal wheel movement to be constructive is that the Eq.(4.24) should be satisfied. By substituting Eq.(4.33) into (4.24) this leads to,

$$\beta_0 \leq 0 \tag{4.34}$$

2. The mechanism should allow the wheel to travel vertically in both directions to generate the desired tilting angle. At upper limits, Point F should avoid in line with ED to circumvent the dead point; while at the lower limit position, Point G is expected to be in the right half of the XZ plane.

$$\varphi_{max} < \alpha_0 \tag{4.35}$$

$$\varphi_{min} + \beta_0 > -\frac{\pi}{2} \tag{4.36}$$

3. To make the system compact in the longitudinal direction, Point E is desired to be in the right half of the XZ plane. For compactness in the lateral direction, the actuator and the trailing-arm are expected to sit in the same plane to leave more space for the cabin. To achieve this without interference, Point F should be placed above Line DG.

$$\beta_0 \leq \gamma_0 \leq \frac{\pi}{2} - \alpha_0 \tag{4.37}$$

4. The suspension ratio, which is defined as vertical wheel displacement Δz over actuator length increment Δl, is specified at the nominal working position as,

$$K_{des} - \varepsilon_K \leq \lim_{\Delta l \to 0} \frac{\Delta z}{\Delta l} \leq K_{des} + \varepsilon_K \tag{4.38}$$

where, K_{des} is the desired suspension ratio [75]; ε_K is the tolerance for the ratio.

5. The stroke length of the actuator is limited by its minimum length, as,

$$l_{EF\max} - l_{EF\min} \le l_{EF\min} + \varepsilon_L \tag{4.39}$$

where, l_{EFmax}, l_{EFmin} are the maximum and minimum length of the actuator which can be solved from Eq.(4.30); ε_L is the required minimum length to assemble the actuator.

6. To avoid interference between the cabin and the ground during tilting, it requires,

$$z_{\max} \le R_W - \varepsilon_H \tag{4.40}$$

where, R_W is the radius of the wheel; ε_H is the height clearance.

7. The lower and upper bounds of the design variables are considered:

$$
\begin{aligned}
&l_{ED}, l_{FD}, l_{GD} \in [100, 650], l_{EF0} \in [300, 600] \\
&\gamma_0 \in [-90°, 90°], \beta_0 \in [-90°, 0°]
\end{aligned} \tag{4.41}
$$

The following optimization targets are considered,

1. The length of the actuator, as well as the trailing arm, should be minimized to reduce the system weight as well as improving the stiffness of the whole structure,

$$J_1 = \max(l_{FD}, l_{GD}) + l_{EF0} \tag{4.42}$$

2. Although the suspension ratio around the nominal working point is formulated as a constraint, it is still desired that, over the whole actuator stroke, the specified ratio is maintained in a linear fashion, as,

$$J_2 = \int_{\Delta l_{\min}}^{\Delta l_{\max}} (\Delta z - K_{des}\Delta l) \, dl \tag{4.43}$$

According to the above description of the design variables, constraints, and the cost functions, the optimal design problem can be formulated as,

$$
\begin{aligned}
\min_{v} : \quad & J(v) = wJ_1(v) + J_2(v) \\
\text{s.t.} \quad & f_i(v) \le 0 \\
& v = [l_{EF0}, l_{ED}, l_{FD}, l_{GD}, \gamma_0, \beta_0]^T
\end{aligned} \tag{4.44}
$$

where, w is the weighting factor; $J_1(v)$ and $J_2(v)$ are the cost functions defined in Eq.(4.42) and (4.43) respectively; $f_i(v)$ are the constraints given in Eq.(4.34)-(4.41).

The initial values for design variables and parameters are chosen as Table 4.1.

Parameter	Description	Value	Unit
K_{des}	Desired suspension ratio	3.33	−
R_W	Wheel Radius	300	mm
ε_K	Suspension ratio tolerance	0.15	−
ε_L	Minimum actuator length for assembly	80	mm
ε_H	Height clearance	100	mm
w	Weighing factor	100	−

Table 4.1: Parameters for the Trailing Arm Mechanism

The interior-point method implemented in Matlab is adopted for solving the optimization problem Eq.(4.44). The tolerance is set to be 1e-6, and the package returns the optimal solution listed in Table 4.2 after 30 iterations.

Design Variable	Initial Value	Optimized Value	Unit
l_{EF0}	380	403	mm
l_{ED}	300	153	mm
l_{FD}	500	368	mm
l_{GD}	600	502	mm
γ_0	50	-9.6	deg
β_0	-10	-17.4	deg

Table 4.2: Design Variables for the for the Trailing Arm Mechanism

The designed mechanism with the vehicle frame is shown in Figure 4.7. It can be seen that, due to the adoption of the trailing arm structure, much of the space in the front trunk of the vehicle is saved for cargo and vehicle equipment. The vehicle in tilting mode is also illustrated with the trailing arm mechanism in Figure 4.8.
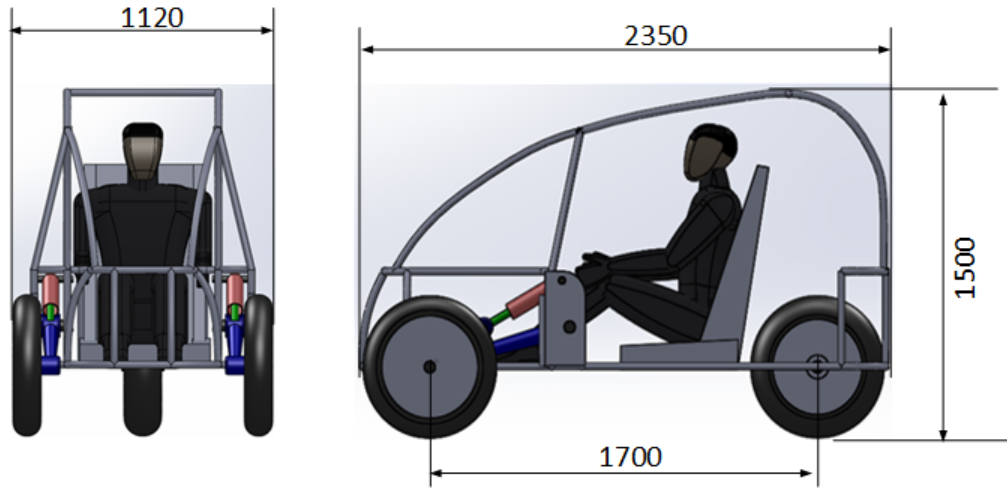
Figure 4.7: Designed NTV in Nominal Position
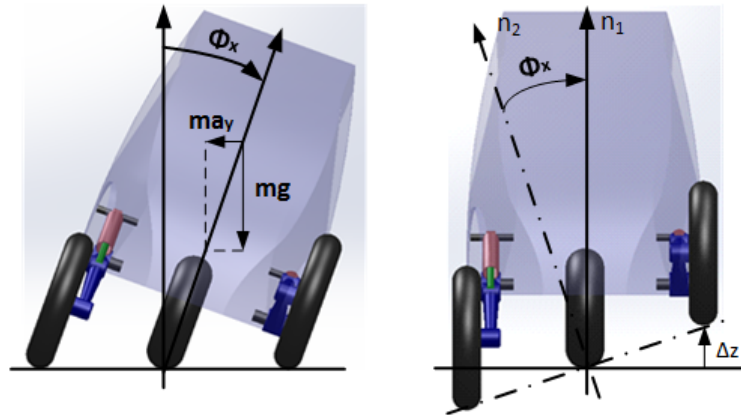
Figure 4.8: Designed NTV in Tilting Mode

4.5   Vehicle Simulation

To confirm the vehicle roll stability is not impaired by the trailing arm design, a tilting three-wheeled vehicle is simulated by using the MapleCar [76] toolbox developed in MapleSim. The topology of the multi-body model of the full tilting vehicle is shown in Figure 4.9. Two suspension mechanisms are considered for this comparison. One is the

designed trailing-arm structure (Figure 4.9(a)), and the other is the sliding pillar mechanism (Figure 4.9(b)) with the same nominal track width. The trailing-arm mechanism is expected to demonstrate the preferred wheel movement pattern as specified during the optimization, while the sliding pillar one is known to generate pure vertical suspension movement without introducing any longitudinal wheel movements.

All bodies in the model are assumed to be rigid, and the motorcycle Magic Formula tire model [63] is adopted. The chassis of the vehicle has 6 degrees of freedom with respect to the inertial system. The rear wheel is steerable and can spin relative to the chassis frame. The front suspension with the sliding pillar mechanism is modeled using two translational joints which can only move in the vertical direction, while the rotational angle of the trailing arm mechanism is determined by changing the length of the actuator. Steering and driving torques are applied so that the vehicle maintains the desired speed $15m/s$ while entering a curve of $60m$ radius from a straight lane.

The vehicle rollover index performance under the same tilting angle but implemented by different suspension mechanisms are shown in Figure 4.10. For the desired traveling speed on the given circular track, the lateral acceleration in steady-state can be estimated, and the tilting angle to eliminate the lateral load transfer can be calculated using Eq.(4.2) as around 21.3 degrees. If the desired angle is successfully tracked, there will be no lateral load transfer, and the rollover index will remain zero for any suspension mechanism designs. However, if that cannot be achieved due to either tilting angle limitations or energy consumption concerns, the benefits of the suggested design can be demonstrated. In Figure 4.10(a), the vehicle is only tilting for 10 degrees. It can be seen that the magnitude of the rollover index is reduced using the proposed trailing-arm design. The same trend is shown in Figure 4.10(b) when the applied tilting angle is 20 degrees. However, as the vehicle is approaching the ideal angle with zero load transfer, there are less unbalanced lateral accelerations. As a consequence, the proposed mechanism is not as effective as before for roll stability enhancement.

The sliding pillar mechanism is chosen in this comparison because it is a fair representation of the widely-adopted vehicle roll model. The proposed trailing arm mechanism, by properly utilizing the longitudinal movement of the wheels as a by-product of the vertical suspension movement, is shown to improve the vehicle roll stability even further. This, along with other benefits of adopting the trailing-arm mechanism, makes the proposed system well suited for narrow tilting vehicles.
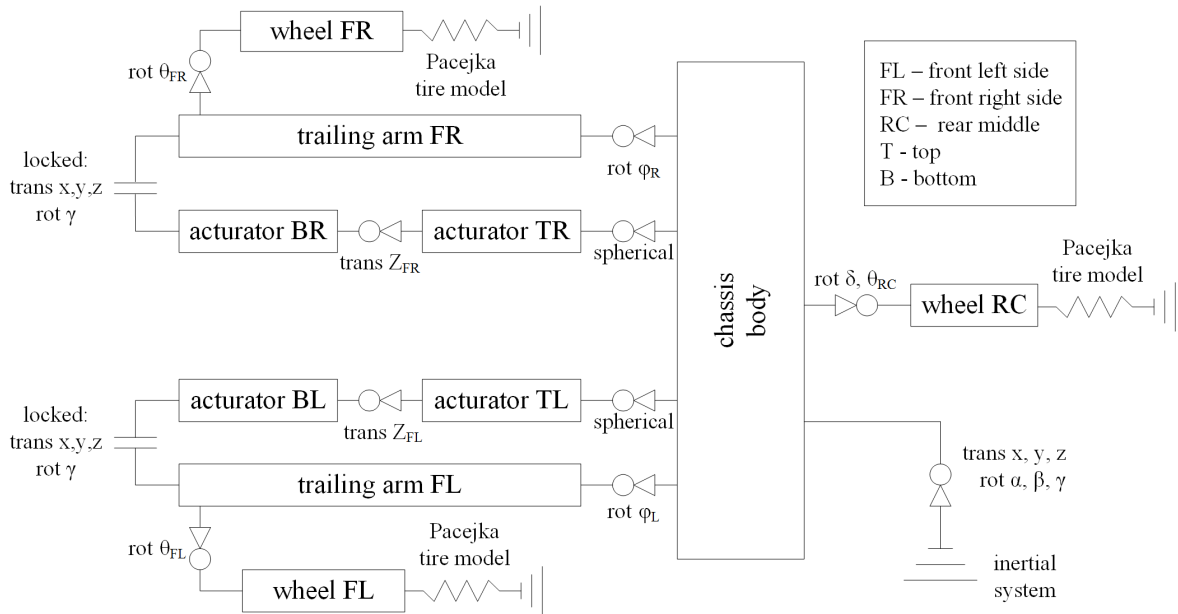
(a) tilting three-wheeler with trailing-arm mechanism
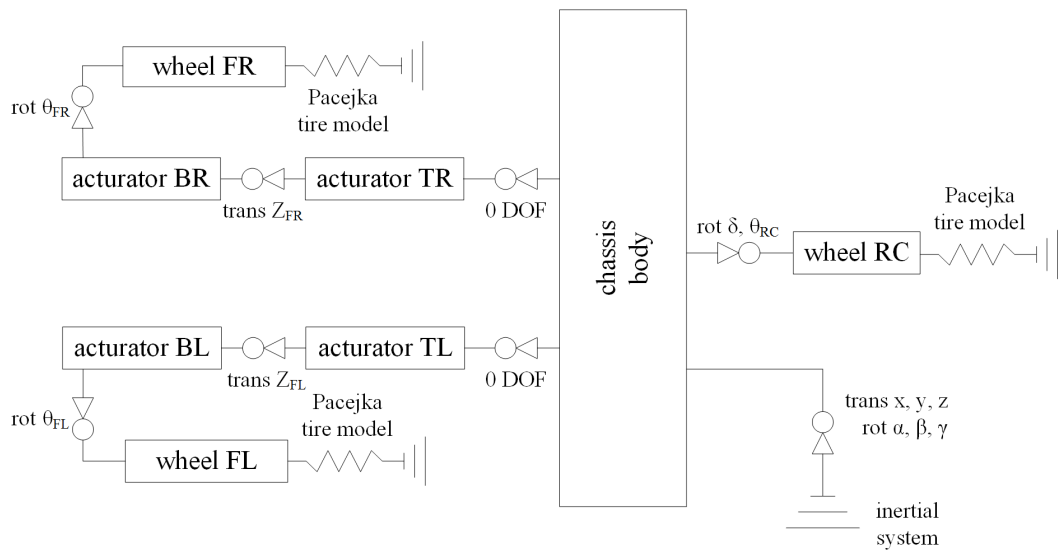
(b) tilting three-wheeler with sliding pillar mechanism

Figure 4.9: Topology of the Multi-body Dynamics Models for Tilting Three-wheelers
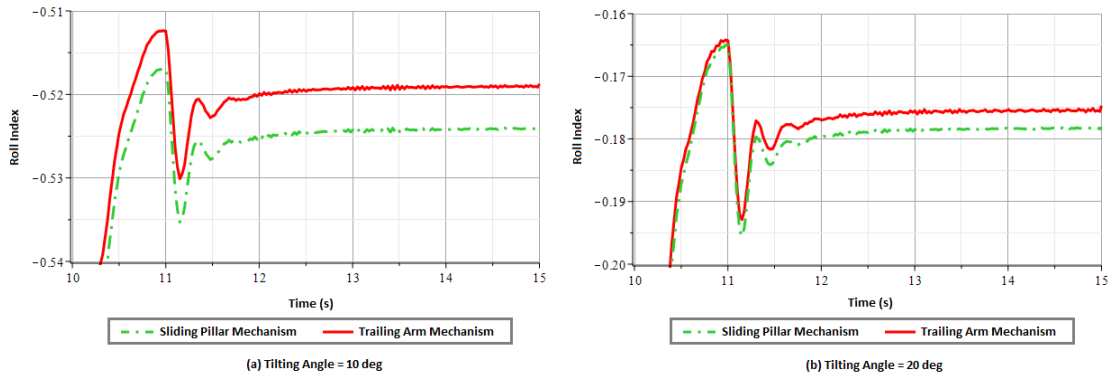
Figure 4.10: Rollover Index with Sliding Pillar and Trailing Arm Mechanisms

4.6 Conclusions

This chapter studied the suspension mechanism for implementing the suggested ISTS on
NTVs. The trailing arm mechanism, through comparison with other suspension mecha-
nisms for its compactness and the simplicity to produce the tilting motion, was identified
to be promising. The tilting vehicle characteristics by adopting the trailing arm mechanism
were studied in detail. The effect of longitudinal wheel movement on roll kinematics and
dynamics was investigated, and a preferred pattern of wheel longitudinal motion was pro-
posed to improve the roll stability of the vehicle. A trailing-arm mechanism was designed
for the target tilting vehicle by utilizing this effect while considering other practical con-
straints. A multi-body simulation of the proposed system showed that, if designed properly,
the longitudinal wheel motion could be used to further reduce the vehicle rollover index
while cornering.

Chapter 5

Envelope-based Vehicle Stability Control for Tilting Vehicles

This chapter presents the controller design for the proposed tilting vehicle. The vehicle roll model is first developed, followed by the derivation for lateral load transfer (LTR) which is adopted as the measure of vehicle rollover tendency in this research. Safe roll envelope is then suggested based on the LTR index. Instead of tracking the desired roll angle calculated from zero LTR index in steady state, a more energy-efficient way is to activate the tilting actuator only when the vehicle states are leaving the safe envelope. Non-minimum phase nature of the active tilting control is revealed, and the MPC controller is suggested for the envelope control of the vehicle roll motion.

An integrated controller considering both the lateral and roll motion is then proposed. The stability requirements are formed as an integrated envelope control problem in both directions. The re-configurable approach is adopted in the controller derivation, which provides the freedom to select various actuator combinations for the system without redesigning the controller. The control effort, thanks to the integrated formulation of handling and roll dynamics, are then optimally distributed to corresponding actuators to ensure the feasibility as well as system robustness.

As an extension to the proposed integrated envelope controller, tilting actuator dynamics is considered using the ISTS as an example. The hybrid model combing the mechanical and hydraulic dynamics is derived and adopted in the model predictive controller. It is shown in CarSim results that, with the proposed control approach, tilting control effort is reduced and the vehicle handling, as well as stability in both lateral and roll motions, can be improved.

5.1 Challenges in Controller Design for NTV Applications

The primary challenge in control of vehicles with tilting capabilities is determining how to systematically integrate the tilting actuators with other control efforts. Previous work for integrated vehicle control on conventional vehicles either ignore the roll dynamics [30, 31, 31] or separately control the roll dynamics from the lateral and longitudinal ones [25, 77]. The literature for the tilting vehicle control [21, 22, 23] suggests incorporating the steering actuators for roll stability control using STC/SDTC methods. Vehicle roll dynamics control via active steering is shown to be effective especially at high speeds. However, its impact on vehicle lateral stability and handling are not systematically considered. The suggested control structure in this chapter considers vehicle roll dynamics along with lateral ones in an integrated fashion, and optimally distributes the control efforts by considering the constraints systematically. Tilting effort can be reduced, benefiting from this integrated approach compared with the separated roll controller design, and the lateral stability can also be maintained within the safe envelope.

Apart from the control integration, the energy consumption is also regarded as a priority issue. The original idea is to build compact and energy efficient cars for urban commuter use. The active safety control is not expected to consume too much energy. Compared with the conventional tilting control algorithms which try to perfectly balance the vehicle all the time, the envelope-based roll stability control is proposed. The vehicle with track width by nature can resist unbalanced lateral accelerations without causing rollover problems. The envelope control based on rollover index threshold is thus proposed to tilt the vehicle in an energy-efficient manner.

The third issue to be addressed is the non-minimum phase problem in active tilting control. Applying the tilting moment can deteriorate the rollover index in transient, which could be a potential issue of the proposed envelope approach. To address this, the controller with the predictive feature (MPC) is adopted. The prediction can be used to detect the possible envelope violation at an early stage to start applying the rollover mitigation control and quantify the rollover index overshoot if it is unavoidable.

Another challenge in designing the controller for tilting cars is their various wheel and actuator configurations, as shown in Table 2.1. A properly designed controller for one specific configuration might not work for others. To address this, a re-configurable control approach is demonstrated with the proposed MPC controller. The suggested framework not only improves flexibility of the control system but also makes it more robust against actuator failure since the control effort can be optimally redistributed online to react to

the failures.

5.2 Roll Motion Control with Envelope-based Approach

The roll motion control is crucial to tilting vehicles. A proper control strategy which efficiently tilts the vehicle while maintains the roll stability is studied in this section. Rather than tracking roll angle or rollover index to be zero, the suggested envelope approach only activates the tilting control when the rollover index reaches pre-defined thresholds.

This section starts with the derivation of the vehicle roll model and the rollover index as a measure of the rollover tendency. The concept of roll envelope control is then proposed based on the rollover index, and different implementations of the envelope constraints are discussed. The non-minimum phase problem with tilting control is also investigated with the vehicle roll model. An MPC controller is then developed to demonstrate its potential for tilting vehicle control.

5.2.1 Vehicle Roll Model and Rollover Index

The vehicle roll model adopted in this section is illustrated in Figure 5.1. The sprung mass (m_s) is assumed to roll with regard to the un-sprung mass (m_u) at the roll center (RC). The suspension is modeled as an equivalent rotational spring (K_ϕ) and damper (C_ϕ). The lateral acceleration (a_y) is treated as a measurable disturbance, and the tilting actuator generates the roll moment (T_x) between the sprung and un-sprung mass for rollover mitigation. The normal forces at left and right side wheels are denoted as $(F_{zl},\ F_{zr})$, and lateral tire forces as $(F_{yl},\ F_{yr})$. Geometrical parameters like sprung mass CoG to roll center distance (h_s), un-sprung mass center height (h_u), roll center height (h_{rc}), and track width (T_w) are illustrated in the figure.
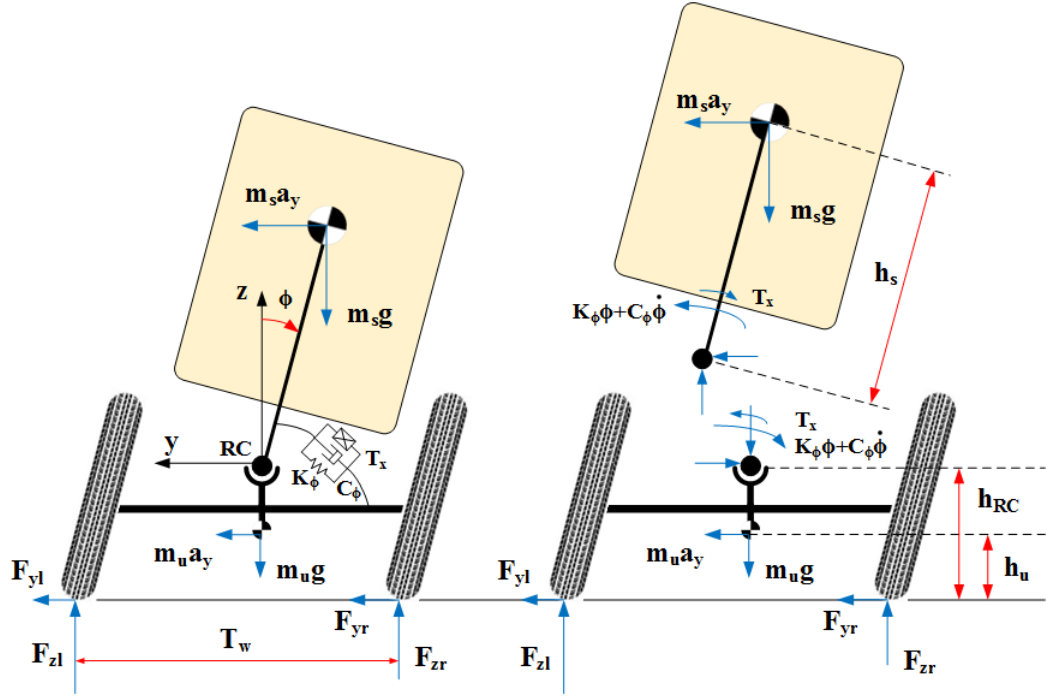
Figure 5.1: Vehicle Roll Model with the Solid Axle

The roll dynamics equation can then be written as,

$$\ddot{\phi} = \frac{1}{I_x}T_x - \frac{m_s h_s \cos(\phi)}{m I_x}a_y - \frac{K_\phi \phi - m_s g h_s \sin(\phi)}{I_x} - \frac{C_\phi}{I_x}\dot{\phi} \tag{5.1}$$

By defining the roll rate and roll angle as the states ($[X_r = \begin{bmatrix} \dot{\phi} & \phi \end{bmatrix}^T$), tilting moment as the control input ($U_r = [T_x]$), and maneuver induced lateral acceleration as disturbance ($W_r = [a_y]$), the roll dynamics under the small angle assumption can be written in the state space form as:

$$\dot{X}_r = A_r X_r + B_r U_r + E_r W_r \tag{5.2}$$

where,

$$A_r = \begin{bmatrix} -\frac{C_\phi}{I_x} & \frac{m_s g h_s - K_\phi}{I_x} \\ 1 & 0 \end{bmatrix}, B_r = \begin{bmatrix} \frac{1}{I_x} \\ 0 \end{bmatrix}, E_r = \begin{bmatrix} -\frac{m_s h_s}{I_x} \\ 0 \end{bmatrix} \tag{5.3}$$

60

For the rollover mitigation control, the lateral load transfer (LTR) [78, 73] ratio is widely adopted as the evaluation metric for rollover tendency, especially for the transient behavior. The vehicle rollover is defined as a situation when one of the wheels lifts off the ground. In other words, it happens when the vertical force of one of the wheels reaches zero. By definition, LTR can be written by vertical tire forces as,

$$\text{LTR} \triangleq \frac{F_{zl} - F_{zr}}{F_{zl} + F_{zr}} \tag{5.4}$$

Since it is no easy to directly measure the vertical tire forces, it is desired to rewrite the LTR in terms of measurable parameters and states, especially for the design of rollover mitigation controllers [79, 80]. Adopting the vehicle roll model in Eq.(5.1) and taking the roll moment around the midpoint of the contact points on the left and right tires gives,

$$F_{zl} - F_{zr} = \frac{2}{T_w} \left(I_x \ddot{\phi} + m_u h_u a_y + m_s h'_s a_y - m_s g h_s \phi \right) \tag{5.5}$$

where, $h'_s = h_s + h_{rc}$ is the CoG height of the sprung mass.

Substituting the roll dynamics Eq.(5.1) into (5.5), and considering the sum of the tire forces equals to gravity $(F_{ZL} + F_{ZR} = (m_s + m_u) g)$, the LTR index can be written as:

$$\text{LTR} \triangleq \frac{F_{zl} - F_{zr}}{F_{zl} + F_{zr}} = \frac{2}{T_w (m_s + m_u) g} \left(I_x \ddot{\phi} + m_u h_u a_y + m_s h'_s a_y - m_s g h_s \phi \right) \tag{5.6}$$

Or equivalently, in state-space form as:

$$\text{LTR} = C_r X_r + D_r U_r + F_r W_r \tag{5.7}$$

where,

$$
\begin{aligned}
C_r &= \left[\begin{array}{cc} \frac{-2C_\phi}{(m_s+m_u)gT_w} & \frac{-2K_\phi}{(m_s+m_u)gT_w} \end{array} \right] \\
D_r &= \frac{2}{(m_s+m_u)gT_w}, F_r = \frac{2(m_s h_{rc}+m_u h_u)}{(m_s+m_u)gT_w}
\end{aligned}
\tag{5.8}
$$

5.2.2 Roll Envelope

The rollover is a major threat to vehicle operational safety, especially for cars with small track width and high center of gravity. On dry roads with high friction coefficients, the rollover can happen before skidding. Under those circumstances, either of the vertical tire force reaches zero or equivalently, the LTR index reaches ± 1 [73]. Thus, it is desired to avoid these situations by keeping the rollover index to smaller values. However, previous studies for tilting vehicle control [10, 1, 78] attempt to regulate LTR by treating the tilting vehicle as a motorcycle with zero track width, and the tilting controller tries to balance the centrifugal force through active tilting all the time during the operation.

This seems to be unnecessary, as the existence of the vehicle track width can help to endure some unbalanced lateral accelerations as illustrated in Figure 5.2. In that sense, the tilting strategy which tries to eliminate the lateral load transfer might be too conservative. Frequent activation of the tilting control system consumes too much energy and conflicts with the original idea to build energy-efficient compact vehicles.

By accepting the rollover index is not necessarily kept at zero but only needs to be bounded within a safe envelope defined by the threshold RI_{lim}, the tilting actuator can be inactive when the vehicle is driven with moderate maneuvers at lower speeds. For harsh maneuvers, the tilting effort can also be reduced since the target is not to perfectly balance the vehicle but only to bring the system back to the predefined safe envelope. Much control effort can be saved when the vehicle is within the safe threshold (RI_{lim}) as demonstrated in [81], which improves the energy efficiency of the vehicle.
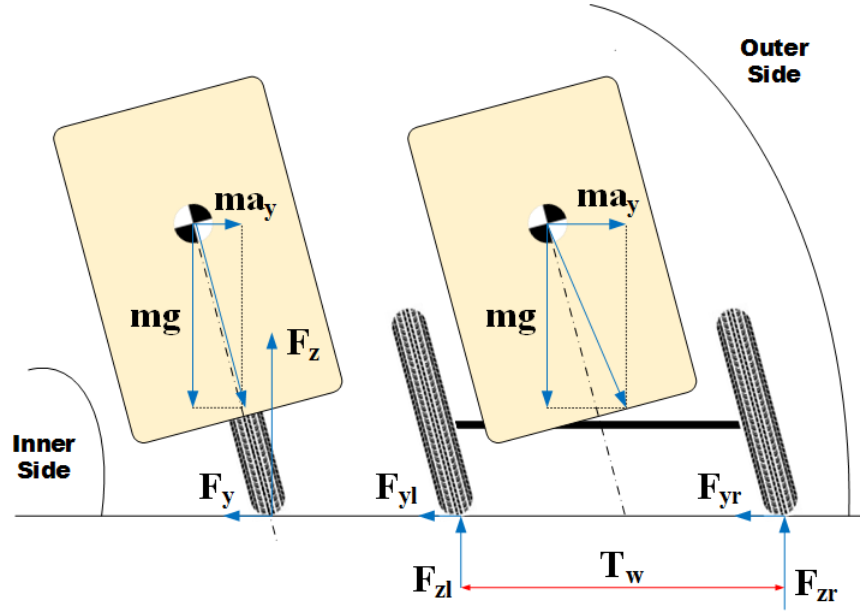
Figure 5.2: Vehicle Model with Zero and Non-zero Track Width

Steady-State Roll Envelope

The first attempt to adopt the desired roll envelope is through re-design of the reference tilting angle. Based on the described roll control envelope, the desired tilting angle can be written as,

$$
\phi_{des} = \begin{cases} \frac{mT_w}{2m_s h_s} sign\left(a_y\right) RI_{lim} - \frac{mh_0}{m_s h_s g} a_y & |a_y| \geq a_y^* \\ \phi_{passive} & otherwise \end{cases}
$$
(5.9)

where, RI_{lim} is the desired rollover index threshold; the lateral acceleration threshold a_y^* to activate the tilting control is solved as,

$$
a_y^* = \frac{mT_w}{2m_s h_s \left(\frac{m_s h_s}{K_\phi - m_s g h_s} + \frac{mh_0}{m_s g h_s} \right)} RI_{\lim}
$$
(5.10)

It should be mentioned that by assuming a zero vehicle track width $(T_w = 0)$, or setting the desired rollover index to be zero $(RI_{lim} = 0)$, the proposed tilting angle reduces to the

form of the conventional approach ($\phi_{des} \approx -a_y/g$). The general expression given in Eq.(5.9) also considers the sprung and un-sprung mass distribution, which can be different for full tilting and partial tilting vehicles as shown in Table 2.1. Equation (5.10) also reveals that, smaller track-width, as well as a lower rollover index threshold, could activate the tilting control at an earlier stage.

A major benefit of the proposed envelope approach for rollover index based control is the energy saving on tilting control efforts. To demonstrate that, the resultant tilting torque under a quasi-static process can be determined using the inverse roll dynamics from Eq.(5.1) as,

$$
T_{xq} = \begin{cases} K_\phi\phi - m_sgh_s\sin(\phi) - m_sa_yh_s\cos(\phi) & |a_y| \geq a_y^* \\ 0 & otherwise \end{cases}
\tag{5.11}
$$

By combining Eq.(5.9)-(5.11), the energy consumption on tilting actuators (J_{tilt}) to achieve the desired roll stability can be calculated. Figure 5.3 illustrates the desired tilting angle and energy consumption for various rollover index thresholds. It can be seen that the energy consumption increases quadratically as the increase of the lateral acceleration. The energy saving with a higher threshold is majorly due to the delayed activation, which applies control efforts only under more severe disturbances. The figure also shows that, under severe driving scenarios, maintaining a zero rollover index could be challenging. The suspension mechanism, as well as the actuator, needs to be properly designed to allow the excessive roll motion.

The energy consumption as a result of the suggested roll envelope approach is very dependent on the driving style. Adopting Eq.(3.28) which describes the steady-state lateral acceleration as a function of steering angle and vehicle speed, the desired tilting angle shown in Eq.(5.9) can be represented as a mapping dependent solely on vehicle longitudinal speed, steering angle, and the rollover index threshold. The contour of the desired roll angle with different RI_{lim} thresholds is visualized in Figure 5.4.
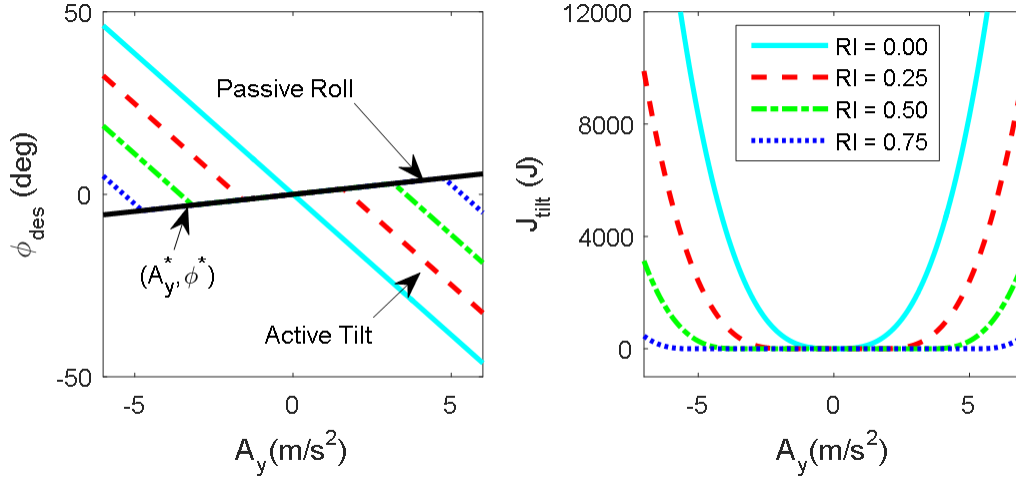
Figure 5.3: Desired Tilting Angle and Energy Consumption under a Quasi-static Process

The lighter color in the figure denotes smaller tilting angles, while the white area represents the scenarios where the rollover index is below the threshold, and no active tilting control is required. As the increase of the rollover index threshold, the area needs no tilting control grows quickly; while the dark area, which denotes the situations with maximum tilting angles, shrinks to the upper right corner. Compared with the conservative case when the desired rollover index is zero (Figure 5.4a), and tilting actuators are activated all the time, the tilting control based on the proposed envelope strategy (Figure 5.4b-d) is only expected to deal with rollover tendency at higher speeds with harsher maneuvers.

Although a higher threshold value helps to improve the energy efficiency, determination of a proper threshold also needs to consider conflicting factors like safety margin, riding comfort, and driving sensations. The existing tilting approaches which track zero rollover index react almost continuously to drivers maneuvers; however, the proposed envelope approach will introduce an elongated delay as shown in Figure 5.3 on top of the existing delays caused by signal processing and actuator dynamics [12, 41]. A lower threshold setting leaves a responsive impression due to the frequent activation of the tilting; while higher threshold setting generates a more calm and sluggish feeling, since the vehicle will tilt less frequently and the magnitude of the tilting angle will be smaller. However, all tuning for the threshold need to be validated by driving simulators [82] or real tests to achieve a balanced solution. Drivers might also be allowed to adjust the settings from the dashboard to meet their specific driving style and the fuel economy preferences.

65
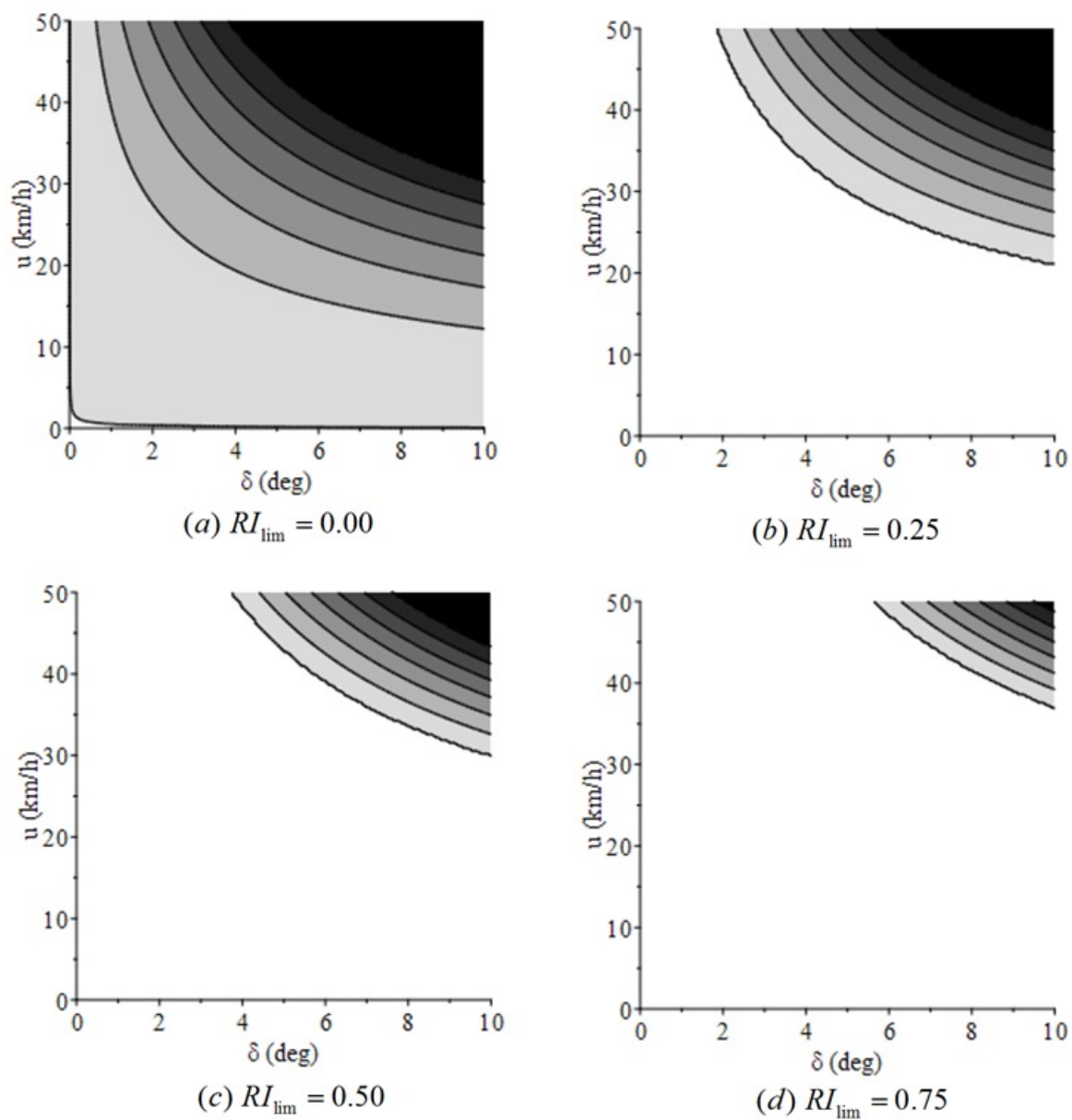
Figure 5.4: Contour Plot of Desired Tilting Angles with Various Rollover Thresholds
(lighter color denotes smaller angles)

Roll Envelope as Constraints

The previous section demonstrates the possibility of implementing the threshold of roll envelope as steady-state tilting angles. The desired tilting angle in the form of Eq.(5.9) is a generalized expression considering the desired rollover index threshold as a tunable parameter. By tracking the desired tilting angle, the design compromise between energy consumption and safety margin improvement can be made [81].

However, since the desired angles are derived under the steady-state assumptions, the transient behavior is not captured. To improve the roll control performances, a direct control against the rollover index is desired.

With the LTR index written in the form of Eq.(5.7), the prediction of rollover tendency is possible with available roll states estimations [83]. Furthermore, with given tilting moment inputs (U_r) and measured disturbances (W_r), the rollover index can be represented as a linear combination of roll states (X_r). If plotted in the roll phase plane ($\phi - \dot{\phi}$), the contour of LTR indices is a set of sloped lines determined by the suspension properties.

Two sets of roll-index boundaries ($\pm RI_{lim}$ and ± 1) are illustrated in Figure 5.5. The sloped dash-dot lines stand for the desired rollover index boundary for roll safety ($RI_{lim} = 0.5$), while the dash lines represent the hard bound for the rollover situation ($RI_{lim} = 1.0$). To form a closed envelope, the roll rate limit for actuator restrictions is also considered, which is illustrated as horizontal lines in the figure. Compared with roll control approaches which track either zero roll angle (y-axis in the phase plane) or zero rollover index (the contour line with ($RI_{lim} = 0.0$)), the envelope approach saves the control effort by only maintaining the roll states within the envelope area to achieve the required level of stability.

The equilibrium point for the roll dynamics can be solved from Eq.(5.2) as,

$$\phi_{ss} = \frac{-m_s h_s a_y + T_x}{K_\phi - m_s g h_s} \tag{5.12}$$

When there are no lateral disturbance or control torques, the passive system should converge to the origin with various initial states located on the rollover index boundaries, as shown in Figure 5.5a. However, as the lateral acceleration increases, the equilibrium point will move along the horizontal axis which makes the vehicle less stable as shown in Figure 5.5b. Some trajectories cross the boundary for rollover index thresholds, with their initial states located on it.

(a) without disturbance ($A_y=0$)   (b) with disturbance ($A_y=0.5g$)
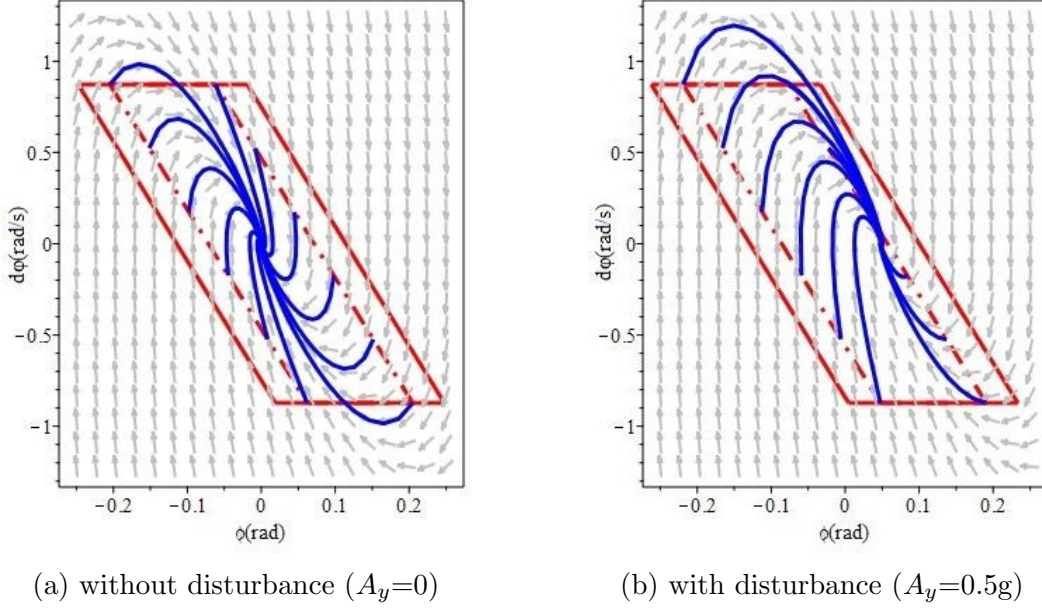
Figure 5.5: Open Loop Vehicle Phase Portrait in Roll Plane

It should also be noted that, the static equilibrium point shown in Eq.(5.12) might not be a good measure to determine whether to activate the roll control. As can be seen in Figure 5.5b, although the static equilibrium point stays within the desired envelope, there might be transient dynamics causing the states to leave the envelope. In that sense, the model-based method which predicts the development of the rollover index during run-time and activates the envelope control accordingly is a preferable approach.

Denoting the desired threshold for rollover index and roll rate as RI_{lim} and $\dot{\phi}_{lim}$, the safe roll envelope defined above can be written as a constraint as,

$$M_{ro}X_r^{(k)} + N_{ro}U_r^{(k)} \leq L_{ro} \tag{5.13}$$

where,

$$M_{ro} = \begin{bmatrix} +C_r \\ -C_r \\ \begin{bmatrix} +1 & 0 \\ -1 & 0 \end{bmatrix} \end{bmatrix}, N_{ro} = \begin{bmatrix} +D_r \\ -D_r \\ O_{2\times1} \\ O_{2\times1} \end{bmatrix} L_{ro} = \begin{bmatrix} RI_{\lim} \\ RI_{\lim} \\ \dot{\phi}_{\lim} \\ \dot{\phi}_{\lim} \end{bmatrix} - \begin{bmatrix} +F_r \\ -F_r \\ 0 \\ 0 \end{bmatrix} W_r^{(k)} \tag{5.14}$$

68

5.2.3 Active Tilting as a Non-minimum Phase Control System

When the disturbance is big enough that even the static equilibrium point falls outside the boundary, active control for rollover mitigation has to be applied. One approach is to decrease the lateral acceleration at the cost of vehicle trajectory change and handling performance degradation which will be examined in the lateral section using the integrated vehicle control approach. In this section, the focus is to solely use tilting moment for roll envelope control.

As shown in Eq.(5.7), the rollover index is dependent on the tilting moment as a control input. The algebraic relationship indicates an instant shift of rollover index boundary when the tilting moment is applied. This could cause problems as demonstrated below.

(a) without tilting torque   (b) with tilting torque
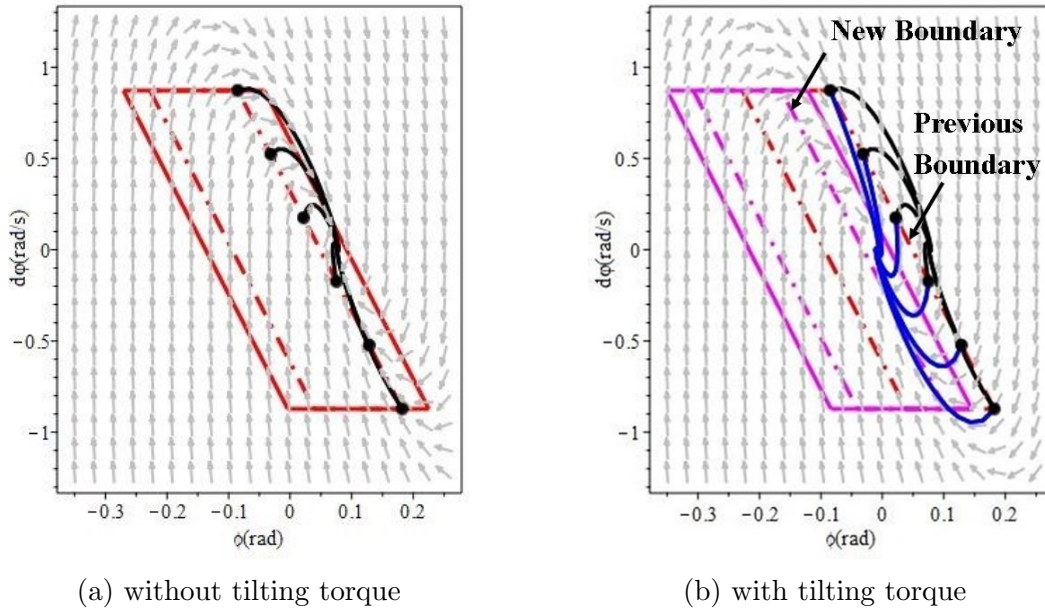
Figure 5.6: Effects of Tilting Torque on the Roll Envelope

The uncontrolled roll dynamics under a high lateral acceleration is shown in Figure 5.6a. Two sets of boundaries for the rollover index ($\pm RI_{lim}$ and ± 1) are plotted. Initial states (denoted by dots) on the rollover index boundary converges to the equilibrium point which locates outside of the safe envelope. Some transient dynamics even cross the hard boundary which indicates a direct rollover.

As a comparison, the dynamics with a constant tilting torque is illustrated in Figure

5.6b. Starting with the same initial states, the new state trajectories in blue are now converging to the inner side of the original boundary compared with uncontrolled trajectories in black. However, this does not guarantee better roll stability due to the boundary shift with the applied torque. The new rollover index boundaries are plotted in pink. Since the roll states transition takes time, at the instant when the torque is applied, the LTR index gets even worse.

Combining Eq.(5.2) and (5.7), the transfer function from tilting moment to rollover index is written as,

$$
\begin{aligned}
H\left(s\right) &= C_r(sI - A_r)^{-1}B_r + D_r \\
&= \frac{2\left(I_x s^2 - m_s h_s g\right)}{(m_s + m_u)T_w g\left(I_x s^2 + C_\phi s + K_\phi - m_s h_s g\right)}
\end{aligned}
\tag{5.15}
$$

The zeros of the above transfer function can be solved as:

$$
s = \pm\sqrt{m_s h_s g / I_x}
\tag{5.16}
$$

which indicates there always exists an RHS zero. This is known as the non-minimum phase system [84] and could cause troubles for the roll envelope control. There exists a fundamental limitation between response time and system overshoot according to [85]. Higher tilting moment helps to change the roll dynamics quicker at the cost of more severe rollover index overshoot. From a physical perspective, this can be explained by referring to the force analysis in Figure 5.1, as,

1. To balance the lateral acceleration (a_y) with gravity, a clockwise roll angle in steady state is desired;

2. The tilting torque applied to the sprung mass needs to be in the clockwise direction, so as the roll acceleration;

3. Treating the sprung and un-sprung mass as a whole, tilting moment as an internal force does not change the load distribution directly, but the inertia moment due to the roll acceleration makes the LTR index worse;

4. The fundamental limitation exists between the desired steady state roll angle and the roll acceleration to achieve that angle.

This transient overshoot should be bounded to ensure it does not cause a direct rollover when the tilting torque is applied, and a quick reaction time is also desired for rollover

mitigation. To address this, an optimal controller based on the vehicle roll model is proposed to compromise between these conflicting targets. The prediction capability in the controller is considered quite beneficial, since it can foresee the arriving of the envelope violation and applies the tilting moment at an early stage to minimize the overshoot. The fact that lateral control can help the rollover index without such negative transient effects also indicates that systematically integrate the handling stability with roll motion control can be promising, which leads to the idea of integrated vehicle stability control to be discussed later.

5.2.4 Implementation of the Roll Envelope Control using MPC

To apply the above-mentioned safe envelope as state constraints in the controller design, the model predictive control approach is adopted due to its straightforward implementation of the constraints regarding the states and inputs in the form of Eq.(5.13). The predictive feature of the controller also enables it to foresee the violation of the envelope and react at an early stage.

As shown in Section 5.2.3, the non-minimum phase phenomenon in active tilting control can pose a problem for the strict formulation of the rollover index constraint. A hard constraint formulation can limit the use of tilting actuator since it always comes with the side-effect of worse rollover index in transient. However, if such overshoot can be bounded and only exists during the transient, perturbation of the states outside of the boundary allows the system to react more quickly for emergency conditions [86]. The slack variable is thus introduced to formulate a softened constraint by allowing constraint violations but minimizing them in the cost function. For later discussions on MPC formulation, the following format for the slack variables is adopted,

$$
\begin{aligned}
\min_{U,S} : \quad & J = \sum_{k=1}^{N} \left\| S^{(k)} \right\|_p^Q \\
s.t. : \quad & X^{(k+1)} = AX^{(k)} + BU^{(k)} + EW^{(0)} \\
& MX^{(k)} + NU^{(k)} \leq L + S^{(k)} \\
& S^{(k)} \geq 0
\end{aligned}
\tag{5.17}
$$

where, $\| \cdot \|_p^Q$ denotes the norm-p of slack variables weighted by matrix Q.

The cost of the slack variable should be minimized to avoid constraint violation in both the magnitude as well as the duration, which are competing objectives for non-minimum

71

phase systems as described. The norm captures the worst-case constraint violation but does not enforce the minimization of the violation time. It is also reported to have non-intuitive parameter tuning issues as well as poor closed-loop performance [87]. The l_∞ norm is chosen for the slack variables for this research. Compared with the l_1 norm which linearly penalizes the constraint violation, the l_2 norm better captures the demand to maintain the vehicle away from the hard boundary for vehicle rollover conditions ($RI = \pm 1$). It should be mentioned that the adoption of l_1 or l_2 norm increases the computational burden, but it has been shown to be real-time tractable [88] with the current hardware limitations.

To study the feasibility of the MPC controller for the roll envelope control, the vehicle roll model derived in Sec 5.2.1 is first examined. The control objective is to maintain the vehicle within the safe boundary for roll stability as well as minimizing the control effort. The control objectives can be written using the envelope approach as the following optimal receding horizon control problem:

$$
\begin{aligned}
\min_{U_r, S_{ro}} : \quad & J = \sum_{k=1}^{N} \left\| U_r^{(k)} \right\|_2^{R_{ro}} + \sum_{k=1}^{N} \left\| S_{ro}^{(k)} \right\|_2^{Q_{ro}} \\
s.t. : \quad & X_r^{(k+1)} = A_{rd} X_r^{(k)} + B_{rd} U_r^{(k)} + E_{rd} W_r^{(0)} \\
& M_{ro} X^{(k)} + N_{ro} U^{(k)} \le L_{ro} + S_{ro}^{(k)} \\
& 0 \le S_{ro}^{(k)} \le S_{ro,\max} \\
& \left| U_r^{(k)} \right| \le U_{\max} \\
& \left| U_r^{(k)} - U_r^{(k-1)} \right| \le U_{slew,\max}
\end{aligned}
\tag{5.18}
$$

where, $S_{ro}^{(k)} \in \mathbb{R}^4$ denotes slack variables for the roll envelope at the $k - th$ prediction step. The disturbance is assumed to remain unchanged during the control horizon as $W^{(0)}$. The total cost to be minimized is the l_2 norm of the control effort and slack variables, which are weighted by R_{ro} and Q_{ro} respectively.

The non-minimum-phase issue discussed in Sec.5.2.3 affects the choice of the prediction horizon. To demonstrate this, the vehicle rollover index response under a step input of tilting torque is shown below.
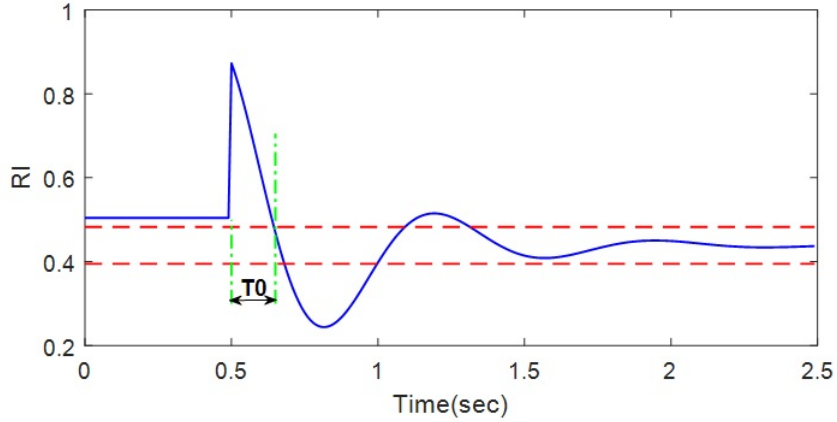
Figure 5.7: Step Response of Rollover Index with Tilting Torque Input

It can be seen from Figure 5.7 that, the rollover index gets worse instantly as the torque is applied, and no improvement on rollover index is seen till T_0. If the prediction horizon is not long enough, the optimizer can be fooled to abandon the use of tilting moment or even apply it in the reverse direction before the ultimate improvement on rollover index shows up in steady state. In such cases, as commented by [84], patience is a virtue. By properly tuning the prediction horizon to correctly foresee systems longer-term reactions, the model predictive controller is shown to work for the tilting control.

A ramp acceleration disturbance of 0.5g is applied to the system, the desired RI threshold is set to be 0.5, and the results from MPC with various prediction horizon settings are shown in Figure 5.8. If the horizon is chosen to be as small as 0.5 sec ($N = 10$, $\Delta T = 50ms$), the calculated tilting moment is shown to have the wrong sign and end up with even worse rollover index of the controlled plant. The optimized solutions start to converge after prediction horizon reaches 1sec. For computational efficiency, a prediction horizon of 1sec is adopted for the control implementations in remaining sections for the target vehicle.
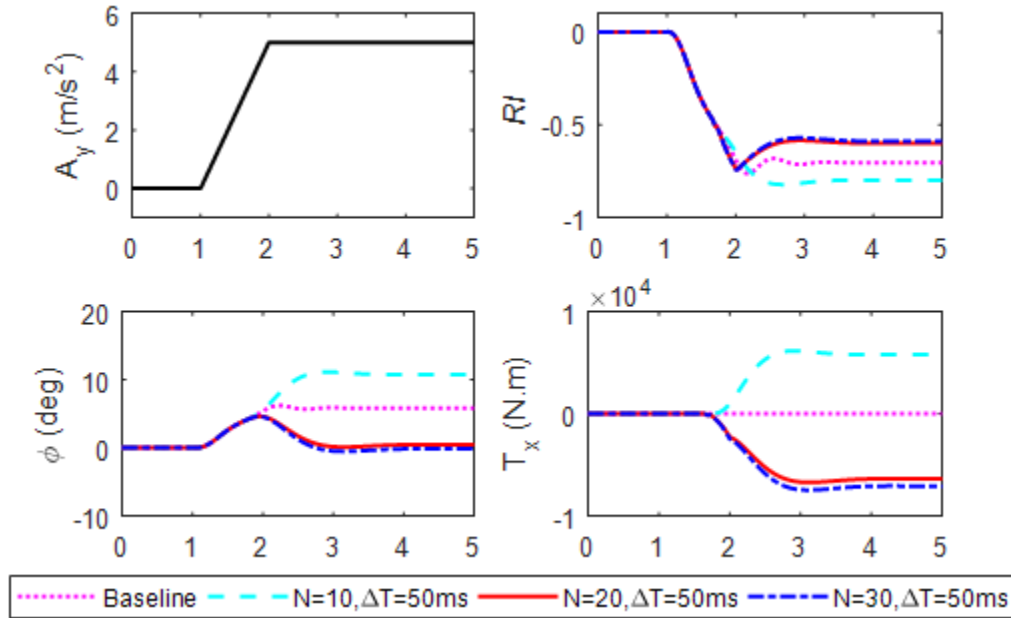
Figure 5.8: Roll Envelope Control with Different Prediction Horizons

It should also be noted that, the rollover index overshoot is still noticeable as shown in Figure 5.8 using the tilting actuator only. To further improve the vehicle roll stability during the transient, the lateral stability control effort should be incorporated, and an integrated approach will be examined in the next section.

5.3   Integrated Envelope Control for Tilting Vehicles

The previous section demonstrates the use of tilting actuators for rollover envelope control based on the model predictive approach. With the properly tuned MPC controller, the rollover danger of the vehicle can be lowered to the desired level. However, due to the non-minimum phase nature of the tilting system, the transient performance, when looking at the rollover index, still has rooms for improvement. A possible way to alleviate the non-minimum-phase problem is to use alternative actuators especially those for lateral control.

To implement that, a vehicle model incorporating the lateral dynamics with a general re-configurable approach is adopted. Based on the derived model, an integrated vehicle

controller with various actuator configurations is demonstrated using the proposed envelope control scheme for both lateral and roll stability. The controller performance, as well as robustness, is shown to be further improved with the proposed integrated approach.

5.3.1 Vehicle Modelling

The double track vehicle handling model for lateral dynamics is adopted due to its generality. The schematic drawing is shown in Figure 5.9. It should be noted that three-wheeled vehicle configurations can be handled by setting the track width at the front or rear axle to be zero.
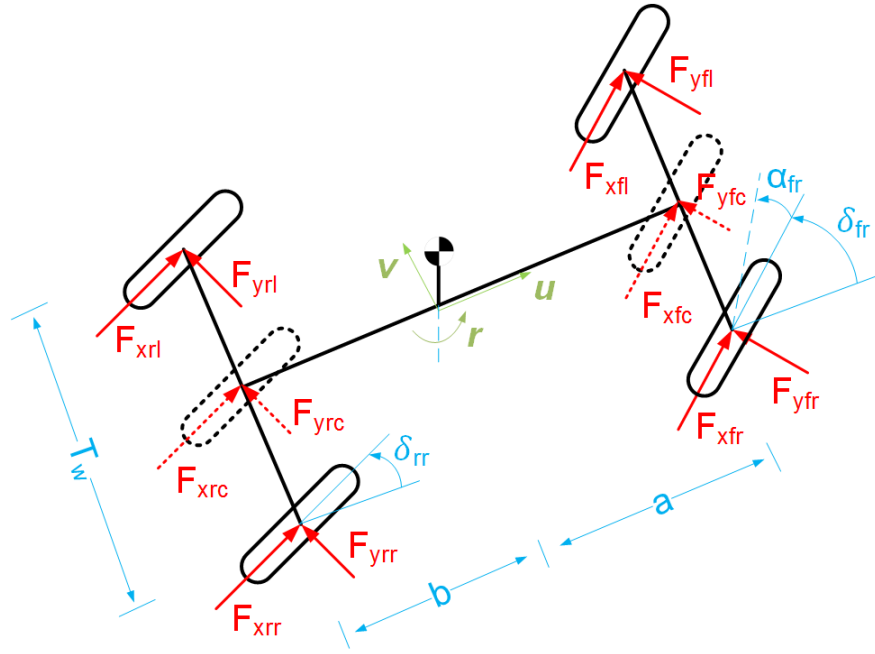
Figure 5.9: Double Track Vehicle Handling Model

The net tire forces in lateral and yaw directions are considered, which gives,

$$\dot{v} = \frac{1}{m}F_y - ur$$
$$\dot{r} = \frac{1}{I_z}M_z$$

(5.19)

75

where, m is the total mass of the vehicle; I_z is the vehicles yaw inertia; u, v and r are vehicle longitudinal, lateral speeds and yaw rate; the generalized external forces acting on the vehicle are denoted as F_y, and M_z respectively.

Generalized forces F_y and M_z on the right-hand side of Eq.(5.19) are dependent on the tire forces at each corner. To cover various wheel configurations, especially the three-wheelers which are common in urban tilting vehicles, a general parameter for track width T_{wj} ($j = left/right/center$) and axle to CoG distance a_i ($i = front/rear$) are introduced. The generalized CoG forces can be calculated from individual longitudinal and lateral tire forces as,

$$
\begin{aligned}
F_y &= \sum_{i,j} \left(F_{xij} sin\left(\delta_{ij} \right) + F_{yij} cos\left(\delta_{ij} \right) \right) \\
M_z &= \sum_{i,j} M_{zij} = \sum_{i,j} \left(\begin{array}{c} \frac{T_{wj}}{2} \left(F_{xij} \cos\left(\delta_{ij} \right) - F_{yij} sin\left(\delta_{ij} \right) \right) \\ + a_i \left(F_{xij} sin\left(\delta_{ij} \right) + F_{yij} cos\left(\delta_{ij} \right) \right) \end{array} \right)
\end{aligned}
\tag{5.20}
$$

where, F_{xij} and F_{yij} are longitudinal and lateral forces at each tire. δ_{ij} denotes the steering angle on each wheel. T_{wj} and a_i are based on the vehicle configuration, as:

$$
T_{wj} = \begin{cases} +T_w & j = \text{right} \\ 0 & j = \text{center} \\ -T_w & j = \text{left} \end{cases}
\tag{5.21}
$$

$$
a_i = \begin{cases} a & i = \text{front} \\ -b & i = \text{rear} \end{cases}
\tag{5.22}
$$

The force produced by pneumatic tires has been studied both theoretically and experimentally [63]. In general, the longitudinal and lateral tire forces can be written as,

$$
\begin{aligned}
F_{xij} &= f_x \left(\alpha_{ij}, S_{ij}, F_{zij}, \gamma_{ij} \right) \\
F_{yij} &= f_y \left(\alpha_{ij}, S_{ij}, F_{zij}, \gamma_{ij} \right)
\end{aligned}
\tag{5.23}
$$

where, α_{ij}, S_{ij}, F_{zij}, γ_{ij} represent the side slip angle, the slip ratio, the normal force and the camber angle for each wheel ij respectively.

The side slip and camber angles are calculated by,

$$
\alpha_{ij} = \delta_{ij} - \frac{v + a_i r}{u}
\tag{5.24}
$$

$$\gamma_{ij} = K_{\gamma_i}\phi \tag{5.25}$$

where, K_{γ_i} is the camber-by-roll coefficient. For wheels assembled on the tilting parts of the vehicle, K_{γ_i} is equal to 1. This enables tilting vehicles to generate extra lateral force like a motorcycle for handling improvement.

For control practice, instead of adopting the tire force in nonlinear form as shown in Eq.(5.23), it is common practice to use the linearized representation of the tire force model. More specifically, the longitudinal force for the tire ij is assumed proportional to the driven or braking torque for small slip ratio, and the longitudinal tire force can be represented as:

$$F_{xij} = \frac{Q_{ij}}{R_{wij}} \tag{5.26}$$

where, R_{wij} is the effective rolling radius of the wheels, Q_{ij} is the torque applied on each wheel.

The nonlinear lateral force model is also approximated with an affine tire model. The lateral forces are linearized at the operation points of side-slip and camber angle by holding the zeroth and first-order terms of the Taylor expansion [39, 89]. Denote the lateral tire force, cornering and camber stiffness of tire ij at the operating point as $\bar{F}_{yij}$, $\tilde{C}_{\alpha i}$, and $\tilde{C}_{\gamma i}$ respectively, the affine tire model can be expressed as,

$$F_{yij} = \bar{F}_{yij} + \tilde{C}_{\alpha ij}\left(\alpha_{ij} - \bar{\alpha}_{ij}\right) + \tilde{C}_{\gamma ij}\left(\gamma_{ij} - \bar{\gamma}_{ij}\right) \tag{5.27}$$

The maximum longitudinal and lateral tire forces are dependent on the normal force and the road friction condition, and for the combined slip situations, they also need to be constrained by the friction ellipse as,

$$\left(\frac{F_{xij}}{F_{xij\,\max}}\right)^2 + \left(\frac{F_{yij}}{F_{yij\,\max}}\right)^2 \leq 1 \tag{5.28}$$

where,

$$\begin{aligned} F_{xij\,\max} &= \mu_x F_{zij} \\ F_{yij\,\max} &= \mu_y F_{zij} \end{aligned} \tag{5.29}$$

with μ_x, μ_y be the longitudinal and lateral friction coefficient respectively.

Combining Eq.(5.19) with the roll dynamics shown in Eq.(5.1), the equation for the full vehicle system can be written in state-space form as:

$$\dot{X} = AX + BRU + EW + G \tag{5.30}$$

where, $X = \begin{bmatrix} v & r & \dot{\phi} & \phi \end{bmatrix}^T$; $U = \begin{bmatrix} \delta_{cfl} & \delta_{cfr} & \delta_{crl} & \delta_{crr} & Q_{cfl} & Q_{cfr} & Q_{crl} & Q_{crr} & T_x \end{bmatrix}^T$; $W = \delta_d$; $R = diag\left(\begin{bmatrix} R_{\delta fl} & R_{\delta fr} & R_{\delta rl} & R_{\delta rr} & R_{Qfl} & R_{Qfr} & R_{Qrl} & R_{Qrr} & R_{Tx} \end{bmatrix}\right)$ is the configuration matrix composed of boolean operators to denote the availability of each actuator [24, 80]. The system matrices are:

$$A = \begin{bmatrix} \dfrac{-\sum\limits_{i,j}\tilde{C}_{aij}}{(m_s+m_u)\cdot u} & \dfrac{-\sum\limits_{i,j}a_i\tilde{C}_{aij}}{(m_s+m_u)\cdot u}-u & 0 & \dfrac{\sum\limits_{i,j}K_{\gamma i}\tilde{C}_{\gamma ij}}{m_s+m_u} \\[3ex] \dfrac{-a\left(\tilde{C}_{afl}+\tilde{C}_{afr}\right)+b\left(\tilde{C}_{arl}+\tilde{C}_{arr}\right)}{I_z\cdot u} & \dfrac{-\sum\limits_{i,j}a_i^2\tilde{C}_{aij}}{I_z\cdot u} & 0 & \dfrac{\sum\limits_{i,j}a_iK_{\gamma i}\tilde{C}_{\gamma ij}}{I_z} \\[3ex] -\dfrac{m_sh_s\sum\limits_{i,j}\tilde{C}_{aij}}{(m_s+m_u)\cdot u\cdot I_x} & \dfrac{-m_sh_s\sum\limits_{i,j}a_i\tilde{C}_{aij}}{(m_s+m_u)\cdot u\cdot I_x} & -\dfrac{C_\phi}{I_x} & \dfrac{m_sh_s\sum\limits_{i,j}K_{\gamma i}\tilde{C}_{\gamma ij}}{(m_s+m_u)\cdot I_x}+\dfrac{m_sgh_s-K_\phi}{I_x} \\[3ex] 0 & 0 & 1 & 0 \end{bmatrix}$$

$$B = \begin{bmatrix} \dfrac{\tilde{C}_{afl}}{m_s+m_u} & \dfrac{\tilde{C}_{afr}}{m_s+m_u} & \dfrac{\tilde{C}_{arl}}{m_s+m_u} & \dfrac{\tilde{C}_{arr}}{m_s+m_u} & 0 & 0 & 0 & 0 & 0 \\[3ex] \dfrac{a\tilde{C}_{afl}}{I_z} & \dfrac{a\tilde{C}_{afr}}{I_z} & -\dfrac{b\tilde{C}_{arl}}{I_z} & -\dfrac{b\tilde{C}_{arr}}{I_z} & -\dfrac{1}{2}\dfrac{T_w}{R_{wfl}I_z} & \dfrac{1}{2}\dfrac{T_w}{R_{wfr}I_z} & -\dfrac{1}{2}\dfrac{T_w}{R_{wrl}I_z} & \dfrac{1}{2}\dfrac{T_w}{R_{wrr}I_z} & 0 \\[3ex] \dfrac{m_sh_s\tilde{C}_{afl}}{(m_s+m_u)\cdot I_x} & \dfrac{m_sh_s\tilde{C}_{afr}}{(m_s+m_u)\cdot I_x} & \dfrac{m_sh_s\tilde{C}_{arl}}{(m_s+M_u)\cdot I_x} & \dfrac{m_sh_s\tilde{C}_{arr}}{(m_s+m_u)\cdot I_x} & 0 & 0 & 0 & 0 & \dfrac{1}{I_x} \\[3ex] 0 & 0 & 0 & 0 & 0 & 0 & 0 & 0 & 0 \end{bmatrix}$$

$$E = \begin{bmatrix} \dfrac{\tilde{C}_{afl}+\tilde{C}_{afr}}{m_s+m_u} \\[3ex] \dfrac{a\left(\tilde{C}_{afl}+\tilde{C}_{afr}\right)}{I_z} \\[3ex] \dfrac{m_sh_s\left(\tilde{C}_{afl}+\tilde{C}_{afr}\right)}{(m_s+m_u)\cdot I_x} \\[3ex] 0 \end{bmatrix}, G = \begin{bmatrix} \dfrac{\sum\limits_{i,j}\left(\bar{F}_{yij}-\tilde{C}_{\alpha ij}\bar{\alpha}_{ij}-\tilde{C}_{\gamma ij}\bar{\gamma}_{ij}\right)}{m_s+m_u} \\[3ex] \dfrac{\sum\limits_{i,j}a_i\left(\bar{F}_{yij}-\tilde{C}_{\alpha ij}\bar{\alpha}_{ij}-\tilde{C}_{\gamma ij}\bar{\gamma}_{ij}\right)}{I_z} \\[3ex] \dfrac{m_sh_s\sum\limits_{i,j}\left(\bar{F}_{yij}-\tilde{C}_{\alpha ij}\bar{\alpha}_{ij}-\tilde{C}_{\gamma ij}\bar{\gamma}_{ij}\right)}{(m_s+m_u)I_z} \\[3ex] 0 \end{bmatrix}$$

$$\tag{5.31}$$

5.3.2 Integrated Stability Envelope

The stability envelope for roll motion control has been proposed and implemented in Section 5.2. To incorporate the lateral stability, the stable handling envelope proposed by

researchers [90, 91] is adopted. The thresholds for yaw rate (r_{max}) and the tire slip angle at rear wheels ($\alpha_{r,sat}$) are used to define the boundary at each discretized control step k,

$$M_{sh}X^{(k)} \leq L_{sh} \tag{5.32}$$

where,

$$M_{sh} = \begin{bmatrix} +1 & -b/u \\ -1 & +b/u \\ 0 & +1 \\ 0 & -1 \end{bmatrix} O_{4\times2} \right], L_{sh} = \begin{bmatrix} \alpha_{r,sat} \\ \alpha_{r,sat} \\ r_{\max} \\ r_{\max} \end{bmatrix} \tag{5.33}$$

Since the constraint is dependent only on vehicle states of lateral speed v and yaw rate r. The handling envelope can be visualized in the phase plane as the boundaries shown in Figure 5.10a. The horizontal boundaries stand for the yaw rate limit, and the sloped lines represent the constraint for rear tire slip angle. For a less harsh maneuver shown in blue, the state trajectory stays within the handling envelope, and no control intervention is required, while for a harsher maneuver shown in red, the trajectory leaves the safe envelope. In that case, active safety control needs to be applied once the system foresees the approaching of envelope violations.

By combining the handling envelope with the proposed roll envelope, an integrated envelope approach is suggested, which defines the state constraints for both lateral and roll motions, as shown in the Figure 5.10. Compared with the conventional tracking approach for stability control, the proposed integrated-envelope-based controller applies the control effort only when the predicted vehicle states are leaving the safe envelopes, which reduce the control intervention while still maintain the desired level of stability.
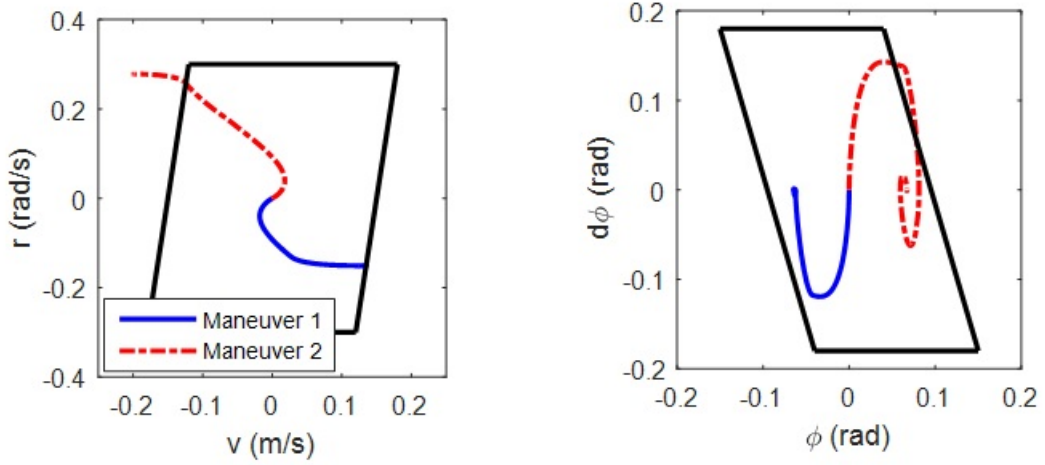
(a) Handling envelope   (b) Roll envelope

Figure 5.10: Effects of Tilting Torque on the Roll Envelope

5.3.3   MPC Formulation

The previously suggested integrated lateral and roll envelope control can be written as an optimal receding horizon control problem:

$$\min_{U,S_{ro},S_{sh}} : J = \tfrac{1}{2}\sum_{k=1}^{N} \left\| U^{(k)} \right\|_{2}^{R_U} + \tfrac{1}{2}\sum_{k=1}^{N} \left\| r^{(k)} - r_{des} \right\|_{2}^{R_X} + ...$$

$$\tfrac{1}{2}\sum_{k=1}^{N} \left\| S_{ro}^{(k)} \right\|_{2}^{Q_{ro}} + \tfrac{1}{2}\sum_{k=1}^{N} \left\| S_{sh}^{(k)} \right\|_{2}^{Q_{sh}}$$

$$s.t. : \quad X^{(k+1)} = A_d X^{(k)} + B_d U^{(k)} + E_d W^{(0)}$$

$$M_{sh} X^{(k)} \le L_{sh} + S_{sh}^{(k)}$$

$$S_{sh}^{(k)} \ge 0 \tag{5.34}$$

$$M_{ro} X^{(k)} + N_{ro} U^{(k)} \le L_{ro} + S_{ro}^{(k)}$$

$$0 \le S_{ro}^{(k)} \le S_{ro,\max}$$

$$\left| U^{(k)} \right| \le U_{\max}$$

$$\left| U^{(k)} - U^{(k-1)} \right| \le U_{slew,\max}$$

where, A_d, B_d and E_d are discretized system matrices. $S_{sh}^{(k)} \in \mathbb{R}^4$ and $S_{ro}^{(k)} \in \mathbb{R}^4$ denotes handling and roll envelope slack variables at the $k - th$ prediction step. The disturbance is assumed to remain unchanged during the control horizon as $W^{(0)}$. The total cost to be minimized is composed of: the control effort, the yaw rate tracking error, and the slack variable for the lateral and roll envelopes, which are weighted by R_U, R_X, Q_{ro} and Q_{sh} respectively.

Compared with the controller formulation for the roll model shown in Eq.(5.18), the added cost terms are the yaw rate tracking errors for handling improvement and the norm of the slack variables for stable handling weighted by Q_{sh}.

The desired yaw rate [8], considering the road friction capacity, can be written as,

$$r_{des} = sign\left(\delta\right) \cdot \min\left(\left|\frac{u}{L + K_{us}u^2}\delta\right|, \frac{\mu g}{u}\right) \tag{5.35}$$

where, μ denotes the road friction condition, which could be estimated by the algorithm as suggested in [92, 93].

Using the batch formulation, the above objective function can be written in a quadratic programming form, with the derivation shown below.

The state trajectory, by adopting the plant model, can be predicted as,

$$\bar{X} = S_X X^{(0)} + S_{U0}U^{(0)} + S_{W0}W^{(0)} + S_U\bar{U} + S_W\bar{W} \tag{5.36}$$

where,

$$
\bar{X} = \begin{bmatrix} X^{(1)} \\ X^{(2)} \\ \vdots \\ \vdots \\ X^{(N)} \end{bmatrix}, \bar{U} = \begin{bmatrix} U^{(1)} \\ U^{(2)} \\ \vdots \\ \vdots \\ U^{(N)} \end{bmatrix}, \bar{W} = \begin{bmatrix} W^{(1)} \\ W^{(2)} \\ \vdots \\ \vdots \\ W^{(N)} \end{bmatrix}
$$

$$
S_X = \begin{bmatrix} A_d^1 \\ A_d^2 \\ \vdots \\ \vdots \\ A_d^N \end{bmatrix}, S_{U0} = \begin{bmatrix} B_d^1 \\ A_d B_d \\ \vdots \\ \vdots \\ A_d^{N-1} B_d \end{bmatrix}, S_{W0} = \begin{bmatrix} E_d^1 \\ A_d E_d \\ \vdots \\ \vdots \\ A_d^{N-1} E_d \end{bmatrix}
$$

$$
S_U = \begin{bmatrix} O & \cdots & \cdots & \cdots & O \\ B_d & O & \cdots & \cdots & O \\ A_d B_d & B_d & O & \cdots & \vdots \\ \vdots & \vdots & \ddots & \ddots & \vdots \\ A_d^{N-2} B_d & A_d^{N-3} B_d & \cdots & B_d & O \end{bmatrix}
$$

$$
S_W = \begin{bmatrix} O & \cdots & \cdots & \cdots & O \\ E_d & O & \cdots & \cdots & O \\ A_d E_d & E_d & O & \cdots & \vdots \\ \vdots & \vdots & \ddots & \ddots & \vdots \\ A_d^{N-2} E_d & A_d^{N-3} E_d & \cdots & E_d & O \end{bmatrix}
$$

(5.37)

The envelope constraints can also be written using the batch form. For example, the roll envelope as,

$$
M_{RO}\bar{X} + N_{RO}\bar{U} \leq L_{RO} + \bar{S}_{ro} \tag{5.38}
$$

where,

$$
\begin{aligned}
M_{RO} &= BlockDiag\left(\begin{bmatrix} M_{ro} & M_{ro} & \cdots & \cdots & M_{ro} \end{bmatrix}\right) \\
N_{RO} &= BlockDiag\left(\begin{bmatrix} N_{ro} & N_{ro} & \cdots & \cdots & N_{ro} \end{bmatrix}\right) \\
L_{RO} &= \begin{bmatrix} L_{ro} & L_{ro} & \cdots & \cdots & L_{ro} \end{bmatrix}^T \\
\bar{S}_{RO} &= \begin{bmatrix} S_{ro}^{(1)} & S_{ro}^{(2)} & \cdots & \cdots & S_{ro}^{(N)} \end{bmatrix}^T
\end{aligned} \tag{5.39}
$$

Combining Eq.(5.36) and (5.38) gives the design variables in the linear constraint form,

$$A_{RO}\eta \leq b_{RO} \tag{5.40}$$

where,

$$
\begin{aligned}
\eta &= \begin{bmatrix} \bar{U} & \bar{S}_{ro} & \bar{S}_{sh} \end{bmatrix}^T \\
A_{RO} &= BlockDiag\left(\begin{bmatrix} M_{RO}S_U + N_{RO} & -I & O \end{bmatrix}\right) \\
b_{RO} &= L_{RO} - M_{RO}\left(S_X X^{(0)} + S_{U0}U^{(0)} + S_{W0}W^{(0)} + S_W\bar{W}\right)
\end{aligned}
\tag{5.41}
$$

Similarly, the handling envelope can be written as,

$$A_{SH}\eta \leq b_{SH} \tag{5.42}$$

with,

$$
\begin{aligned}
A_{SH} &= BlockDiag\left(\begin{bmatrix} M_{SH}S_U & O & -I \end{bmatrix}\right) \\
b_{SH} &= L_{SH} - M_{SH}\left(S_X X^{(0)} + S_{U0}U^{(0)} + S_{W0}W^{(0)} + S_W\bar{W}\right)
\end{aligned}
\tag{5.43}
$$

Equation (5.40) and (5.42), along with the constraints on the design variables and their slew rate, forms the linear constraint in the quadratic programming problem. The objective function can be rewritten by considering Eq.(5.36) as,

$$J = \frac{1}{2}\eta^T H\eta + f\eta + Const. \tag{5.44}$$

where,

$$
\begin{aligned}
H &= BlockDiag\left(\begin{bmatrix} \left(R_U + S_U^T R_X S_U\right) & Q_{ro} & Q_{sh} \end{bmatrix}\right) \\
f &= \begin{bmatrix} \left(S_X X^{(0)} + S_{U0}U^{(0)} + S_{W0}W^{(0)} + S_W\bar{W} - \bar{X}_{des}\right)^T R_X S_U & O & O \end{bmatrix}^T
\end{aligned}
\tag{5.45}
$$

The quadratic programming can then be written in the form as,

83

$$\begin{aligned} \min_{\eta} : \quad & J = \tfrac{1}{2}\eta^T H \eta + f\eta \\ s.t. : \quad & \begin{bmatrix} A_{RO} \\ A_{SH} \end{bmatrix} \eta \leq \begin{bmatrix} b_{RO} \\ b_{SH} \end{bmatrix} \\ & \eta_{\min} \leq \eta \leq \eta_{\max} \\ & \left| \eta^{(k)} - \eta^{(k-1)} \right| \leq \eta_{slew,\max} \end{aligned} \tag{5.46}$$

5.3.4 Simulation Results

To evaluate the performance of the suggested controller, especially with the introduction of the tilting actuators, simulation studies are implemented in CarSim, which is a well-known simulation platform widely-used by automotive researchers. Conventional vehicles with active suspensions or active anti-roll bars are considered to demonstrate the feasibility of the proposed integrated envelope controller. Four-wheeled configuration is thus adopted and the desired tilting moment is considered as the output of the upper-level controller for a general case. A three-wheeler demonstration with the proposed ISTS actuator is shown in the next section.

An SUV model with 15 mechanical degrees of freedom is adopted. The vehicle is equipped with the trailing arm suspension, and its track width is intentionally reduced to better demonstrate the tilting control performances [15]. A tire model based on look-up tables is used, which considers the longitudinal force, lateral force, aligning moments and overturning moments as functions of slip, load, and camber. The system diagram for the simulation is shown in Figure 5.11, and the vehicle parameters are listed in Table 5.1.

To focus on the discussion of tilting control, the allocation on non-tilting forces is simplified by assuming only active front steering (AFS) is available in the first two scenarios. The benefit of the envelope control approach along with the integration of roll and lateral stability control is demonstrated. The re-configurable model is then used to compare the control performances with various actuator configurations. The robustness of the proposed approach is also shown via the scenario considering the tilting actuator failure.
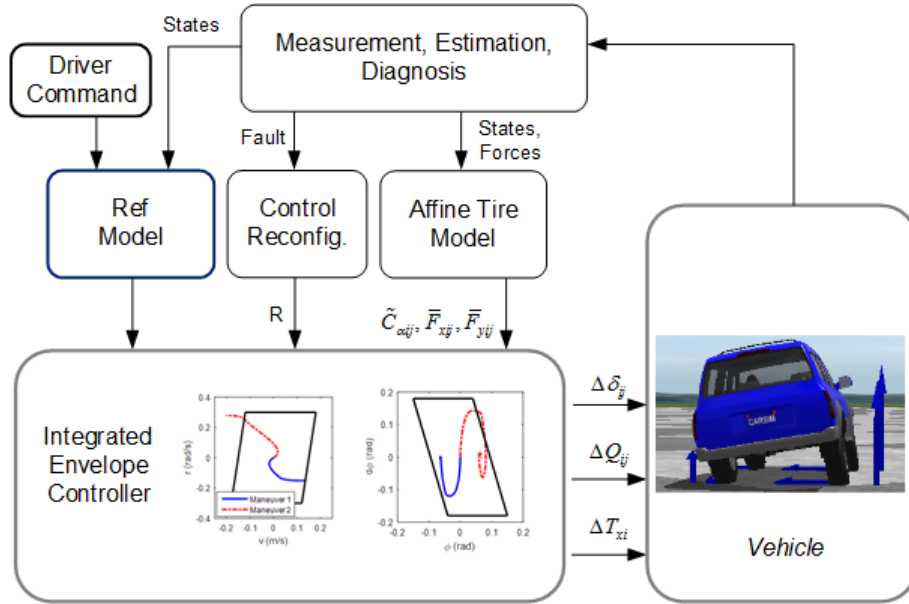
Figure 5.11: Re-configurable Integrated Envelope Control

Symbol	Parameter Description	Value	Unit
m_s	Sprung mass	1590	kg
m	Vehicle mass	1830	kg
I_x	Roll inertia	894.4	$\text{kg} \cdot \text{m}^2$
I_z	Yaw inertia	2687.1	$\text{kg} \cdot \text{m}^2$
a	Front axle to CoG distance	1.18	m
b	Rear axle to CoG distance	1.77	m
h_s	CoG to roll center distance	0.72	m
h_u	Un-sprung mass CoG height	0.2	m
T_w	Vehicle track width	1.2	m
K_ϕ	Effective Roll Stiffness	81363	$\text{N} \cdot \text{m/rad}$
C_ϕ	Effective Roll Damping	4432	$\text{N} \cdot \text{m/rad}$

Table 5.1: Parameters for the CarSim Vehicle Model

Roll Envelope Control with Various Thresholds

To show the effectiveness of the envelope approach for roll stability control compared with the conventional rollover index regulation, a ramp steering ($\delta_d = 3.8\,\mathrm{deg}$) scenario is simulated with the vehicle traveling at $60km/h$. Weights on yaw rate tracking (R_x) are intentionally set to be low to promote using active reverse steering for rollover prevention. Different rollover index thresholds are adopted, and the results are shown in Figure 5.12.
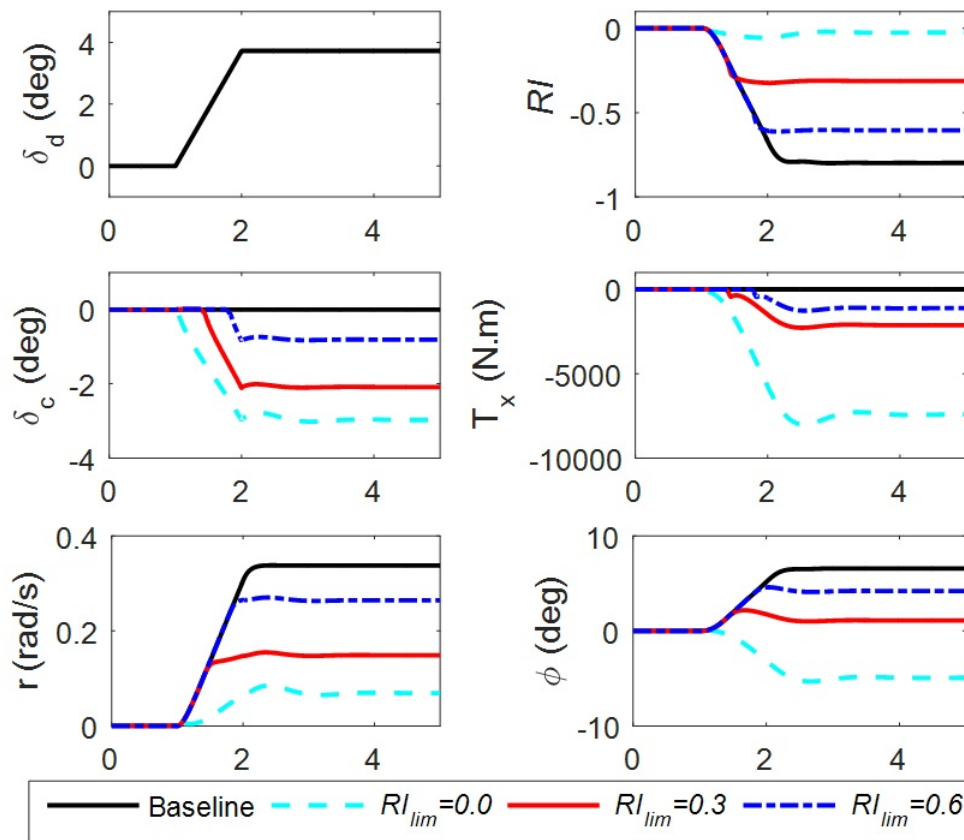
Figure 5.12: Ramp Steer Maneuver with different RI Thresholds

For the uncontrolled baseline case, the rollover index can be as high as 0.8. All other controlled case maintained the vehicle states within the stable handling envelope as well as the roll stability envelope. Compared with the results using only the tilting actuator as shown in Figure 5.8, the transient overshoot of the rollover index, in addition to the tilting

effort, has been dramatically reduced by using the steering actuators.

Although the proposed controller can maintain the vehicle rollover index under various thresholds, the control efforts to achieve the required level of stability are quite different. This demonstrates the significance of the proposed integrated envelope approach for roll stability control.

To maintain the rollover index around zero ($RI_{lim} = 0.0$) during the whole operation time, the tilting torque demand (T_x) is quite high compared with other two cases which only regulates the roll motion when it is about to leave the pre-defined safe envelope. This can also be verified by checking the roll angle (ϕ). The cabin rolls towards the outside bend of the curve for the uncontrolled case, while the perfect balancing approach actively tilts the cabin towards the reverse direction to use gravity for eliminating the lateral load transfer. The proposed envelope approach, which accepts the tracked vehicle can endure some lateral acceleration without rollover danger, only needs to reduce the roll angle to a safe bound. This should alleviate the energy consumption for these narrow vehicles while still maintain the vehicle roll stability.

It can also be seen from the active steering inputs (δ_c) that, to maintain the vehicle under a smaller rollover index threshold, the active reverse steering needs to be activated at an early stage along with more steady-state steering corrections. This can affect the handling performance since the vehicle yaw rate (r) is altered to be less responsive to give compromise to rollover stability.

Integrated Vehicle Control with Envelope Approach

In the previous scenario, it was shown that active steering is very effective in reducing the vehicle rollover tendency at the cost of degraded handling performance. The integrated control approach, by proper allotment of the control actions, is shown to coordinate different actuators to meet the conflicting objectives. The following simulations demonstrate the vehicle performances with different turning maneuvers under the integrated control framework.
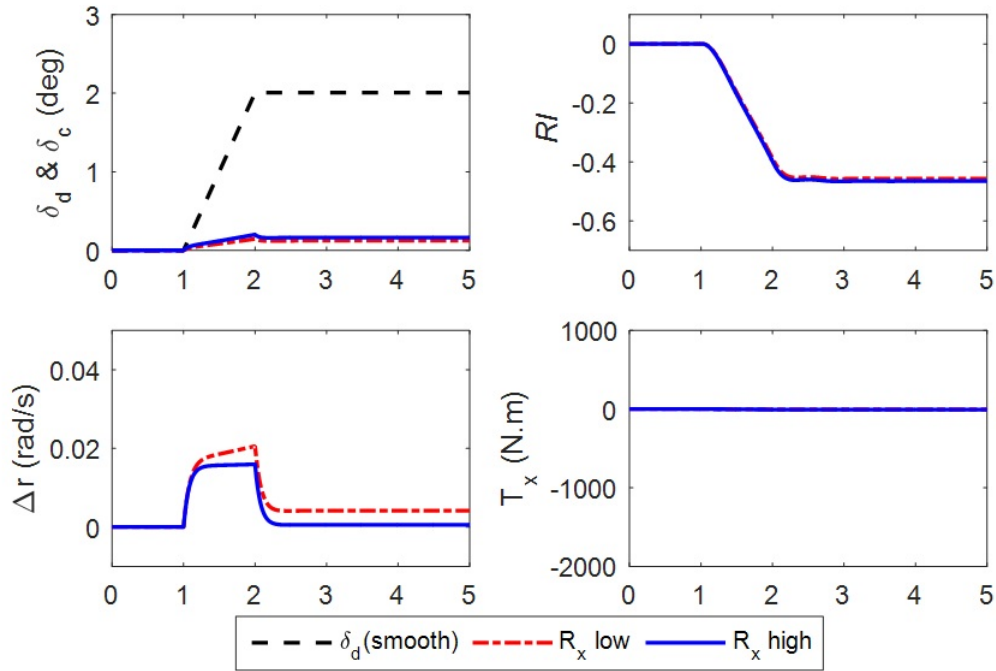
Figure 5.13: Performances under a Smooth Maneuver

The first case applies a smooth ramp steered wheel angle of $2deg/s$ at a speed of $60km/h$, with the results shown in Figure 5.13. The roll stability envelope is defined by the rollover index threshold of 0.6. It can be seen from the results that, since the vehicle states are within the stability envelope, no tilting torque is applied, and the active steering is used only for handling improvement by steering more aggressively to make the vehicle more responsive. The difference (Δr) between the desired and measured yaw rate is maintained at a low level.
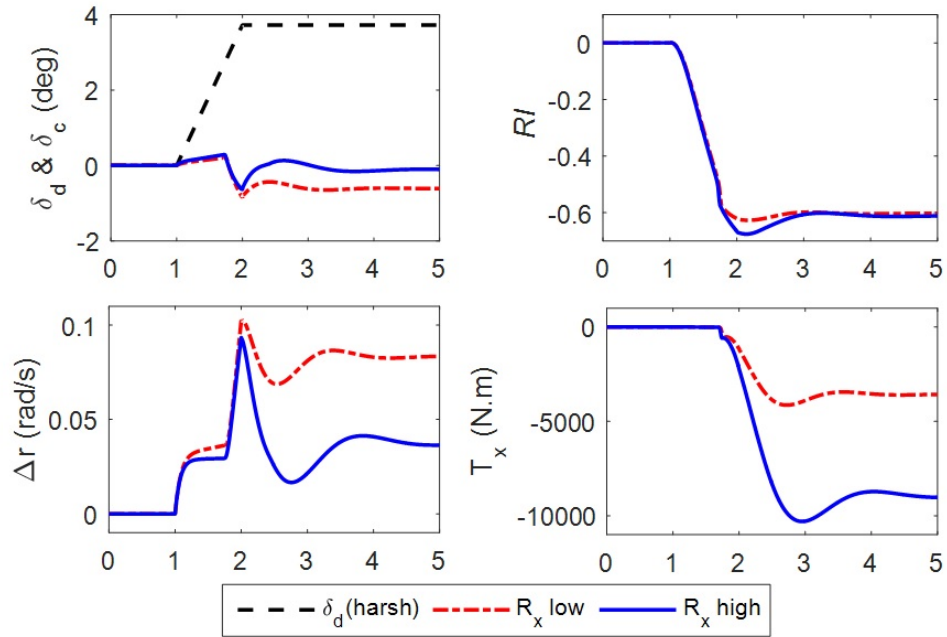
Figure 5.14: Performances under a Harsh Maneuver

As a comparison, a harsher ramp steering of $3.8deg$ is applied at the same speed with the same roll envelope ($RI_{lim} = 0.6$) as illustrated in Figure 5.14. The rollover index for the uncontrolled vehicle is 0.8, and the roll envelope control will be activated at around $1.7sec$. Before activation of the envelope condition, the active steering acts as before for handling improvement (same sign of δ_c and δ_d). However, once the predictive controller foresees the violation of the rollover index threshold, the tilting torque (T_x) will be applied along with the reverse steering (opposite sign of δ_c and δ_d) to give prior to rollover prevention. It is also shown in the figure that, a higher weight (R_x) on handling improvement can successfully reduce the yaw rate tracking error (Δr) and eliminate the use of reverse steering. As a consequence of that, more tilting torque is required to maintain the vehicle within the safe roll envelope at the steady-state. More severe overshoots of rollover index during transient are expected.

Re-configurable Integrated Vehicle Control

In this scenario, the re-configurable feature of the suggested controller is demonstrated. The ramp steering signal is applied to both front wheels at $t = 1.0sec$ with vehicle longitudinal

speed maintained at $60km/h$. The following four actuator configurations are considered,

- Base - Four wheel torque vectoring, no roll control:
  $R_{case1} = diag\left(\begin{bmatrix} 0 & 0 & 0 & 0 & 1 & 1 & 1 & 1 & 0 \end{bmatrix}\right)$

- AT+AFS - Front active steering + tilting:
  $R_{case2} = diag\left(\begin{bmatrix} 1 & 1 & 0 & 0 & 0 & 0 & 0 & 0 & 0 \end{bmatrix}\right)$

- AT+TV Active tilting + four wheel torque vectoring:
  $R_{case3} = diag\left(\begin{bmatrix} 0 & 0 & 0 & 0 & 1 & 1 & 1 & 1 & 1 \end{bmatrix}\right)$

- AT+AFS+TV - Front active steering + four wheel torque vectoring + Tilting:
  $R_{case4} = diag\left(\begin{bmatrix} 1 & 1 & 0 & 0 & 1 & 1 & 1 & 1 & 1 \end{bmatrix}\right)$

Since the roll dynamics is very dependent on the lateral acceleration as the disturbance, for a fair comparison, the vehicle equipped with torque vectoring (Case 1) for yaw rate tracking is chosen as the baseline for the scenario. The active steering applied to the front two tires are assumed to be of the same magnitude and the tilting moment is distributed to the two axles proportionally to their roll stiffness. The desired rollover threshold is chosen as 0.5 for to demonstrate the tracking performance for the roll control. Results are shown in Figure 5.15. It can be seen that, compared with base case when no rollover control is applied, all other configurations can mitigate the rollover danger by decreasing the rollover index from more than 0.8 down to the desired threshold 0.5.

Compared with Case 2 (AT+AFS), which has been demonstrated in the last session for integrated stability control, the Case 3 (AT+TV) is shown to offer similar performances by replacing active steering actuators with torque vectoring ones. This extends the existing STC or SDTC controller designs for tilting vehicles by incorporating more generalized lateral control approaches. When all actuators (AT+AFS+TV) are available, much smoother performance can be obtained. More reverse steering are applied to ease the tilting, while the desired yaw rate is still maintained by the torque vectoring as shown in the figure.
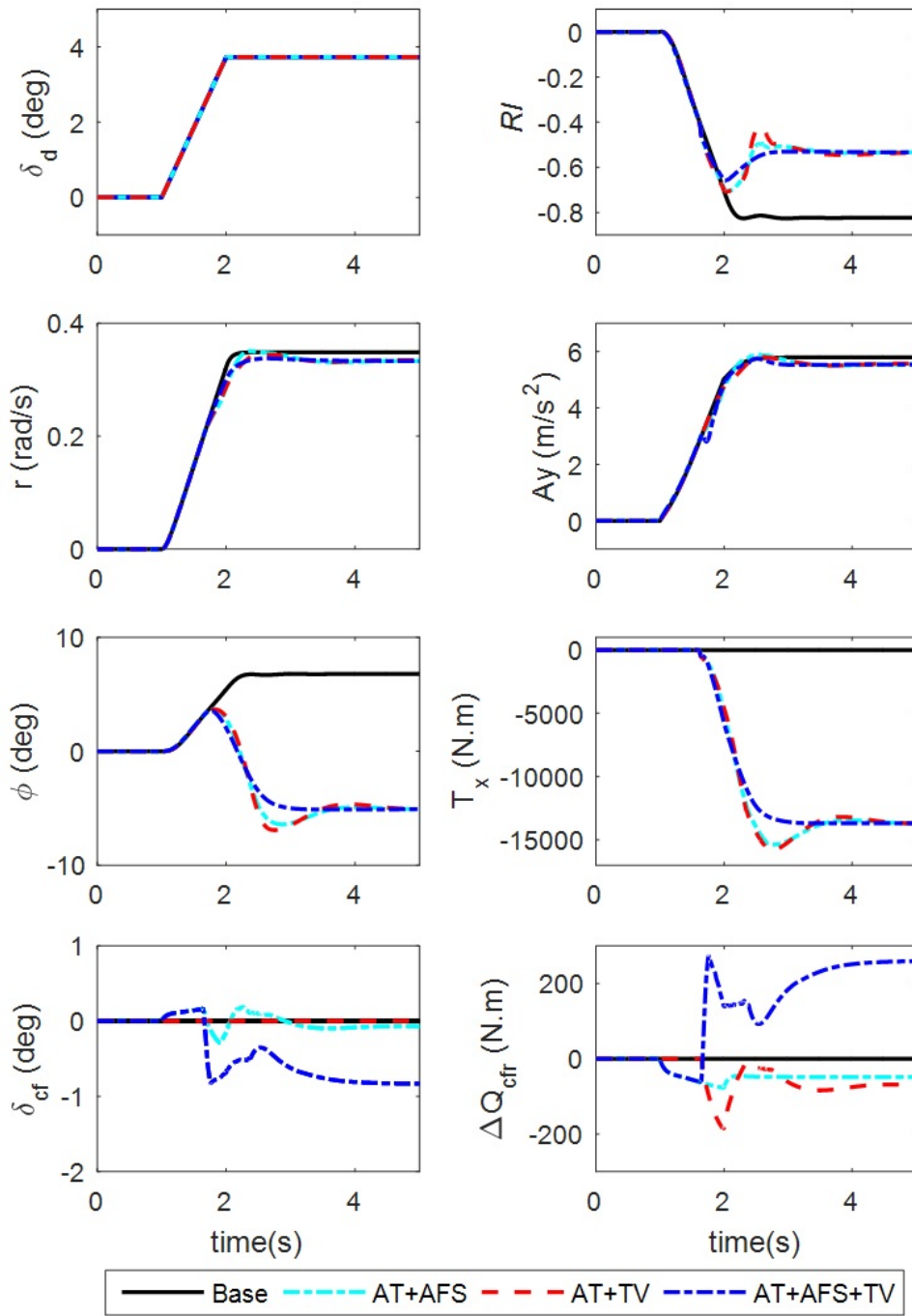
Figure 5.15: Various Actuator Configurations with the Integrated Envelope Control

Robustness to Tilting Actuator Failure

To demonstrate the robustness of the proposed controller, especially under the situation of tilting actuator failure, the vehicle with control configuration in Case 4 (i.e., AT+AFS+TV) from the last session is adopted, and actuator failure is injected into the simulation model by enforcing the tilting moment output to be zero. The failure is triggered at t = 4s and is expected to be captured by the fault-diagnostic system, and the re-configurable structure of the proposed controller can be updated in the form of,

$$R_{case4} = diag\left(\begin{bmatrix} 1 & 1 & 0 & 0 & 1 & 1 & 1 & 1 & R_{Tx}(t) \end{bmatrix}\right)$$

where, $R_{Tx}(t)$ is the diagnosis of the actuator health condition which can be determined by algorithms suggested in [38, 39, 1].

The torque vectoring case with no roll motion control is chosen as the baseline. Under the fishhook maneuver with a travelling speed of $60km/h$, the vehicle is approaching its tipping limit. The rollover tendency can be greatly reduced with the suggested integrated control when all actuators are working properly.

After the triggering of the tilting actuator fault, the suggested controller can be re-constructed due to the re-configurable approach. The steering control will be more active after tilting actuator failure. The torque vectoring will also compromise between rollover mitigation and yaw rate tracking. As a consequence of this redistribution, the vehicle will behave more under-steer compared with the normal case, but the rollover index of the vehicle is successfully reduced to the pre-defined threshold, which gives driver enough time to handle the situation.
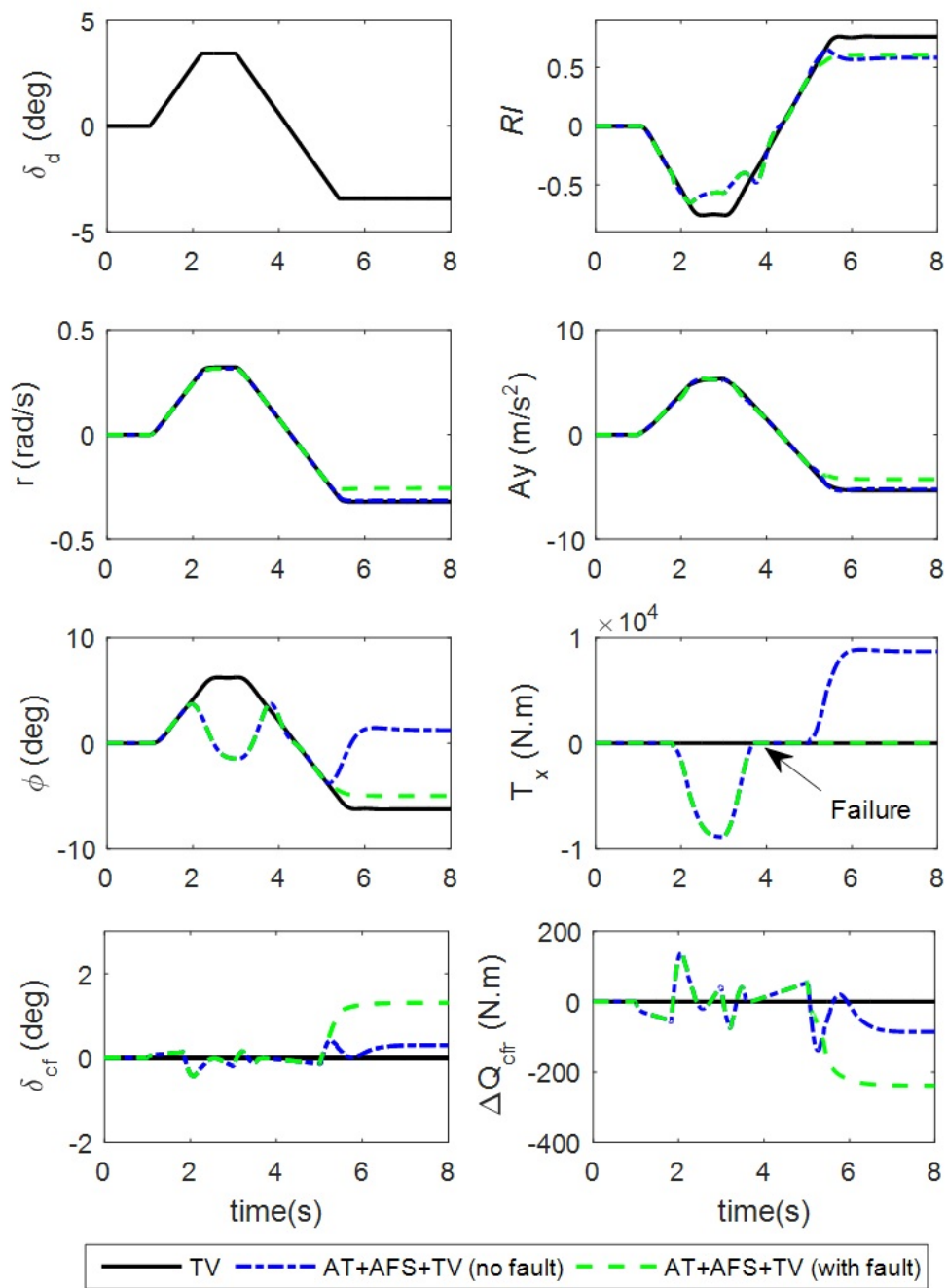
Figure 5.16: Integrated Envelope Control with Actuator Failure

5.4 Integrated Envelope Control for Tilting Vehicles with ISTS

The previous section demonstrates the performance of the integrated envelope controller. For generality, a vehicle roll model with the solid axle is adopted, and the output of the controller is the desired tilting moment which can be implemented on active/semi-active suspension actuators. In this section, a detailed ISTS model is adopted for a three-wheeled NTV to demonstrate the extension of the proposed general approach to incorporate specific actuator designs. The feasibility of the ISTS for NTV is further studied.

5.4.1 Vehicle Modelling with ISTS

The solid axle roll model derived in Section 5.2.1 is widely adopted for rollover studies of conventional vehicles. However, the lumped rotational spring-damper-actuator model restricts its application for detailed suspension components studies, like the ISTS proposed in this thesis. The vehicle roll model with independent suspensions is thus derived in this section first, as shown in Figure 5.17.
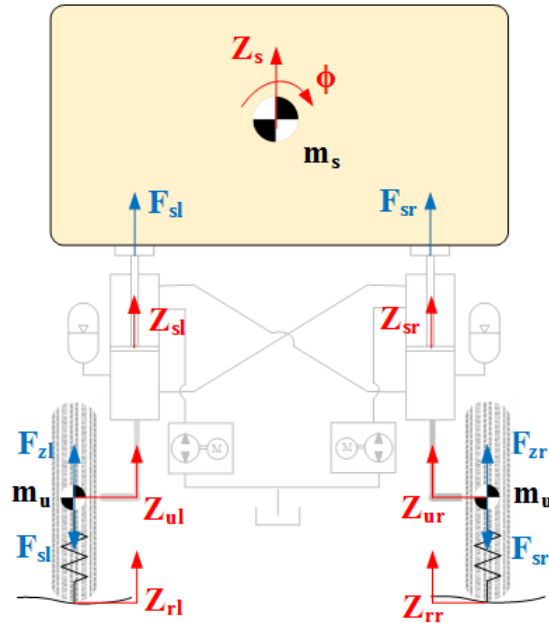
Figure 5.17: Vehicle Roll Model with Independent Suspensions

The vehicle unsprung mass is no longer treated as one single-piece but divided into two, both of which allow the independent bump motion. The DOFs to be considered are: sprung mass bump (z_s) and roll (ϕ), and unsprung mass bump at both left (z_{ul}) and right sides (z_{ur}). The road excitations are considered as disturbance inputs (z_{rl}, z_{rr}) applied to unsprung mass though vertical tire stiffness (k_t). To simplify the final equation for the integrated ISTS, the vertical displacements of the connection points at left (z_{sl}) and right strut (z_{sr}) are chosen as the states, which can be written as a linear transformation of sprung mass bump (z_s) and roll (ϕ) under the small angle assumption as shown in Eq.(3.11).

The dynamics equations can be written as,

$$
\begin{aligned}
m_s \ddot{z}_s &= F_{sl} + F_{sr} - m_s g \\
m_u \ddot{z}_{ul} &= F_{zl} - F_{sl} - m_u g \\
m_u \ddot{z}_{ur} &= F_{zr} - F_{sr} - m_u g \\
I_x \ddot{\phi} &= (F_{sl} - F_{sr})\frac{T_w}{2} + m_s a_y h + m_s g h \phi
\end{aligned}
\tag{5.47}
$$

where, I_x denotes the roll moment of inertia; h is the CoG height; F_{sl} and F_{sr} stand for the suspension strut forces (e.g., output forces of the ISTS as shown in Chapter 3); F_{zl} and F_{zr} are the vertical tire forces calculated by,

$$
F_{zi} = K_t \left(Z_{ri} - Z_{ui} \right) i = l, r
\tag{5.48}
$$

where, K_t is the vertical stiffness of the tire.

The dynamic equations of the mechanical system can be derived by combining lateral (Eq.(5.19)) and roll dynamics (Eq.(5.47)). With the active front steering (AFS) as an additional control input for active safety improvement, the state-space equation can then be written as,

$$
\dot{X}_{me} = A_{me} X_{me} + B_{me} U_{me} + E_{me} W + G_{me} + H_{me} U_{hf}
\tag{5.49}
$$

where the states, inputs, and disturbances are defined as,

$$
\begin{aligned}
X_{me} &= \begin{bmatrix} v & r & \dot{z}_{sl} & \dot{z}_{sr} & z_{sl} & z_{sr} & \dot{z}_{ul} & \dot{z}_{ur} & z_{ul} & z_{ur} \end{bmatrix}^T \\
W &= \begin{bmatrix} \delta_d & z_{rl} & z_{rr} \end{bmatrix}^T, U_{me} = \delta_c, U_{hf} = \begin{bmatrix} F_{sl} & F_{sr} \end{bmatrix}^T
\end{aligned}
\tag{5.50}
$$

95

The system matrices are,

$$A_{me} = \begin{bmatrix} A_1 & O_{4\times 2} & A_2 & & O_{6\times 4} \\ O_{2\times 2} & I_{2\times 2} & O_{2\times 2} & & \\ & O_{4\times 6} & & O_{2\times 2} & -\frac{K_t}{m_u}\cdot I_{2\times 2} \\ & & & I_{2\times 2} & O_{2\times 2} \end{bmatrix}$$

$$B_{me} = \begin{bmatrix} B_1 & O_{6\times 1} \end{bmatrix}^T, E_{me} = \begin{bmatrix} B_1^T & O_{4\times 2} \\ O_{6\times 1} & E_1^T \end{bmatrix}$$

$$G_{me} = \begin{bmatrix} f_1 & f_2 & f_3 & f_4 & 0 & 0 & -g & -g & 0 & 0 \end{bmatrix}^T$$

$$H_{me} = \begin{bmatrix} O_{2\times 2} & G_1 & O_{2\times 2} & \frac{-1}{m_u}\cdot I_{2\times 2} & O_{2\times 2} \end{bmatrix}^T$$

(5.51)

with,

$$A_1 = \begin{bmatrix} -\frac{2(\tilde{C}_{\alpha f}+\tilde{C}_{\alpha r})}{u(m_s+2m_u)} & -\frac{2(a\tilde{C}_{\alpha f}-b\tilde{C}_{\alpha r})}{u(m_s+2m_u)}-u \\ -\frac{2(a\tilde{C}_{\alpha f}-b\tilde{C}_{\alpha r})}{u\cdot I_z} & -\frac{2(a^2\tilde{C}_{\alpha f}+b^2\tilde{C}_{\alpha r})}{u\cdot I_z} \\ -\frac{(\tilde{C}_{\alpha f}+\tilde{C}_{\alpha r})}{u(m_s+2m_u)}\frac{m_s h T_w}{I_x} & \frac{(-a\tilde{C}_{\alpha f}+b\tilde{C}_{\alpha r})}{u(m_s+2m_u)}\frac{m_s h T_w}{I_x} \\ \frac{(-a\tilde{C}_{\alpha f}+b\tilde{C}_{\alpha r})}{u(m_s+2m_u)}\frac{m_s h T_w}{I_x} & -\frac{(\tilde{C}_{\alpha f}+\tilde{C}_{\alpha r})}{u(m_s+2m_u)}\frac{m_s h T_w}{I_x} \end{bmatrix},$$

$$A_2 = \begin{bmatrix} \frac{2(\tilde{C}_{\gamma f}K_{\gamma f}+\tilde{C}_{\gamma r}K_{\gamma r})}{(m_s+2m_u)T_w} & -\frac{2(\tilde{C}_{\gamma f}K_{\gamma f}+\tilde{C}_{\gamma r}K_{\gamma r})}{(m_s+2m_u)T_w} \\ \frac{2(a\tilde{C}_{\gamma f}K_{\gamma f}-b\tilde{C}_{\gamma r}K_{\gamma r})}{I_z T_w} & -\frac{2(a\tilde{C}_{\gamma f}K_{\gamma f}-b\tilde{C}_{\gamma r}K_{\gamma r})}{I_z T_w} \\ \frac{m_s h(\tilde{C}_{\gamma f}K_{\gamma f}+\tilde{C}_{\gamma r}K_{\gamma r})}{(m_s+2m_u)I_x}+\frac{m_s g h}{2I_x} & -\frac{m_s h(\tilde{C}_{\gamma f}K_{\gamma f}+\tilde{C}_{\gamma r}K_{\gamma r})}{(m_s+2m_u)I_x}-\frac{m_s g h}{2I_x} \\ -\frac{m_s h(\tilde{C}_{\gamma f}K_{\gamma f}+\tilde{C}_{\gamma r}K_{\gamma r})}{(m_s+2m_u)I_x}-\frac{m_s g h}{2I_x} & \frac{m_s h(\tilde{C}_{\gamma f}K_{\gamma f}+\tilde{C}_{\gamma r}K_{\gamma r})}{(m_s+2m_u)I_x}+\frac{m_s g h}{2I_x} \end{bmatrix}$$

(5.52)

$$B_1 = \begin{bmatrix} \frac{2\tilde{C}_{\alpha f}}{m_s+2m_u} & \frac{2\tilde{C}_{\alpha f}a}{I_z} & \frac{m_s\tilde{C}_{\alpha f}hT_w}{(m_s+2m_u)I_x} & -\frac{m_s\tilde{C}_{\alpha f}hT_w}{(m_s+2m_u)I_x} \end{bmatrix}$$

$$E_1 = \begin{bmatrix} O_{2\times 2} & \frac{K_t}{m_u}\cdot I_{2\times 2} & O_{2\times 2} \end{bmatrix}, G_1 = \begin{bmatrix} \frac{1}{m_s}+\frac{1}{4}\frac{T_w^2}{I_x} & \frac{1}{m_s}-\frac{1}{4}\frac{T_w^2}{I_x} \\ \frac{1}{m_s}-\frac{1}{4}\frac{T_w^2}{I_x} & \frac{1}{m_s}+\frac{1}{4}\frac{T_w^2}{I_x} \end{bmatrix}$$

$$f_1 = \frac{2(\bar{F}_{yf}-\tilde{C}_{\alpha f}\bar{\alpha}_f-\tilde{C}_{\gamma f}\bar{\gamma}_f)+2(\bar{F}_{yr}-\tilde{C}_{\alpha r}\bar{\alpha}_r-\tilde{C}_{\gamma r}\bar{\gamma}_r)}{m_s+2m_u}$$

$$f_2 = \frac{2a(\bar{F}_{yf}-\tilde{C}_{\alpha f}\bar{\alpha}_f-\tilde{C}_{\gamma f}\bar{\gamma}_f)-2b(\bar{F}_{yr}-\tilde{C}_{\alpha r}\bar{\alpha}_r-\tilde{C}_{\gamma r}\bar{\gamma}_r)}{I_z}$$

$$f_3 = \frac{1}{2}\frac{m_s h T_w}{I_x}f_1-g, f_4 = -\frac{1}{2}\frac{m_s h T_w}{I_x}f_1-g$$

To incorporate the actuator dynamics, the ISTS equations derived in Chapter 3 are then incorporated with the above mechanical system equations to form a hybrid model. The augmented states and control inputs are considered as,

$$X = \begin{bmatrix} X_{me} \\ Q_{PL} \\ Q_{PR} \end{bmatrix}, U = \begin{bmatrix} U_{me} \\ q_{PL} \\ q_{PR} \end{bmatrix} \tag{5.53}$$

The state-space representation of the mechanical system (Eq.(5.49)) can then be rewritten as,

$$\dot{X} = \tilde{A}_{me}X + \tilde{B}_{me}U_{me} + \tilde{E}_{me}W + \tilde{G}_{me} + \tilde{H}_{me}U_{hf} \tag{5.54}$$

where, $(\tilde{*})_{me}$ denotes the augmented system matrices.

The ISTS strut forces Eq.(3.8) can be rewritten with the new states definition as,

$$U_{hf} = A_{hy}X + B_{hy}U + F_{hy} \tag{5.55}$$

where,

$$A_{hy} = \begin{bmatrix} O_{2\times2} & A_{ds} & A_s & -A_{ds} & -A_s & A_p \end{bmatrix}$$
$$B_{hy} = \begin{bmatrix} 0 & (r_h + r_o)A_U & -A_Lr_o \\ 0 & -A_Lr_o & (r_h + r_o)A_U \end{bmatrix}, F_{hy} = \begin{bmatrix} (A_U - A_L)P_a \\ (A_U - A_L)P_a \end{bmatrix} \tag{5.56}$$

Substituting Eq.(5.55) into (5.54), the mechanical-hydraulic model can be written as,

$$\dot{X} = AX + BU + EW + F \tag{5.57}$$

where,

$$A = \tilde{A}_{me} + \tilde{H}_{me}A_{hy}, B = \tilde{B}_{me} + \tilde{H}_{me}B_{hy},$$
$$E = \tilde{E}_{me}, F = \tilde{F}_{me} + \tilde{H}_{me}F_{hy} \tag{5.58}$$

5.4.2 Stability Envelope for Independent Suspensions

LTR for Models with Independent Suspensions

Due to the adoption of the ISTS model which considers the un-sprung mass at each corner, the tire force can be written as the states (Z_{ui}) and disturbances (Z_{ri}). By substituting Eq.(5.48) into Eq.(5.4), the rollover index can be derived as,

$$\text{LTR} = \frac{Z_{rl} - Z_{rr} - Z_{ul} + Z_{ur}}{Z_{rl} + Z_{rr} - Z_{ul} - Z_{ur}} \tag{5.59}$$

For the use of the LTR index in control purposes, the above expression for LTR index is linearized around the nominal position at,

$$Z_{rl0} = Z_{rl0} = 0, Z_{ul0} = Z_{ur0} = -\frac{1}{2}\frac{(m_s + 2m_u)\,g}{K_t} \tag{5.60}$$

The rollover index in the linearized form can then be written as,

$$\text{LTR} = CX + GW \tag{5.61}$$

where,

$$C = \begin{bmatrix} O_{1\times8} & \frac{-K_t}{(m_s+2m_u)g} & \frac{K_t}{(m_s+2m_u)g} & O_{1\times2} \end{bmatrix}$$
$$G = \begin{bmatrix} 0 & \frac{K_t}{(m_s+2m_u)g} & \frac{-K_t}{(m_s+2m_u)g} \end{bmatrix} \tag{5.62}$$

It should be noted that, with the proposed ISTS, the suspension strut displacement and force can be measured. Road disturbance information is assumed to be available via estimation based on acceleration measurements [94, 95], and latest advancements in vision and LIDAR sensors [96, 97]. Particularly, when road disturbances are zero ($Z_{rl} = Z_{rr} = 0$), the model reduces to the one for un-tripped rollover studies on the flat road.

State Constraints on Independent Suspensions Model

Adopting the rollover index derived in linear form in Eq.(5.61), the safe region for rollover index threshold can be visualized as a band in the $Z_{ul} - Z_{ur}$ plane as shown in Figure 5.18.
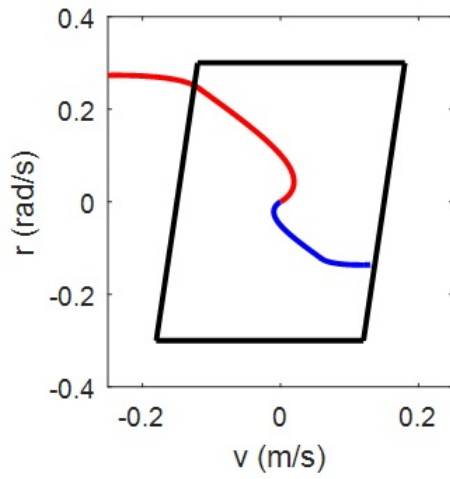
More specifically, at each discretized control step k, it can be represented as a constraint in linear form as,
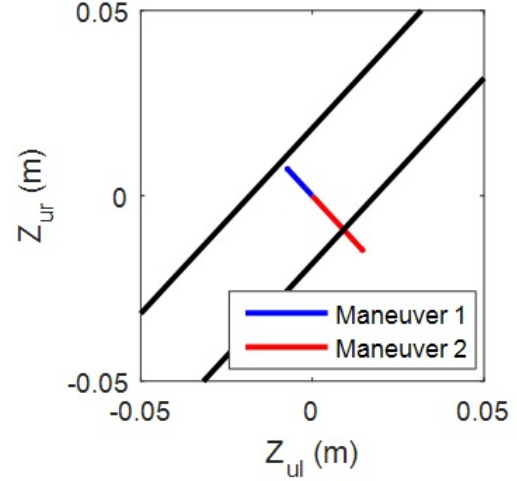
$$M_{ro}X_r^{(k)} \le L_{ro} \tag{5.63}$$

where,

$$M_{ro} = \begin{bmatrix} O_{4\times2} & \begin{matrix} O_{2\times6} & M_1 \\ M_2 & O_{2\times6} \end{matrix} & O_{4\times2} \end{bmatrix}, L_{ro} = \begin{bmatrix} RI_{\lim} \\ RI_{\lim} \\ \dot{\phi}_{\lim} \\ \dot{\phi}_{\lim} \end{bmatrix} - \begin{bmatrix} G \\ -G \\ O_{3\times1} \\ O_{3\times1} \end{bmatrix} W^{(k)} \tag{5.64}$$

$$M_1 = \frac{K_t}{(M_s+2M_u)g} \begin{bmatrix} -1 & 1 \\ 1 & -1 \end{bmatrix}, M_2 = \frac{1}{T_w} \begin{bmatrix} 1 & -1 \\ -1 & 1 \end{bmatrix}$$

(a) Handling envelope (b) Roll envelope

Figure 5.18: Integrated Stability Envelope with Independent Suspensions

It should be mentioned that leaving the pre-defined boundary does not mean the vehicle will roll over instantly. Instead, according to the LTR definition, vehicle rollover is defined as the situation when the rollover index reaches ± 1. The LTR reserve between the defined thresholds to the true rollover condition can be utilized to achieve a quicker system reaction considering the non-minimum phase issue in active tilting control.

5.4.3 MPC Formulation

Using the previously proposed integrated envelope control approach, the receding horizon optimal control problem can be similarly implemented as shown in the Eq.(5.34). The system matrices are substituted with the ones derived in Eq.(5.57), which considers the actuator model of the ISTS. The state constraints for the roll envelope is also replaced with the ones derived in Eq.(5.53).

Due to the incorporation of actuator dynamics, the discrete prediction step-size needs to be adjusted accordingly. For the proposed ISTS on the target vehicle, a step-size bigger than $0.002s$ is found to cause system divergence. This imposes a computational challenge for the model predictive control approach, since a prediction horizon of $1sec$ can lead to a prediction step $N = 500$. This scale of the optimization problem is too big to be solved in a reasonable time.

It is also found to be unnecessary to calculate the control input and perform the envelope constraint check at such a high sampling rate. A reduced formulation is proposed in this section to deal with this problem. More specifically, it is desired to have a different sampling rate for the control signal updates and the system behavior predictions. This can be achieved with the reduction matrix as shown below,

$$\bar{U} = U_{RN}\bar{U}_N \tag{5.65}$$

where, $\bar{U}$ is the full control vector discretized at a small step-size with repetitions; $\bar{U}_N$ is the reduced design variables at a much lower sampling rate; U_{RN} is the reduction transformation matrix which specifies the pattern of repetitions.

$$U_{RN} = \begin{bmatrix} I & O & & \cdots & & O \\ \vdots & & & \cdots & & \\ I & O & & \cdots & & O \\ O & I & O & \cdots & & O \\ & \vdots & & \cdots & & O \\ O & I & O & \cdots & & O \\ & & \vdots & \vdots & \vdots & \\ O & & & \cdots & O & I \\ O & & & \cdots & O & \vdots \\ O & & & \cdots & O & I \end{bmatrix} \left.\begin{matrix} \\ \\ \\ \end{matrix}\right\} \#of\,repeats = \frac{\Delta T_c}{\Delta T} \tag{5.66}$$

The same idea can be applied during the search for the slack variables which leads to the reduction matrix S_{RN} as,

$$\bar{S}_{ro} = S_{RN}\bar{S}_{roN}$$
$$\bar{S}_{sh} = S_{RN}\bar{S}_{shN}$$

(5.67)

Instead of searching for a fine boundary for the envelope violations, a rougher boundary is explored in pursuit for a better computational performance. The envelope constraint can be derived as before, with modifications to the constraint matrices as well as the final quadratic terms, as below.

$$\min_{\eta} : \quad J = \tfrac{1}{2}\eta^T H\eta + f\eta$$

$$s.t. : \quad \begin{bmatrix} A_{RO} \\ A_{SH} \end{bmatrix} \eta \leq \begin{bmatrix} b_{RO} \\ b_{SH} \end{bmatrix}$$

$$\eta_{\min} \leq \eta \leq \eta_{\max}$$

$$\left| \eta^{(k)} - \eta^{(k-1)} \right| \leq \eta_{slew,\max}$$

(5.68)

where,

$$\eta = \begin{bmatrix} \bar{U}_N & \bar{S}_{roN} & \bar{S}_{shN} \end{bmatrix}^T$$
$$H = BlockDiag\left(\begin{bmatrix} \left(R_U + U_{RN}^T S_U^T R_X S_U U_{RN} \right) & Q_{ro} & Q_{sh} \end{bmatrix} \right)$$
$$f = \begin{bmatrix} \left(S_X X^{(0)} + S_{U0}U^{(0)} + S_{W0}W^{(0)} + S_W \bar{W} - \bar{X}_{des} \right)^T R_X S_U U_{RN} & O & O \end{bmatrix}^T$$
$$A_{RO} = BlockDiag\left(\begin{bmatrix} M_{RO} S_U U_{RN} & -S_{RN} & O \end{bmatrix} \right)$$
$$b_{RO} = L_{RO} - M_{RO}\left(S_X X^{(0)} + S_{U0}U^{(0)} + S_{W0}W^{(0)} + S_W \bar{W} \right)$$
$$A_{SH} = BlockDiag\left(\begin{bmatrix} M_{SH} S_U U_{RN} & O & -S_{RN} \end{bmatrix} \right)$$
$$b_{SH} = L_{SH} - M_{SH}\left(S_X X^{(0)} + S_{U0}U^{(0)} + S_{W0}W^{(0)} + S_W \bar{W} \right)$$

(5.69)

5.4.4   Simulation Results

The above MPC problem is implemented with the structure shown in Figure 5.19. Different from the MPC controller in the last section which outputs the desired tilting moment, the controller here considers the actuator dynamics and calculates the control actions of active

steering angles and pump flow rates. The previously adopted SUV model is modified for a three-wheeler with tadpole configuration. The hydraulic circuits of ISTS are modeled as a co-simulation block using the equations derived in Chapter 3, and the suspension strut forces are sent to CarSim as external forces applied at the front axle.
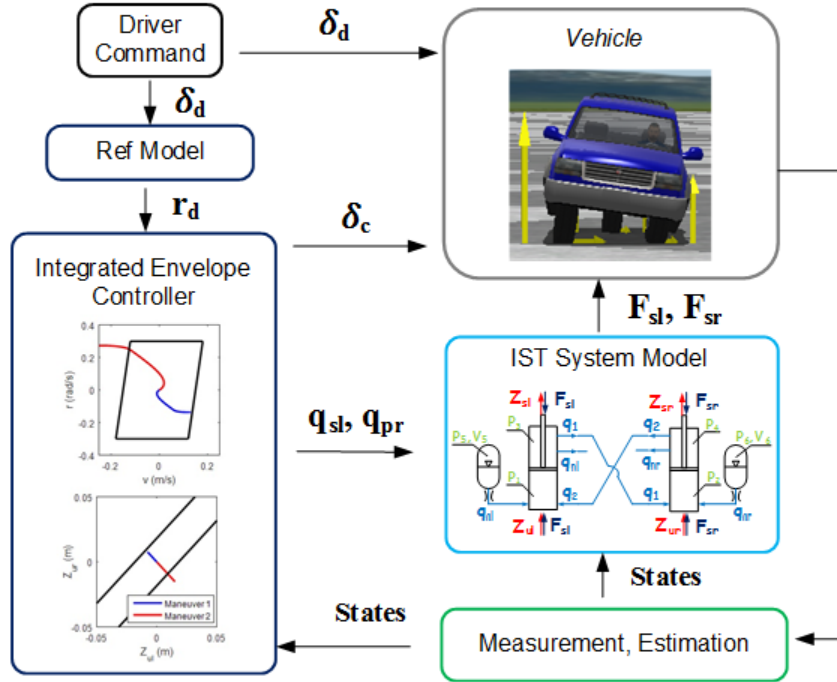

Figure 5.19: Integrated Envelope Controller with ISTS

Roll Envelope Control with ISTS

It has been shown in [98, 99] that the passive hydraulic interconnected suspension (HIS) can improve the roll stability. The proposed ISTS, as an active version of the HIS system, is expected to improve this roll stability even further. This section demonstrates the roll envelope control with ISTS as the only actuator.

As shown in Figure 5.20, two ramp steering maneuvers are considered at the vehicle speed of $60km/h$ to demonstrate the effectiveness of the envelope control: a harsher maneuver with the passive $RI = 0.7$ and a smoother one with the passive $RI = 0.4$. The rollover index threshold is chosen as $RI_{lim} = 0.5$.
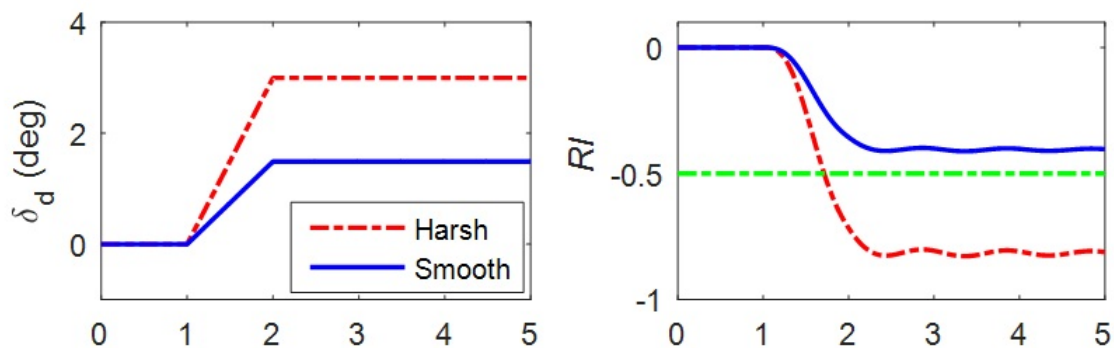
Figure 5.20: Different Ramp Maneuvers and Resultant Rollover Index

The results are shown in Figure 5.21. It can be seen that, for the smooth maneuver, due to the adoption of the envelope control, the tilting actuators are not activated since the rollover index is within the safe boundary. This could save much of the control efforts compared with the endeavors to entirely balance the vehicle [10, 38, 1], and is beneficial for energy efficiency improvements. Such feature makes it quite attractive for NTV applications which need the tilting capability while having constraints on power consumption.

Figure 5.21: Un-tripped Rollover Mitigation with ISTS

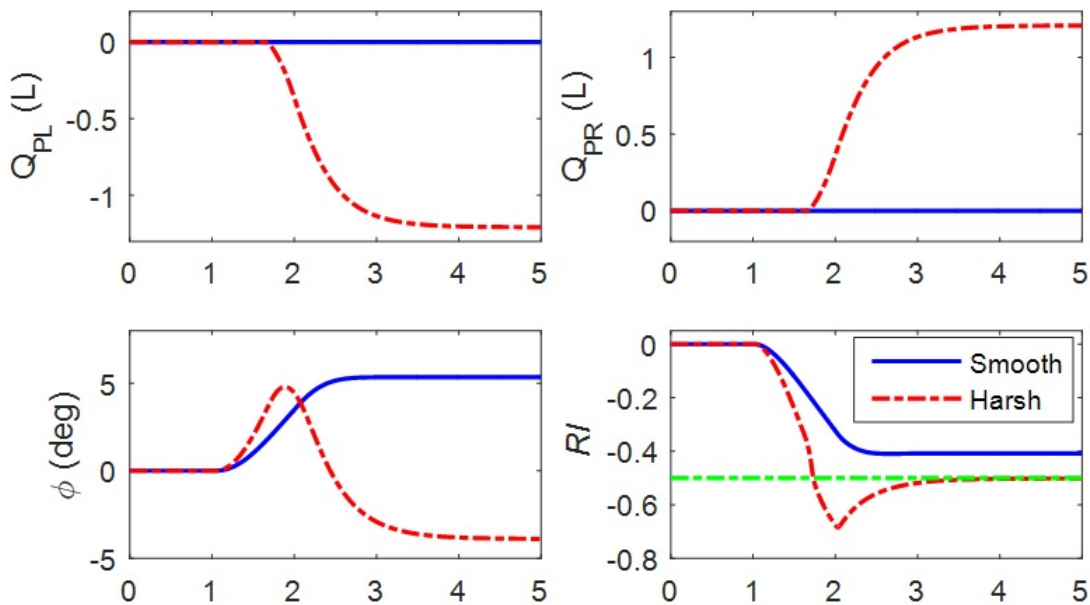Another observation from Figure 5.21 is the non-minimum phase in direct roll control with tilting actuators. Activation of the tilting actuators when the controller foresees the violation of the roll envelope will inevitably worsen the rollover index in transient. Under such circumstances, the soft RI boundary formulation enables the optimizer to explore a better feasible solution with minimal transient violations.

Integrated Un-tripped Rollover Mitigation with ISTS

To overcome non-preferable transient rollover index overshot due to the activation of the tilting actuator, the lateral control approaches can be an excellent complimentary, especially for transient rollover mitigation. Same maneuvers used in Section 5.4.4.1 are adopted, and the results using the integrated controller are illustrated in Figure 5.22.
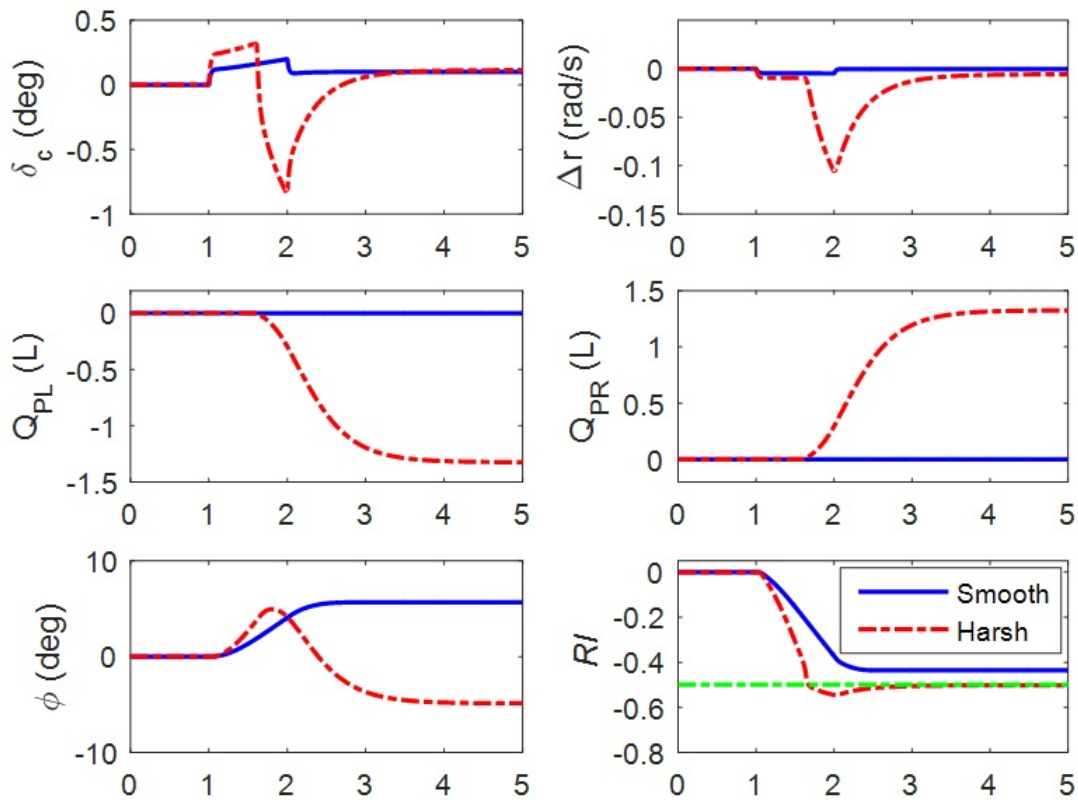

Figure 5.22: Integrated Vehicle Stability Envelope Control with ISTS

For the smoother maneuvers, since the roll envelope boundary is not activated, the focus of the integrated controller is on the handling improvement by steering more aggressively in the direction of drivers steering, while still maintain the vehicle within the safe handling envelope.

However, once the rollover boundary condition is activated, the tuning of the weights gives priority to rollover mitigation. The tilting actuators start to tilt the vehicle into the inner bend of the curve by activating the hydraulic pumps, and counter-steering is also applied to reduce the lateral acceleration in transient to reduce the overshoot of the rollover index. Handling performance is comprised but the vehicle roll stability is greatly enhanced under the coordination of the active steering and the proposed ISTS.

Tripped Rollover Mitigation with ISTS

The proposed model with the independent suspension also enables the tripped rollover to be studied. The scenario is to drive vehicle through a road bump on the left wheel side at different speeds. Duration (ΔT) of the half-sine bump excitation is recorded as a measure of the harshness of the disturbance.

Figure 5.23 demonstrates one of the simulated cases when the duration of the bump in time-domain is $1.5s$. For the uncontrolled scenario, the vehicle almost tips over as indicated by the rollover index. With the proposed integrate controller, a quick steering correction along with the pump actuation is applied for tripped rollover mitigation.
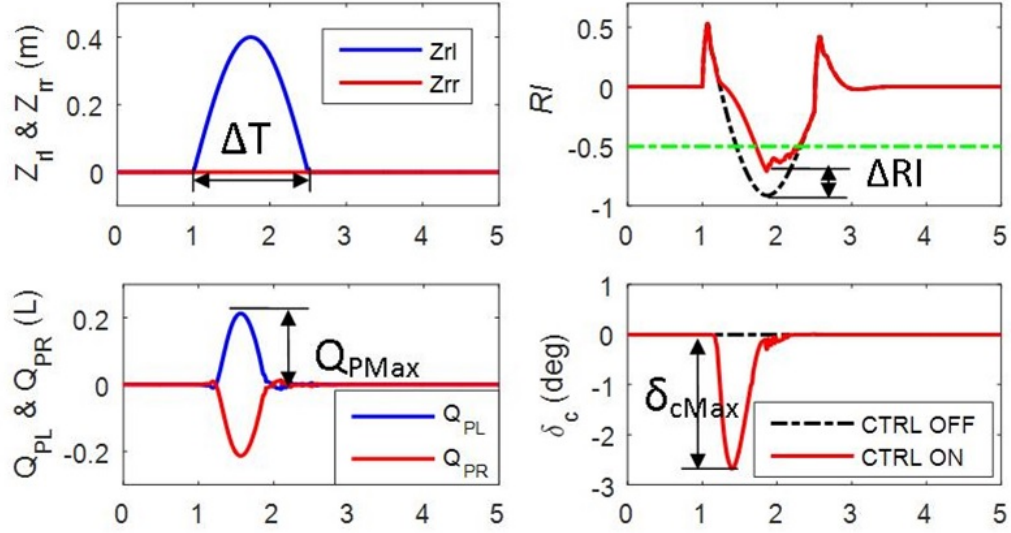
Figure 5.23: Tripped Rollover Mitigation at $\Delta T = 1.5s$

To demonstrate the significance of the proposed ISTS for tripped rollover mitigation, this scenario is simulated with different excitation duration. For each case, three different controller configurations are considered (i.e. uncontrolled, active steering only, and integrated control with ISTS). The improvements on rollover index results are shown in Figure 5.24. It can be seen that, with the proposed integrated suspension tilting system, the rollover index can be further reduced compared with the situation using active steering only. Such improvements are more distinguishable for harsher cases as the time duration of the bump becomes smaller (vehicle travels at a higher speed).

Figure 5.24: Tripped Rollover Mitigation with Integrated Envelope Control

5.5 Conclusions

This chapter identified the challenges in controller design for NTVs and then proposed an integrated envelope controller based on MPC scheme to address them. The i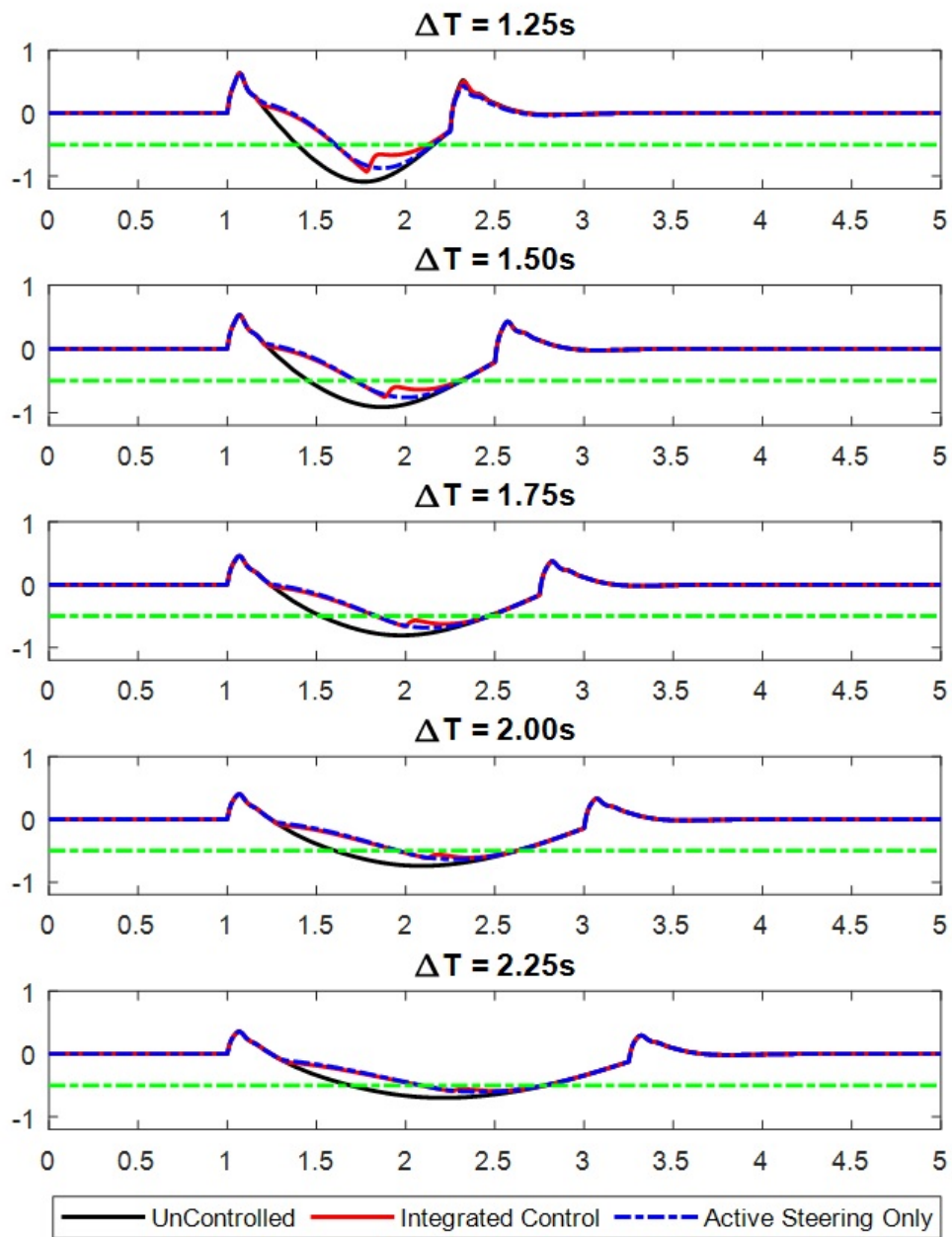dea of the roll envelope control was first illustrated with a general solid-axle roll model. The energy savings with the proposed envelope approach was discussed, and the non-minimum-phase issue using active titling moment for roll control was studied. The MPC controller, due to its predictive feature, was shown to be effective in addressing the tilting control problem. The concept of roll envelope control was then expanded to include the vehicle lateral motions to form an integrated vehicle stability controller. Combining the handling envelope with the proposed roll envelope, an integrated stability envelope for both lateral and roll motion was suggested. An MPC controller which coordinated re-configurable control efforts for stability, as well as handling improvement, was studied. After that, the actuator dynamics of the proposed ISTS was incorporated in the controller design. The proposed controller demonstrated the ISTS could further improve the vehicle stability in an energy efficient manner, which made it ideal for NTV applications.

Chapter 6

Conclusion and Future Work

6.1 Conclusions

This study investigated the active tilting system for narrow tilting vehicles (NTVs) from the conceptual, mechanism, to dynamics and control.

Existing tilting mechanisms were firstly reviewed, and the designs based on four-bar mechanisms were found to take much of the lateral footprint on narrow vehicles. To leave more space to the passengers and cargo, alternative methods to synchronize the wheel motions without mechanical linkages were explored. A tilting concept named Integrated Suspension Tilting System (ISTS) which used hydraulics to replace the mechanical parts was proposed. The wheel synchronization problem which used to be enforced by mechanical linkages were tackled by the coordination of hydraulic pumps via control algorithms. Apart from regulating the desired vehicle roll motion, the proposed system could also adjust the vehicle riding height, thanks to the feature of ISTS for generating both synchronous and asynchronous wheel motions. To make the suggested system even more compact, suspension functionalities were embedded in the design of tilting systems. By using interconnected hydro-pneumatic accumulators, high roll stiffness could be achieved without sacrificing the riding comfort, which enhanced the passive roll stability of NTVs and reduced the tilting control effort accordingly. The proposed system was modeled and simulated to demonstrate its feasibility.

To implement the ISTS on narrow vehicles, the suspension mechanism for NTVs was also investigated. Different from those used on conventional cars, the major challenges for the mechanisms on NTVs were identified as achieving a long suspension stoke in a

compact manner. The trailing arm mechanism was thus suggested as a promising solution due to their simplicity as well as compactness in lateral footprint. The effect of suspension kinematics on vehicle roll stability was then studied. The longitudinal wheel motions for trailing arm mechanisms during tilting were modeled to study their impact on vehicle roll angles as well as the rollover index, and a preferred pattern of wheel longitudinal movement to improve vehicle roll stability was suggested. A design example of a trailing-arm mechanism for NTV was proposed by utilizing the desired longitudinal move pattern of the wheels, and the simulation evaluation confirmed that the suspension kinematics could be utilized to improve the stability of NTVs even further.

The design of a controller to alleviate the energy consumption for tilting was also investigated. An envelope approach based on rollover index was suggested to balance the tilting energy consumption with improvements on the safety margin. Compared with existing tilting strategies which tried to eliminate the lateral load transfer during vehicle cornering, the proposed envelope approach was featured by less frequent activation of tilting actuators and was shown to save the titling effort especially during the non-harsh urban driving scenarios. Different implementations of the roll stability envelope were presented. Instead of using steady-state roll angle, the constraint formulation captured the transient behavior of the rollover index and was adopted for the envelope control.

The non-minimum-phase issue with the active tilting control was studied, and an MPC-based approach was suggested. The predictive feature, along with the proposed envelope formulation, was shown to ease the design compromise between transient and steady-state performances.

By integrating the proposed roll envelope with the one for lateral stability in the literature, an integrated envelope control for vehicle stability was suggested. The integrated framework not only synthesized the stability envelope constraints but also suggested systematic coordination of the actuators for performance improvement. The steering tilting control (STC) in the literature could be regarded as a particular case of this generalized approach. A re-configurable approach was also suggested on top of the integrated controller to optimally distribute the required control efforts to available actuators. This enabled the control algorithm to be easily adapted to various vehicle configurations, and enhance the system robustness to actuator failures as well.

The proposed controller was demonstrated on a conventional SUV along with a three-wheeled NTV in CarSim. The simulation results of the SUV indicated the potential of the suggested controller to be used on conventional vehicles with active suspensions, while the NTV case with the previously introduced ISTS further demonstrated the feasibility of ISTS for rollover mitigation of tilting vehicles.

6.2 Future Work

- Integrated height control for vehicle stability

  One of the features in the proposed ISTS is its capability for height adjustment, which is currently designed only to ease the entering and exiting when the vehicle is not in motion. Vehicle CoG height is known as a key factor in vehicle roll and pitch dynamics. The direct control of it during operation can help to stabilize the vehicle. However, the energy consumption, its effectiveness on rollover mitigation comparing with other actuators, and its impact on the riding comfort should be carefully examined before incorporating the height control as a part of active safety control scheme.

- Riding comfort improvement via ISTS

  The suggested interconnected hydraulic suspensions enable the decoupled design for bump and roll stiffness, which helps the riding comfort in passive mode. When the pumps are activated, the suspension strut forces can be regulated by pump control inputs. This indicates the possibility of using the proposed ISTS as an active suspension system for riding comfort improvement. However, the bandwidth and efficiency of the proposed system should be analyzed in detail for the feasibility.

- Suspension force control via orifice control for ISTS

  The proposed ISTS currently uses the hydraulic pump as the only source for strut force generation. The energy consumption on the pumps might be alleviated by introducing alternative ways for force regulation. Orifices in the hydraulic circuits of ISTS can be utilized as seen on semi-active suspensions for luxury vehicles. The effectiveness of the force regulation via the orifices as well as the control coordination with existing actuators needs to be studied.

- Employment of nonlinear model predictive control

  To overcome the computation burden with NMPC programming, the nonlinear vehicle dynamics model is linearized around the operating point in this research to form a tractable quadratic programming problem at each sampling time. Performance of the proposed controller can be further improved by incorporating the nonlinear tire model as well as the longitudinal dynamics.

- System prototyping and experiments

  The urban vehicle currently being tested in the Mechatronics Vehicle Systems Laboratory can be used as an evaluation platform for the suggested integrated envelope

control algorithm. The integrated suspension tilting system should also be proto-typed for further evaluations.

References

[1] H.M. Kroonen C.R. van den Brink. DVC The banking technology driving the CARVER vehicle class. In *AVEC 2004*, Arnhem (The Netherlands), 2004.

[2] Johan J. H. Berote and web support@bath.ac.uk. *Dynamics and Control of a Tilting Three Wheeled Vehicle.* Ph.D. Thesis, University of Bath, 2010.

[3] Samuel Kidane, Rajesh Rajamani, Lee Alexander, Patrick J. Starr, and Max Donath. Development and Experimental Evaluation of a Tilt Stability Control System for Narrow Commuter Vehicles. *IEEE Transactions on Control Systems Technology*, 18(6):1266–1279, November 2010.

[4] Johannes Edelmann, Manfred Plchl, and Peter Lugner. Modelling and analysis of the dynamics of a tilting three-wheeled vehicle. *Multibody System Dynamics*, 26(4):469–487, December 2011.

[5] K. M. Kockelman and Y. Zhao. BEHAVIORAL DISTINCTIONS: THE USE OF LIGHT-DUTY TRUCKS AND PASSENGER CARS. *Journal of Transportation and Statistics*, 3(3), December 2000.

[6] Robin Hibbard and Dean Karnopp. Twenty First Century Transportation System Solutions - a New Type of Small, Relatively Tall and Narrow Active Tilting Commuter Vehicle. *Vehicle System Dynamics*, 25(5):321–347, May 1996.

[7] Jeffrey C. Huston, Brian J. Graves, and David B. Johnson. Three Wheeled Vehicle Dynamics. In *SAE Technical Paper*, February 1982.

[8] T. D Gillespie and Society of Automotive Engineers. *Fundamentals of vehicle dynamics.* Society of Automotive Engineers, Warrendale, Pa., 1992.

[9] Patrick L. Boyd. NHTSA's NCAP Rollover Resistance Rating System. In *19th International Technical Conference on the Enhanced Safety of Vehicles (ESV)*, June 2005.

[10] S. Kidane, L. Alexander, R. Rajamani, P. Starr, and M. Donath. A fundamental investigation of tilt control systems for narrow commuter vehicles. *Vehicle System Dynamics*, 46(4):295–322, April 2008.

[11] Frank Will, James Nicholas Davdison, Paul Couchman, and David Bednall. Tomorrow's Car-For Today's People: Can Tilting Three Wheeled Vehicles be a Solution for the Problems of Today and the Future? Technical report, SAE Technical Paper, 2011.

[12] Matthew Iain Barker. *Chassis design and dynamics of a tilting three-wheeled vehicle.* Ph.D., University of Bath, 2006.

[13] Nicola Amati, Andrea Festini, Luigi Pelizza, and Andrea Tonoli. Dynamic modelling and experimental validation of three wheeled tilting vehicles. *Vehicle System Dynamics*, 49(6):889–914, June 2011.

[14] Chen Tang, Avesta Goodarzi, and Amir Khajepour. A novel integrated suspension tilting system for narrow urban vehicles. *Proceedings of the Institution of Mechanical Engineers, Part D: Journal of Automobile Engineering*, page 095440701773827, November 2017.

[15] Chen Tang, Ling He, and Amir Khajepour. Design and analysis of an integrated suspension tilting mechanism for narrow urban vehicles. *Mechanism and Machine Theory*, 120:225–238, February 2018.

[16] Jin-Chern Chiou and Chih-Liang Chen. Modeling and verification of a diamond-shape narrow-tilting vehicle. *IEEE/ASME transactions on Mechatronics*, 13(6):678–691, 2008.

[17] marsMediaSite. The curve master F 300 Life Jet.

[18] Carver Technology. The unique self-balancing vehicle technology hold by Carver Technology.

[19] S. Maakaroun, W. Khalil, M. Gautier, and P. Chevrel. Modeling and Simulating a Narrow Tilting Car Using Robotics Formalism. *IEEE Transactions on Intelligent Transportation Systems*, 15(3), June 2014.

114

[20] Toyota Motor Corporation. Toyota Global Site | Personal Mobility | TOYOTA i-ROAD.

[21] Auguste Van Poelgeest. *The dynamics and control of a three-wheeled tilting vehicle.* Ph.D. Thesis, University of Bath, 2011.

[22] James Robertson. *Active Control of Narrow Tilting Vehicle Dynamics.* Ph.D. Thesis, University of Bath, February 2014.

[23] Hasan Alipour, Mohammad Bagher Bannae Sharifian, and Mehran Sabahi. A modified integral sliding mode control to lateral stabilisation of 4-wheel independent drive electric vehicles. *Vehicle System Dynamics*, 52(12):1584–1606, December 2014.

[24] M. Ataei, A. Khajepour, and S. Jeon. A Novel Reconfigurable Integrated Vehicle Stability Control with Omni Actuation Systems. *IEEE Transactions on Vehicular Technology*, PP(99):1–1, 2017.

[25] Avesta Goodarzi, Amir Soltani, Mohammad Hassan Shojaeefard, and Amir Khajepour. An integrated vehicle dynamic control strategy for three-wheeled vehicles. *Proceedings of the Institution of Mechanical Engineers, Part K: Journal of Multi-body Dynamics*, 229(3):225–244, September 2015.

[26] Amir Khajepour, M. Saber Fallah, and Avesta Goodarzi. *Electric and Hybrid Vehicles: Technologies, Modeling and Control - A Mechatronic Approach.* Wiley, Chichester, West Sussex, United Kingdom, May 2014.

[27] Department of Transportation. National Highway Traffic Safety Administration. Traffic safety facts 2012: a compilation of motor vehicle crash data from the fatality analysis reporting system and the general estimates system. Technical report, National Highway Traffic Safety Administration, 2012.

[28] Jangyeol Yoon, Wanki Cho, Juyong Kang, Bongyeong Koo, and Kyongsu Yi. Design and evaluation of a unified chassis control system for rollover prevention and vehicle stability improvement on a virtual test track. *Control Engineering Practice*, 18(6):585–597, June 2010.

[29] Van Tan Vu, Olivier Sename, Luc Dugard, and Peter Gaspar. Enhancing roll stability of heavy vehicle by LQR active anti-roll bar control using electronic servo-valve hydraulic actuators. *Vehicle System Dynamics*, 55(9):1405–1429, September 2017.

[30] David J. M. Sampson and David Cebon. Active Roll Control of Single Unit Heavy Road Vehicles. *Vehicle System Dynamics*, 40(4):229–270, October 2003.

[31] Nong Zhang, Guang-Ming Dong, and Hai-Ping Du. Investigation into untripped rollover of light vehicles in the modified fishhook and the sine maneuvers. Part I: Vehicle modelling, roll and yaw instability. *Vehicle System Dynamics*, 46(4):271–293, April 2008.

[32] Guang-Ming Dong, Nong Zhang, and Hai-Ping Du. Investigation into untripped rollover of light vehicles in the modified fishhook and the sine manoeuvres, part II: effects of vehicle inertia property, suspension and tyre characteristics. *Vehicle System Dynamics*, 49(6):949–968, June 2011.

[33] Garrett A. Mattos, Raphael H. Grzebieta, Mike R. Bambach, and Andrew S. McIntosh. Validation of a dynamic rollover test device. *International Journal of Crashworthiness*, 18(3):207–214, June 2013.

[34] S. Yim, Y. Park, and K. Yi. Design of active suspension and electronic stability program for rollover prevention. *International Journal of Automotive Technology*, 11(2):147–153, April 2010.

[35] Thomas J. Wielenga and Milton A. Chace. A Study in Rollover Prevention Using Anti-Rollover Braking. In *SAE 2000 Automotive Dynamics and Stability Conference*, May 2000.

[36] B. Schofield and T. Hagglund. Optimal control allocation in vehicle dynamics control for rollover mitigation. In *2008 American Control Conference*, pages 3231–3236, June 2008.

[37] Jangyeol Yoon and Kyongsu Yi. A rollover mitigation control scheme based on rollover index. In *2006 American Control Conference*, pages 5372–5377, June 2006.

[38] J.-S. Jo, S.-H. You, J. Y. Joeng, K. I. Lee, and K. Yi. Vehicle stability control system for enhancing steerabilty, lateral stability, and roll stability. *International Journal of Automotive Technology*, 9(5):571, October 2008.

[39] Craig Earl Beal. *Applications of model predictive control to vehicle dynamics for active safety and stability.* Ph.D. Thesis, Stanford University, 2011.

[40] J. Gohl, R. Rajamani, L. Alexander, and P. Starr. Active Roll Mode Control Implementation on a Narrow Tilting Vehicle. *Vehicle System Dynamics*, 42(5):347–372, December 2004.

[41] James W Robertson, Jos Darling, and Andrew R Plummer. Combined steeringdirect tilt control for the enhancement of narrow tilting vehicle stability. *Proceedings of the Institution of Mechanical Engineers, Part D: Journal of Automobile Engineering*, 228(8):847–862, July 2014.

[42] Johannes Edelmann and Manfred Plchl. Electronic Stability Control of a Narrow Tilting Vehicle. *SAE International Journal of Materials and Manufacturing*, 4(1):1006–1013, April 2011.

[43] SANG-GYUN SO and DEAN KARNOPP. Active Dual Mode Tilt Control for Narrow Ground Vehicles. *Vehicle System Dynamics*, 27(1):19–36, January 1997.

[44] ANTONY SNELL. An Active Roll-Moment Control Strategy for Narrow Tilting Commuter Vehicles. *Vehicle System Dynamics*, 29(5):277–307, May 1998.

[45] Lama Mourad, Fabien Claveau, and Philippe Chevrel. Direct and Steering Tilt Robust Control of Narrow Vehicles. *IEEE Transactions on Intelligent Transportation Systems*, 15(3):1206–1215, June 2014.

[46] Johan Berote, Jos Darling, and Andrew Plummer. Lateral dynamics simulations of a three-wheeled tilting vehicle. *Proceedings of the Institution of Mechanical Engineers, Part D: Journal of Automobile Engineering*, 229(3):342–356, February 2015.

[47] R. Rajamani, J. Gohl, L. Alexander, and P. Starr. Dynamics of Narrow Tilting Vehicles. *Mathematical and Computer Modelling of Dynamical Systems*, 9(2):209–231, June 2003.

[48] Rhyse Maryniuk. Development of a Modular Urban Electric Vehicle. Master's thesis, University of Waterloo, December 2017.

[49] Mohammad-Amin Rajaie. Design and Fabrication of a Novel Corner Wheel Module for Urban Vehicles. Master's thesis, University of Waterloo, September 2016.

[50] Allison Waters. A Novel Universal Corner Module for Urban Electric Vehicles: Design, Prototype, and Experiment. Master's thesis, University of Waterloo, August 2017.

[51] Julian Marsh. Citron XM technical specification.

[52] Wolfgang Bauer. *Hydropneumatic Suspension Systems*. Springer, 2011.

[53] Grand River Transit. Accessibility on GRT buses, May 2017.

[54] Tesla Motors. Model S Owner's Manual, December 2018.

[55] Anthony Esposito. *Fluid Power With Applications*. Prentice Hall College Div, Upper Saddle River, N.J, 4 edition edition, July 1996.

[56] Peijun Liu and Peijun Liu. An analytical study of ride and handling performance of an interconnected vehicle suspension. Master's thesis, Concordia University, 1994.

[57] Nong Zhang, Wade A. Smith, and Jeku Jeyakumaran. Hydraulically interconnected vehicle suspension: background and modelling. *Vehicle System Dynamics*, 48(1):17–40, January 2010.

[58] Wade A. Smith, Nong Zhang, and William Hu. Hydraulically interconnected vehicle suspension: handling performance. *Vehicle System Dynamics*, 49(1-2):87–106, February 2011.

[59] Brian J. Kirby. *Micro- and Nanoscale Fluid Mechanics: Transport in Microfluidic Devices*. Cambridge University Press, Cambridge, reprint edition edition, August 2013.

[60] Zhilin Jin, Lei Zhang, Jiale Zhang, and Amir Khajepour. Stability and optimised H control of tripped and untripped vehicle rollover. *Vehicle System Dynamics*, 54(10):1405–1427, October 2016.

[61] Mansour Ataei, Amir Khajepour, and Soo Jeon. A general rollover index for tripped and un-tripped rollovers on flat and sloped roads. *Proceedings of the Institution of Mechanical Engineers, Part D: Journal of Automobile Engineering*, page 0954407017743345, December 2017.

[62] MapleSoft. MapleSim User Guide, 2014.

[63] Hans B Pacejka. *Tire and Vehicle Dynamics*. SAE International, Warrendale, PA, 2006.

[64] Tianjun Zhu, Amir Khajepour, Avesta Goodarzi, Shih-Ken Chen, and Bakhtiar Litkouhi. Development of an optimal driver command interpreter for vehicle dynamics control. *International Journal of Vehicle Autonomous Systems*, 13(1):43–64, January 2015.

[65] J Berote, J Darling, and A Plummer. Development of a tilt control method for a narrow-track three-wheeled vehicle. *Proceedings of the Institution of Mechanical Engineers, Part D: Journal of Automobile Engineering*, 226(1):48–69, January 2012.

[66] Dean Karnopp. *Vehicle Dynamics, Stability, and Control, Second Edition.* CRC Press, Boca Raton, FL, January 2013.

[67] John C. Dixon. *Suspension Geometry and Computation.* Wiley, Chichester, U.K, December 2009.

[68] J. P. Sadler, H. C. Chou, and G. R. George. On the Application of Straight-Line Linkages to Vehicle Suspension. *Journal of Mechanisms, Transmissions, and Automation in Design*, 111(2):208–214, June 1989.

[69] Jing-Shan Zhao, Fulei Chu, and Zhi-Jing Feng. Synthesis of Rectilinear Motion Generating Spatial Mechanism With Application to Automotive Suspension. *Journal of Mechanical Design*, 130(6):065001–065001–8, April 2008. 00017.

[70] Neil Sclater. *Mechanisms and Mechanical Devices Sourcebook, 5th Edition.* McGraw-Hill Education, New York, 5 edition edition, August 2011.

[71] P. A. Simionescu and D. Beale. Synthesis and analysis of the five-link rear suspension system used in automobiles. *Mechanism and Machine Theory*, 37(9):815–832, September 2002.

[72] K. Vikranth Reddy, Madhu Kodati, Kishen Chatra, and Sandipan Bandyopadhyay. A comprehensive kinematic analysis of the double wishbone and MacPherson strut suspension systems. *Mechanism and Machine Theory*, 105:441–470, November 2016.

[73] Mansour Ataei, Amir Khajepour, and Soo Jeon. Rollover stabilities of three-wheeled vehicles including road configuration effects. *Proceedings of the Institution of Mechanical Engineers, Part D: Journal of Automobile Engineering*, 231(7):859–871, June 2017.

[74] M. Barker, B. Drew, J. Darling, K. A. Edge, and G. W. Owen. Steady-state steering of a tilting three-wheeled vehicle. *Vehicle System Dynamics*, 48(7):815–830, July 2010.

[75] William F Milliken and Douglas L Milliken. *Race car vehicle dynamics.* SAE International, Warrendale, PA, U.S.A, 1995.

[76] Chen Tang and Amir Khajepour. MapleCAR - A New Topology-Based Simulation Tool in Vehicle Modeling and Control. In *North America Modelica Users' Group Conference*, 2016.

119

[77] Daofei Li, Shangqian Du, and Fan Yu. Integrated vehicle chassis control based on direct yaw moment, active steering and active stabiliser. *Vehicle System Dynamics*, 46(sup1):341–351, September 2008.

[78] Rajesh Rajamani. *Vehicle Dynamics and Control*. Springer, 2012.

[79] R. Rajamani, D. Piyabongkarn, V. Tsourapas, and J. Y. Lew. Parameter and State Estimation in Vehicle Roll Dynamics. *IEEE Transactions on Intelligent Transportation Systems*, 12(4):1558–1567, December 2011.

[80] Xinjie Zhang, Yi Yang, Konghui Guo, Jiming Lv, and Tao Peng. Contour line of load transfer ratio for vehicle rollover prediction. *Vehicle System Dynamics*, 55(11):1748–1763, November 2017.

[81] Chen Tang, Mansour Ataei, and Amir Khajepour. A Reconfigurable Integrated Control for Narrow Tilting Vehicles. *IEEE Transactions on Vehicular Technology*, 2018.

[82] Tetsunori Haraguchi, Tetsuya Kaneko, Ichiro Kageyama, Yukiyo Kuriyagawa, and Masanori Kobayashi. Study of Tilting Type Personal Mobility Vehicle by the Immersive Driving Simulator with Five Large Screens. *Transactions of Society of Automotive Engineers of Japan*, 48(3):693–698, 2017.

[83] Milad Jalali, Ehsan Hashemi, Amir Khajepour, Shih-ken Chen, and Bakhtiar Litkouhi. Model predictive control of vehicle roll-over with experimental verification. *Control Engineering Practice*, 77:95–108, August 2018.

[84] J. B. Hoagg and D. S. Bernstein. Nonminimum-phase zeros - much to do about nothing - classical control - revisited part II. *IEEE Control Systems*, 27(3):45–57, June 2007.

[85] L. Qiu and E. J. Davison. Performance limitations of non-minimum phase systems in the servomechanism problem. *Automatica*, 29(2):337–349, March 1993.

[86] Chen Tang and Amir Khajepour. Integrated Stability Control for Narrow Tilting Vehicles: An Envelope Approach. *IEEE Transactions on Intelligent Transportation Systems*, 2018. (under review).

[87] Scokaert Pierre O. M. and Rawlings James B. Feasibility issues in linear model predictive control. *AIChE Journal*, 45(8):1649–1659, April 2004.

[88] Matthew Brown, Joseph Funke, Stephen Erlien, and J. Christian Gerdes. Safe driving envelopes for path tracking in autonomous vehicles. *Control Engineering Practice*, 61:307–316, April 2017.

[89] M. Ataei, A. Khajepour, and S. Jeon. Reconfigurable Integrated Stability Control for Four- and Three-wheeled Urban Vehicles With Flexible Combinations of Actuation Systems. *IEEE/ASME Transactions on Mechatronics*, 23(5):2031–2041, October 2018.

[90] Carrie Gwendolene Bobier. *A phase portrait approach to vehicle stabilization and envelope control*. Ph.D. Thesis, Stanford University, 2012.

[91] S. M. Erlien, S. Fujita, and J. C. Gerdes. Shared Steering Control Using Safe Envelopes for Obstacle Avoidance and Vehicle Stability. *IEEE Transactions on Intelligent Transportation Systems*, 17(2):441–451, February 2016.

[92] Y. H. J. Hsu, S. M. Laws, and J. C. Gerdes. Estimation of Tire Slip Angle and Friction Limits Using Steering Torque. *IEEE Transactions on Control Systems Technology*, 18(4):896–907, July 2010.

[93] Ehsan Hashemi. *Full Vehicle State Estimation Using a Holistic Corner-based Approach*. Ph.D. Thesis, University of Waterloo, 2017.

[94] W. Fauriat, C. Mattrand, N. Gayton, A. Beakou, and T. Cembrzynski. Estimation of road profile variability from measured vehicle responses. *Vehicle System Dynamics*, 54(5):585–605, May 2016.

[95] H. Imine, Y. Delanne, and N. K. M'Sirdi. Road profile input estimation in vehicle dynamics simulation. *Vehicle System Dynamics*, 44(4):285–303, April 2006.

[96] H. T. Chen, C. Y. Lai, C. C. Hsu, S. Y. Lee, B. S. P. Lin, and C. P. Ho. Vision-Based Road Bump Detection Using a Front-Mounted Car Camcorder. In *2014 22nd International Conference on Pattern Recognition*, pages 4537–4542, August 2014.

[97] Joy Sucgang Nathalie, Ramos Jr. Manuel, and Ann Arriola Nicolette. Road Surface Obstacle Detection using Vision and LIDAR for Autonomous Vehicle. In *Proceedings of the International MultiConference of Engineers and Computer Scientists*, 2017.

[98] Dongpu Cao, Subhash Rakheja, and Chun-Yi Su. Roll- and pitch-plane coupled hydro-pneumatic suspension. Part 1: Feasibility analysis and suspension properties. *Vehicle System Dynamics*, 48(3):361–386, March 2010.

[99] Dongpu Cao, Subhash Rakheja, and Chun-Yi Su. Roll- and pitch-plane-coupled hydro-pneumatic suspension. Part 2: dynamic response analyses. *Vehicle System Dynamics*, 48(4):507–528, April 2010.

[100] Hibbard R and Karnopp D. Methods of controlling the lean angle of tilting vehicles. *ASME DSC (Am Soc Mech Eng Dyn Syst Control)*, 52:311–320, 1993.